COMBUSTION ASSISTED GRAVITY DRAINAGE (CAGD): AN IN-SITU COMBUSTION METHOD TO RECOVER HEAVY OIL AND BITUMEN FROM GEOLOGIC FORMATIONS USING A HORIZONTAL INJECTOR/PRODUCER PAIR

A Dissertation

by

HAMID RAHNEMA

Submitted to the Office of Graduate Studies of
Texas A&M University
in partial fulfillment of the requirements for the degree of

DOCTOR OF PHILOSOPHY

Approved by:

Chair of Committee,	Maria A. Barrufet
Committee Members,	Robert H. Lane
	Jerome J. Schubert
	Yuefeng Sun
Head of Department,	A. Daniel Hill

December 2012

Major Subject: Petroleum Engineering

ABSTRACT

Combustion assisted gravity drainage (CAGD) is an integrated horizontal well air injection process for recovery and upgrading of heavy oil and bitumen from tar sands. Short-distance air injection and direct mobilized oil production are the main features of this process that lead to stable sweep and high oil recovery. These characteristics identify the CAGD process as a high-potential oil recovery method either in primary production or as a follow-up process in reservoirs that have been partially depleted. The CAGD process combines the advantages of both gravity drainage and conventional in-situ combustion (ISC). A combustion chamber develops in a wide area in the reservoir around the horizontal injector and consists of flue gases, injected air, and mobilized oil. Gravity drainage is the main mechanism for mobilized oil production and extraction of flue gases from the reservoir.

A 3D laboratory cell with dimensions of 0.62 m, 0.41 m, and 0.15 m was designed and constructed to study the CAGD process. The combustion cell was fitted with 48 thermocouples. A horizontal producer was placed near the base of the model and a parallel horizontal injector in the upper part at a distance of 0.13 m. Peace River heavy oil and Athabasca bitumen were used in these experiments. Experimental results showed that oil displacement occurs mainly by gravity drainage. Vigorous oxidation reactions were observed at the early stages near the heel of the injection well, where peak temperatures of about 550ºC to 690ºC were recorded. Produced oil from CAGD was upgraded by 6 and 2ºAPI for Peace River heavy oil and Athabasca bitumen respectively. Steady O2 consumption for both oil samples confirmed the stability of the process.

Experimental data showed that the distance between horizontal injection and production wells is very critical. Close vertical spacing has negative effect on the process as coke deposits plug the production well and stop the process prematurely.

CAGD was also laboratory tested as a follow-up process. For this reason, air was injected through dual parallel wells in a mature steam chamber. Laboratory results showed that the process can effectively create self-sustained combustion front in the previously steam-operated porous media. A maximum temperature of 617ºC was recorded, with cumulative oil recovery of 12% of original oil in place (OOIP). Post-experiment sand pack analysis indicated that in addition to sweeping the residual oil in the steam chamber, the combustion process created a hard coke shell around the boundaries. This hard shell isolated the steam chamber from the surrounding porous media and reduced the steam leakage.

A thermal simulator was used for history matching the laboratory data while capturing the main production mechanisms. Numerical analysis showed very good agreement between predicted and experimental results in terms of fluid production rate, combustion temperature and produced gas composition. The validated simulation model was used to compare the performance of the CAGD process to other practiced thermal recovery methods like steam assistance gravity drainage (SAGD) and toe to heel air injection (THAI). Laboratory results showed that CAGD has the lowest cumulative energy-to-oil ratio while its oil production rate is comparable to SAGD.

DEDICATION

To my family

ACKNOWLEDGEMENTS

I would like to thank my committee chair, Dr. Barrufet, and my committee members, Dr. Lane, Dr. Schubert and Dr. Sun, for their guidance and support throughout the course of this research.

I would like to express heartfelt gratitude to Dr. Mamora for his support and guidance through my study at Texas A&M University in the Department of Petroleum Engineering.

Thanks also go to my friends and colleagues and the department faculty and staff for making my time at Texas A&M University a great experience. I also want to extend my gratitude to the Crisman Petroleum Research Institute for supporting this project.

NOMENCLATURE

HTO	high temperature oxidation
LTO	low temperature oxidation
H	thickness of the model or prototype, m
w	width of the model or prototype, m
X_1, X_2, X_3	cartesian coordinates, m
ϕ	porosity, %
K	permeability, D
t	time, hr
ΔP	pressure difference between injection and production well, kpa
P_{inj}	injection pressure, kpa
P_{sc}	atmospheric pressure, kpa
μ	viscosity, cp
So	oil saturation, %
Sg	gas saturation, %
Sw	water saturation, %
β	scaling ratio
C	thermal heat capacity, kJ/(kg K)
$\overline{K}$	thermal conductivity, W/ (m. K)
ρ	density, Kg/m^3
α	thermal diffusivity, m^2/hr.

T_{In}	temperature at the inner surface, °C
T_{Out}	temperature at the outer surface, °C
ΔT	temperature difference across the inner surface of insulation, °C
$h_{Insulation}$	inner insulation thickness, m
L	vertical well spacing, m
E	energy. KJ
V	volume, m^3
OOIP	original oil in place
THAI	toe-to-heel air injection
SAGD	steam assisted gravity drainage
CAGD	combustion assisted gravity drainage

TABLE OF CONTENTS

Page

LIST OF FIGURES

LIST OF TABLES

1. INTRODUCTION

1.1 In-Situ Combustion

In-situ combustion (ISC) is an effective thermal recovery process that provides a promising alternative to the steam-injection methods. However, the conventional ISC process has many apparent failures, which are mainly related to inappropriate reservoir application and instability issues. Operational difficulties like gravity segregation, air channeling, unfavorable air-to-oil ratio and low sweep efficiency affect the performance of ISC. Horizontal well air injection is a promising concept which attempts to overcome the problems that make ISC challenging through positioning of horizontal wells.

Application of horizontal wells for ISC operations brings new advantages by providing a larger contact area between the formation and combustion front. Also, mobilized oil does not necessarily pass through the cold oil bank to reach to the production well. Combustion assisted gravity drainage (CAGD) is an integrated horizontal well air injection process for in-situ recovery and upgrading of heavy oil and tar sands bitumen. Short-distance air injection and direct mobilized oil production are the main features of this process that lead to stable sweep and high oil recovery. In this well configuration, vertical well distance is about 19 m in the field, which corresponds to 13 cm of laboratory scale. These characteristics identify CAGD as a high-potential oil recovery method for either primary production or as a follow-up process in a reservoir that has been partially depleted by cold production or steam injection.

The CAGD process combines the advantages of both gravity drainage and the conventional ISC. The combustion front initiates along the horizontal injection well and

develops in lateral and vertical directions as the process continues. The combustion chamber consists of the flue gases, injected air, and hot oil. Gravity drainage is the main mechanism for the mobilized oil production and extracting the flue gases from the reservoir. Fig. 1 shows the concept of the CAGD process. In this well configuration a horizontal injector is drilled in the upper section of the formation, with a horizontal producer in the bottom section. The combustion front initiates near the heel of injection well and develops in the lateral and forward directions. Generated heat increases the temperature of the adjacent crude oil. Mobilized oil drains through the production well by gravity drainage.

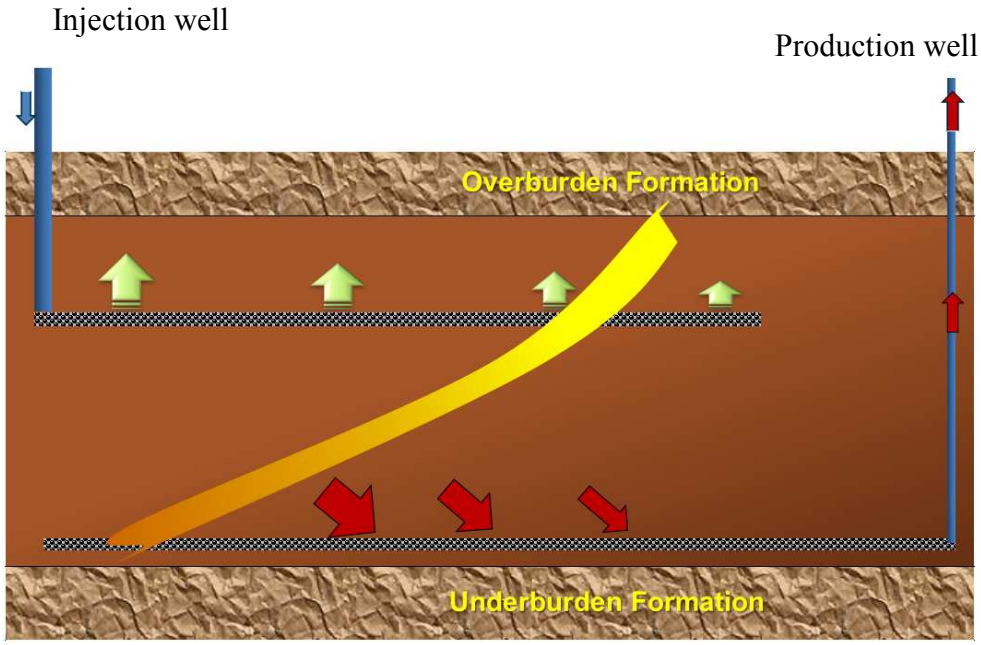

Fig. 1- Schematic diagram of CAGD process. Short-distance air injection and direct mobilized oil production are the main features of this process that lead to stable sweep and high oil recovery.

The main research objectives of this study were to conduct laboratory experiments using a scaled 3D cell and numerical study to investigate the oil recovery

mechanisms and feasibility of this process. Two oil samples of Peace River and Athabasca heavy oil were tested in this study. This research was divided into two main stages of experimental and simulation phases.

A 3D combustion cell with dimensions of 0.62 m, 0.41 m, and 0.15 m was designed to study the CAGD process. The combustion cell was fitted with 48 thermocouples. A horizontal producer was placed near the base of the model, with a horizontal injector in the upper part. Different vertical well spacings of far distance and close distance were investigated. Moreover, the effect of operating conditions such as preheating period, injected gas composition and oxygen partial pressure were studied. Also, CAGD process was tested in a mature SAGD chamber as a follow-up process.

In the simulation phase, a commercial thermal simulator (CMG STARS^{TM}) was used for the numerical study. The simulation model was based on the physical properties of the laboratory cell and used for history matching of experimental data. In addition, the validated numerical model was used for comparison of CAGD performance with other thermal processes like toe to heel air injection (THAI) and steam assistance gravity drainage (SAGD) at the field scale.

2. LITERATURE REVIEW

In-situ combustion (ISC) has been recognized for many years as a high-potential thermal process for recovery of heavy oil and bitumen deposits. This process has been extensively investigated at both laboratory and field scale. Several pilot projects have been tested since 1933. Technically, ISC is a gas injection process which causes heat wave propagation inside the porous medium. This heat front and produced gases enhance oil production (Hascakir et al., 2011; Turta and Bhattacharya, 2005). The combustion front develops by continuous air injection through the reservoir. The ISC operation begins with preheating the injection well perforations using a downhole electrical heater or chemical reactions (Abuhesa and Hughes, 2009; Nasr and Ayodele, 2005). When the target temperature is recorded at the formation sandface, air is injected. In some cases auto ignition has been reported, especially when the initial reservoir temperature exceeds 80°C (Abuhesa and Hughes, 2009). Despite extensive laboratory investigation and the promises of this technique for challenging environments, many field application of this process have failed. These operational difficulties are generally associated with unfavorable gas gravity segregation, low sweep efficiency, and poor directional control of combustion front movement (Bhattacharya and Chattopadhyay, 2007; Carcoana, 1990; Gates and Sklar, 1971).

2.1 Conventional in-situ combustion

In the conventional ISC process, air is injected through a vertical injection well surrounded by a number of production wells. In this way, combustion initiates near a

central injector and in an ideal case, it uniformly sweeps the pattern volume toward the production wells. However, the gravity override of the displacing gases causes the combustion front to move unevenly in the vertical direction reducing total sweep efficiency as the displacing gases flows preferentially to one well of the pattern. Another problem that is frequently encountered is the presence of a cold oil bank in front of the mobilized oil (Fig. 2). The well configuration of a conventional ISC process requires the mobilized oil ahead of the combustion front to pass through the colder, immobile oil. This can cause other problems such as crude oil mobility reduction and injectivity issues (Coates et al., 1995).

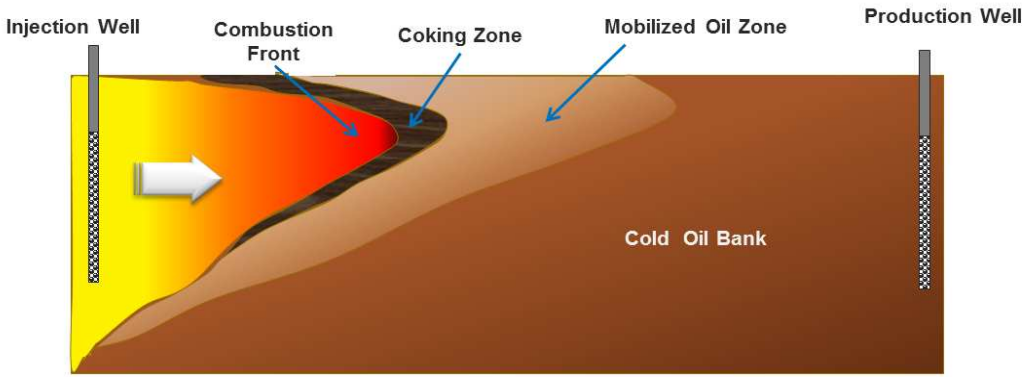

Fig. 2- Schematic of in-situ combustion using vertical wells. Operational difficulties like gravity segregation, air channeling, unfavorable air-to-oil ratio and low sweep are the main challenges of the ISC process.

Most laboratory studies of the ISC process have been conducted using a 1D combustion tube. This physical setup can be used for sensitivity analysis and investigating the performance of combustion reactions, but it will not provide information on either areal or vertical sweep (Akin et al., 2000). Garon et al. (1986a, 1986b) conducted a series of ISC experiments by using a 3D scaled laboratory model. Two vertical wells were used as the injector and producer. Investigated of the sweep

efficiency of dry and wet combustion demonstrated the application of 3D laboratory models for a better understanding the basics of combustion and the effect of various injection and production parameters. Akin et al. (2000) conducted a series of in-situ combustion experiment by a 3D semi-scaled laboratory model and concluded that a vertical injector and horizontal producers shows better efficiency compared to vertical well configurations.

2.2 In-situ upgrading

Several research projects have been conducted to improve the ISC process. Hydrogen donors and catalysts have received enormous interest over the past few years.

Ovalles et al. (2001) tested downhole upgrading of heavy oil using tetralin and pressurized methane in a batch reactor with natural formation as a catalyst. Experimental results highlighted the efficiency of this procedure in upgrading crude oil up to 4°API and 8% reduction in asphaltene content.

He et al. (2005) conducted a set of laboratory experiments to study the cation exchange between metallic salt and formation clay minerals in an effort to improve oxidation reactions. They concluded that this method improves the combustion reactions. Higher oxygen consumption and lower activation energy are the main advantages of this process. Experimental results also indicated that the presence of a catalyst improves coke deposition in porous media and results in efficient high temperature oxidation (HTO) reactions. In other research, Ramirez et al. (2007) studied heavy oil upgrading in the presence of a catalyst for a Gulf of Mexico oil sample in a

combustion tube. Laboratory results showed stable front development and higher oil production rate. Nares and Schachat (2007) confirmed previous laboratory data. In their experiments, Gulf of Mexico heavy crude oil with 12.5 °API gravity was mixed with 500 ppm of Al_2O_3 in a batch reactor. The experiment was conducted at a high temperature of 270°C. Experimental data showed an increase in API gravity and reduction in sulfur and metal content in the produced oil samples.

Later on, Cristofari et al. (2008) tried to analyze the feasibility of solvent injection along with in-situ combustion. They used Hamaca and West Sak oil samples. A mixture of pentane and n-decane was used as a solvent in the first stage of the experiment. Results demonstrated the effectiveness of this procedure where the Hamaca oil sample showed better oxidation reaction characteristics and the West Sak crude oil sample had more stable combustion. Solvent injection changed the initial crude oil composition and extracted the lighter components of the crude oil. Then the follow-up ISC process burned the heavy residue and generated higher energy.

One of the main problems associated with application of the ISC process in heavy oil reservoirs is the low initial mobility of crude oil. This issue could cause severe operational problems and affect the stability of the ISC. Ramirez et al. (2008) focused on this issue and proposed to use a nickel catalyst and tetralin (150 ppm in liquid phase) along with air injection. In this study they used a relatively low-density oil sample (12.5° API) from the Gulf of Mexico mixed with 40-US-mesh crushed dolomite carbonate and packed inside the combustion tube. They aimed to increase the oil mobility and enhance the oxidation reactions of crude oil during combustion. Experiments with nickel ionic

solution as a catalyst showed faster oil production and more stable and efficient combustion than the experiment without a catalyst. These results imply that using a low-concentration nickel ionic solution resulted in higher recovery factor and oil upgrading. Recently, Mohammad and Mamora (2008) conducted a laboratory study on the applicability of in-situ upgrading of heavy crude oil by using a mixture of tetralin and an organometallic catalyst. Tetralin increased oil recovery by 15% and the catalyst enhanced the ultimate oil recovery by 20%.

2.3 Wet combustion

In dry air injection, a significant portion of the generated heat accumulates behind the combustion front. One alternative approach is wet combustion. In this method, water is injected along with air and the goal is to recover a portion of the accumulated heat behind the oxidation zone and transfer it into the zone ahead of the combustion front. In this process, the air requirement also decreases with the reduction in the residual oil on the surface of the grains. Several research projects (Chien et al., 1976; Joseph and Pusch, 1980) have evaluated the mechanism of wet combustion to find the most important parameters for optimum water/air co injection rate. Excess water injection can have a negative effect on oxidation reaction by decreasing the partial pressure of the oxygen in the combustion zone (Lapene et al., 2009).

Shokoya et al. (2002) classified wet combustion as normal-wet and super-wet combustion based on the ratio of injected air and water. In normal-wet combustion the average combustion front temperature is about 600°C. The front temperature declines as

combustion moves away from the injection well. In super-wet combustion, the front temperature is much lower (about 250°C) because of higher injected-water/air ratio. The driving mechanisms in wet combustion are ISC, steam, and hot water. However, in dry combustion, air and flue gases are the displacement forces.

2.4 Horizontal production well air injection

Kisman and Lau. (1994a, 1994b) came up with a novel well arrangement for ISC. They proposed to use lateral wells to vent flue gases out of the reservoir. Their COSH process (combustion override split production horizontal well) uses a series of vertical wells for air injection. Flue gases are produced by vertical or horizontal wells that are drilled far away from the injection point. Also, mobilized oil and condensates drain through a bottom horizontal production well. Gravity drainage stabilizes the combustion front development along the production well. The COSH process allows gases and liquids to be produced separately through different wells and maintains control of the process as it evolves. Fig. 3 shows different parts of this method including a section of the formation with air-injection, gas-production, and oil production wells.

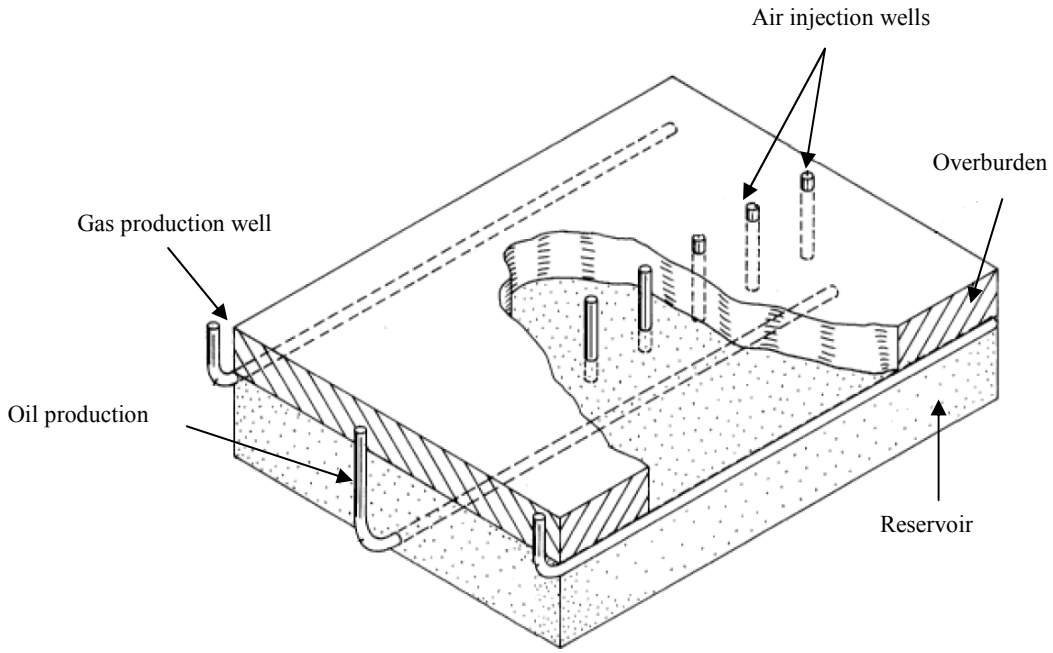

Fig. 3- Schematic view of COSH well configuration. This method allows gases and liquids to be produced separately through different wells and maintains control on the process.

2.5 Toe-to-heel air injection

Toe-to-heel air injection (THAI) is a relatively new, close-distance oil displacement process that results in stable combustion process with ability to produce mobilized oil directly into a section of the horizontal producer. (Ayasse et al., 2005; Greaves and Al-Honi, 2000; Greaves and Al-Shamali, 1996; Greaves et al., 1993; Greaves et al., 2005; Xia et al., 2003). THAI process uses the advantages of horizontal production and vertical injection wells. The process is based on gravity drainage and short distance oil production. Therefore, it avoids some conventional ISC problems. Fig. 4 is a schematics of THAI well configuration. At early stages of the process, steam is circulated in the wells to establish thermal and pressure communication. Heating up the injector and the follow-up air injection creates a combustion front around the heel

portion of the horizontal producer. The combustion front is more developed in the upper layer inside the formation, and mobilized oil drains vertically into the production well by gravity forces.

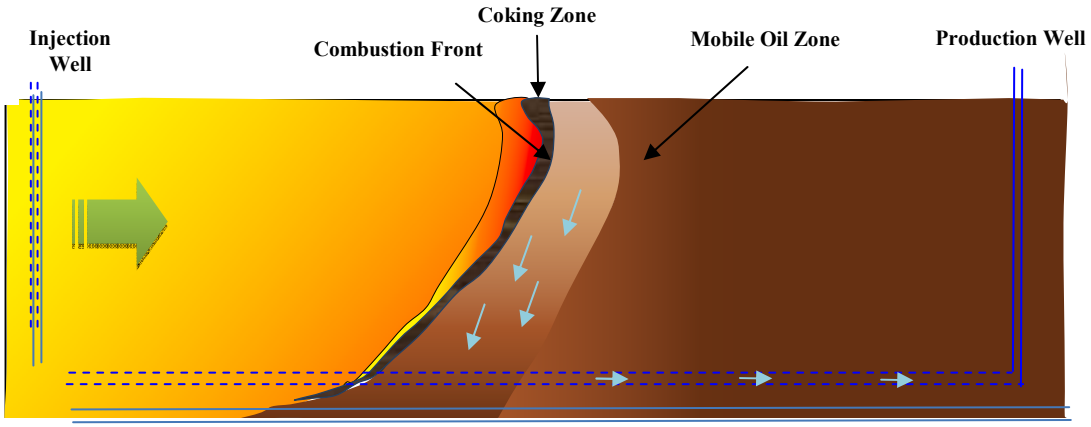

Fig. 4-THAI well configuration. THIA is a close-distance oil displacement process that results in stable combustion process with ability to produce mobilized oil directly into a section of the horizontal producer.

A THAI pilot test was started in the McMurray formation of the Athabasca oil sands in 2005 (Ayasse et al.). Three pairs of vertical horizontal wells and 19 vertical observation wells were used for recovery of bitumen (Fig. 5). Air injection was started on the first pair in 2006 and two other well pairs were fired later in 2007. This pilot targeted the peak production rate of 600 BOD for each production well (Petrobank, 2009).

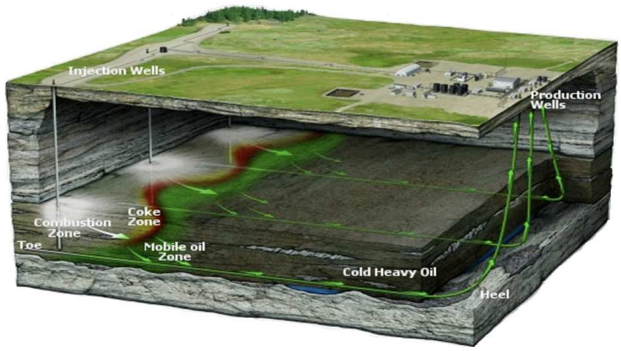

Fig. 5- White Sand THAI pilot test. This pilot targeted peak production rate of 95 m^3/day (600 bbl/day) per well (Petrobank, 2009).

2.6 Hybrid ISC-steam injection

The idea of air and water co injection has been studied for many years, and several papers and patents have presented different aspects of this process (Allen and Shum, 1976; Ayasse et al., 2002; Brown et al., 1985; Cram and D.A.Redford, 1978; Graue, 2001; Gussis, 1987; Horton and Brandt, 1995; Kisman et al., 1995; Leaute, 1994; Pebdani and Shu, 1986; 1990; Redford, 1978a, 1978b). This method in simple form can be described as wet injection in which a combination of oxygen and water is injected into the formation.

Allen and Shum (1976) proposed a technique in which superheated steam was injected into the formation followed by high pressure air injection. In later stages of the process, steam and air are injected at the same time to enhance the viscosity reduction of crude oil. Redford (1978a) patented an idea where water was injected into the post-ISC-operated formation to preserve the in-situ accumulated heat and transfer it to the upstream section of the reservoir. Redford (1978b) later patented a process where steam

was injected with air in cyclic periods. To optimize the procedure and the air to steam ratio Cram and Redford (1978) outlined a recovery process which focused on low-temperature oxidation by injection of a mixture of steam and oxygen. Brown et al. (1985) proposed to inject a sequence of high-quality steam, air, and water into the reservoir to create a steam chamber in the formation. Based on their results, wet combustion showed significant improvement over dry combustion, and the cost of the process was much lower than steam flooding. Graue et al. (2001) explained a method where steam and air were injected by continuous and cyclic modes. Venkatesan et al. (1988) reduced the viscosity of heavy oil by in-situ steam generation. In this method, combustion heat converted the injected water into the steam phase in the reservoir. At the beginning of the process, pressure and thermal communication between wells was established by steam injection. After that, high pressure air was injected through the reservoir and created combustion front behind the steam front. Oxygen reacted with the residual oil and generated heat, converted the water into steam. In an ideal case, the combustion front followed the steam front by controlling the air injection rate. In addition, flue gases moved in the upstream part of the formation and reduced the oil viscosity. Horizontal well air injection can also be used along with other thermal processes. Oskouei et al. (2010, 2011) confirmed the feasibility of starting the combustion process in a mature SAGD chamber. They used a semi scaled physical cell to show the performance of air injection through paired SAGD wells. Their experimental observations showed that the combustion front does not advance beyond steam boundaries, but it creates a continuous hard coke shell around the SAGD chamber. This

Shell minimizes steam leakage from adjacent steam chambers. Yang et al. (2009, 2008a, 2008b) simulated the feasibility of hybrid in-situ combustion and steam injection. They concluded that in addition to low overall energy consumption, the hybrid technique also reduces gas emissions. Nevertheless, the overall recovery of the hybrid process is lower than SAGD. Experimental data regarding feasibility of this hybrid technique has bot been addressed through the literature.

2.7 Simulation of combustion process

Thermal simulation is a promising tool for translating laboratory results to the field scale. The most important criterion in numerical simulation of the ISC process is oxidation kinetics. The high temperature gradient in the reservoir and the complex nature of fluids are the main obstacles to characterizing the kinetic parameters. Several researchers (Abu-Khamsin et al., 1988; Bae, 1977; Barzin et al., 2010; Dabbous and Fulton, 1974; Evans, 1937; Fassihi et al., 1984a, 1984b; Glatz et al., 2011; Lewis, 1967; Ren et al., 2007; Verkoczy and Jha, 1986; Vossoughi et al., 1982) have investigated kinetic parameters of oxidation reactions and rock and fluid property variation with respect to temperature.

Gutierrez et al. (2009) reviewed the challenges associated with simulation of ISC processes. They summarized the potential parameters in history matching of laboratory data like pressure drop, temperature profile, front location and heat losses. Grid-size sensitivity is one of the crucial factors, especially in the field-scale simulation. They indicated that combustion tube laboratory data cannot thoroughly represent the physics

and mechanism of fire flooding. They emphasized that other laboratory data related to the kinetic modeling such as kinetic cell, Thermo-gravimetric analysis (TGA), and differential scanning calorimetric (DSC) are necessary to have reliable and meaningful ISC simulation. The main difficulty with simulation of ISC processes is the modeling of the combustion reaction zone. This area is narrow and three main thermal reactions take place in this region: thermal cracking, Low temperature oxidation (LTO) and high temperature oxidation (HTO) (Bagci, 1998; Gerritsen et al., 2004; Thiez and Lemonnier, 1990). Thickness of combustion front has been addressed through several papers that suggested the combustion thickness is very narrow in comparison to drainage area and formation thickness (Fassihi et al., 1980; Kumar and Garon, 1991; Bagci, 1998). Bousaid and Ramey (1968) reported a combustion zone thickness of about 25 mm. Fassihi et al. (1980) observed 89- mm thickness using a combustion-tube experiment. Kumar and Garon (1991) estimated the combustion thickness at about 25 mm, and they also theorized that the specific surface area of porous media has a direct effect on combustion thickness: higher specific area results in larger combustion thickness. This was confirmed by Belgrave et al. (1990) where they came up with thicknesses of 70 to 100 mm based on combustion tube experiments for wet and dry combustion in low permeability pores media. They also concluded that the grid refinement is essential for ISC simulation to capture the combustion front thickness.

Another issue is the complexity of bitumen composition which requires the number of components to be lumped and reduced. However, lumping should be consistent with the reaction model. Some reports have addressed this issue regarding

characterization of bitumen based on soluble fractions. In this method, bitumen is lumped into the four main classes: saturates aromatics, resins and asphaltenes (SARA) (Adegbesan et al., 1987). Others (Jia et al., 2003 Belgrave et al., 1993b) used different names such as maltenes, asphaltenes, and coke. The properties of coke components are similar to carbon.

2.8 Kinetic modeling

The reaction kinetics of heavy oil is one of the complex parameters that are measured indirectly in the laboratory. Many parallel reactions occur at the same time and at different temperatures. Modeling all these reactions is not possible. Significant experimental studies have been conducted to present reliable and practical kinetic models that can be used directly through thermal simulators. Because of the complexity of the fluid composition and oxidation reactions, many researchers lump these reactions into three major groups:

Thermal cracking: includes cracking and visbreaking, which produces a solid phase on the surface of the sand grains. This solid phase (coke) is consumed by oxygen as fuel. The concentration of this residue depends on the heavy fraction (asphaltene and wax) of the crude oil sample.

Low temperature oxidation (LTO): is a heterogeneous reaction between gases and condensates which generates oxygenates hydrocarbons. In this phase, oxygen added to the structure of carbon-carbon increases oil viscosity and density. This stage of combustion occurs when sufficient oxygen is present at lower temperature (250°C to

350°C) like in front of a combustion front. Lower flue gas emission is one of the characteristics of this stage.

High temperature oxidation (HTO): includes heterogeneous reactions between gas and solid phases. It is the main source of heat generation in the ISC process, and it uses the deposited coke on the surface of grains as fuel. Dart et al. (1949) conducted extensive study on oxidation rate of carbonaceous residue in the presence of a clay catalyst. They concluded that the combustion reactions are first order in respect to partial pressure of oxygen and second order in respect to fuel concentration for carbon concentrations less than 2% by weight. In LTO, the oxygen is added to the hydrocarbon components and creates oxidized hydrocarbons which are ultimately converted to coke. On the other hand in HTO, all components of the original oil are broken by bond scission reactions and produce CO_2 and H_2O. HTO and LTO are dominant in certain temperature ranges: LTO occurs between 250 and 300°C and HTO between 350 and 800°C depending on the composition of the crude oil. At the combustion front, thermal cracking converts maltenes to asphaltenes and asphaltenes to coke. At the upstream section of the formation where oxygen concentration is low, LTO is the dominant reaction. On other hand, in high-temperature combustion zones HTO reactions are dominant and consume deposited coke and generate heat. At the downstream end, unburned coke, flue gases, and injected air are present.

Bousaid and Ramy (1968) studied the isothermal combustion of extracted coke from crude oil in a kinetic cell. They confirmed the results of previous researchers about effects of fuel concentration and oxygen partial pressure on the oxidation reactions. One

of the other kinetic parameters is the oxidation reaction rate, which is related to temperature by the Arrhenius equation. The fuel combustion rate, R_c, can be described as:

$$R_c = -\frac{dC_c}{dt} = kP_{O_2}{}^{m}C_c^n \quad \ldots\ldots\ldots\ldots\ldots\ldots\ldots\ldots\ldots\ldots\ldots\ldots\ldots\ldots\ldots \quad (1)$$

where k is the rate constant, P_{O_2} is the oxygen partial pressure, m and n are the reaction orders, and t is the reaction time. Rate constant, k is a function of temperature, and its dependency can be expressed by Eq. 2.

$$k = A\exp(-\frac{E_a}{RT}) \quad \ldots\ldots\ldots\ldots\ldots\ldots\ldots\ldots\ldots\ldots\ldots\ldots\ldots\ldots\ldots\ldots\ldots \quad (2)$$

where R is the universal gas constant, and E_a is the activation energy, and A is the Arrhenius constant. Fassihi et al. (1984a, 1984b) showed that in different temperature ranges oxidation reactions can be categorized into three distinct groups (cracking, LTO and HTO). Later on, Mamora et al. (1995) investigated the gas composition and mass changes during combustion process using a kinetic cell and estimated the temperature range of each of these dominant reaction groups. TGA and DSC are two useful tools for thermal analysis of the ISC process. TGA is based on mass changes of sample in the presence of oxygen or other gases and DSC is used for heat exchange between the sample and the outer environment. These two pieces of equipment can be used for estimation of the reaction heat.

Lin and Hanson (1991) used TGA technique for extracting the activation energy of coked sand's. They reported activation energy in the range of 127 to 148 kj/mol. Verkoczy et al. (1986) studied the thermo-oxidation of two heavy oil samples using both the TGA and the DSC methods. Later on, Coats and Redfern (1988) proposed a

mathematical model to calculate the kinetics based on laboratory data. They assumed a first-order reaction for coke oxidation. In another study, Vossoughi et al. (1982) developed a procedure for kinetics modeling of oxidation reactions using TGA/DSC. Their experimental results showed a very good match between laboratory data and predicted reaction rate. A review through literature shows more attention has been given to kinetic than to complete oil samples. This procedure reduces the level of complexity in the combustion modeling (Freitag and Verkoczy, 2006; Freitag and Verkoczy, 2005; Karacan and Mustafa, 1997; Ranjbar, 1995; Verkoczy and Freitag, 1997).

Several kinetic studies have been reported for Athabasca bitumen. Hayashitani et al. (1978) proposed using six pseudo components for modeling oxidation reactions. They used these lumped components in history matching of laboratory data, but they didn't address the importance of each of these pseudo components. In another study, Belgrave et al.(1993a) conducted 10 air-injection experiments using combustion tubes at high pressure. They concluded that the use of enriched oxygen cause instability in ISC with high coke load deposition at the surface of the grains. Later on, Dabbous and Elkins (1976) conducted a comprehensive study on Athabasca kinetic modeling. They showed that oxygen partial pressure has direct effects on both LTO and HTO. In their experiment they used a packed reactor with differential flow to distinguish the composition of produced gases. Also they showed the effect of steam on the partial pressure of oxygen. These results are useful for understanding the mechanism of wet combustion and the effect of water saturation on ISC processes. In another study, Jia et al. (2003, 2006) examined the compositional variation of Athabasca oil in the presence

of N_2 and air at different experimental condition. Crude oil properties such as density, viscosity, asphaltene content and coke deposition were tested for each case. They proposed a kinetic model for compositional variation of Athabasca bitumen under oxidation. Characterization of bitumen based on its solubility (SARA) is one of the most preferred procedures in the literature. However, it is not clear how reliable this method is in representing the reactions in the combustion process. Sequera and Marin (2007) studied this problem and concluded that for Athabasca oil sample, the SARA fraction gives a better description for LTO reactions. However, in combustion process, different sets of reaction occur, and capturing all of these reactions using SARA fractions is not feasible. In addition, using a larger set of components brings a significant level of uncertainty for simulators. These uncertainties are related to the properties of pseudo components and how they participate in the oxidation reactions. Also higher number of pseudo components makes it difficult to tune the simulator and increases the numerical convergence problems. No laboratory equipment is capable of providing fully detailed compositional variation during the combustion process. So a compromise between the number of lumped components and the reaction modeling should be an optimum solution. One of the most cited kinetic models for Athabasca bitumen is Belgrave (1990) model. Belgrave et al. (1993a, 1993b) documented detailed description of fluid and kinetic modeling of Athabasca oil sample. They reported the kinetic data, heat of reactions, pseudo components viscosity correlations, and fluid and rock properties. Based on this model, bitumen was characterized by three pseudo-components of maltenes, asphaltenes, and coke. In addition, they used other auxiliary components such

as water, oxygen methane, carbon dioxide, carbon monoxide, and nitrogen.

2.9 Field applications of ISC

Despite all challenges and operational difficulties of ISC process, several reports describe successful air injection processes (Chu, 1982). The following is a summary of successful ISC projects.

Sloss field, Kimball, Nebraska: Several pilot projects have been reported since 1963 and full field operation started in 1967. A combination of air injection and waterflooding were implemented in this field using five-spot patterns. One of the challenges in this field was igniting the injection wells as they were drilled in water-swept zones. For ignition, a downhole burner was used, and gas was injected at the surface as fuel. Low injectivity, corrosion and emulsion were the operational problems associated with this project. Economical constraints put an end to the project (Buxton and Pollock, 1974; Craig and Parrish, 1974; ParrishPollock and Craig Jr., 1974; Parrish et al., 1974; Popa, 1976).

May-Libby field, Delhi, Louisiana: this producing formation is in the Cretaceous age. The initial field production phase was solution-gas drive with original oil saturation of 70% followed by water injection which resulted in 44% oil recovery. Five-spot well patterns were considered for the injection /production configuration. A gas burner was used as an igniter at the sand face. In later stages of fire flooding, water slugs were added in addition to air. In total, 25,928 m^3 (163,084 bbl) oil was produced and 66.00e6 Sm^3 air was injected on a cumulative basis. Low air injectivity was reported as the

operational issue (Hardy et al., 1972).

Buffalo field, north edge of South Dakota: this is the longest fire flooding project. The air injection project was started in 1979 and continued until the present. The primary production mechanism was pressure depletion. Several improved oil recovery methods were tested, and ultimately air injection was selected based on economical considerations. A Horizontal well was used as the producer. By 2010, over 2.6 billion m^3 (18 billion bbl) oil was recovered from this field (Gutierrez et al., 2008; Gutierrez et al., 2007; Gutierrez et al., 2008; Kumar et al., 2010).

Marguerite Lake, Cold Lake, Canada: primarily, the field was underdeveloped by cyclic steam stimulation (CSS) since 1961 and later an air-injection process was implemented (Galas and Ejlogu, 1993; Hajdo et al., 1985; Hallam, 1991; Hallam et al., 1989). The first stage of the project consisted of three pilot tests of wet air injection. Later on the field was converted to five-spot patterns with an infill-drilled wet combustion. Fracturing of the formation appeared to assists in increasing injectivity and higher mobility of the original crude oil. In all wells, steam was injected with pressure higher than the formation fracturing pressure. Under steam injection, daily production reached near 1,272 m3 per day (8,000 bbl per day). The results of the pilot test were promising however, as Hallam et al., (1989) found that the formation heterogeneity prevented uniform development of the combustion front inside the reservoir. The presence of channels inside the formation was the main reason for the problems with controlling the combustion front. Pressure cycling, injection rate control, fracturing,

production rate control, and stimulations were the technical solutions for controlling the combustion front.

3. EXPERIMENTAL APPARATUS

3.1 Apparatus and procedure

The CAGD experimental apparatus is divided into five main parts, including: the Injection control panel, the CAGD cell, fluid production and data acquisition (Fig. 6). The following sections describe each of these main parts.

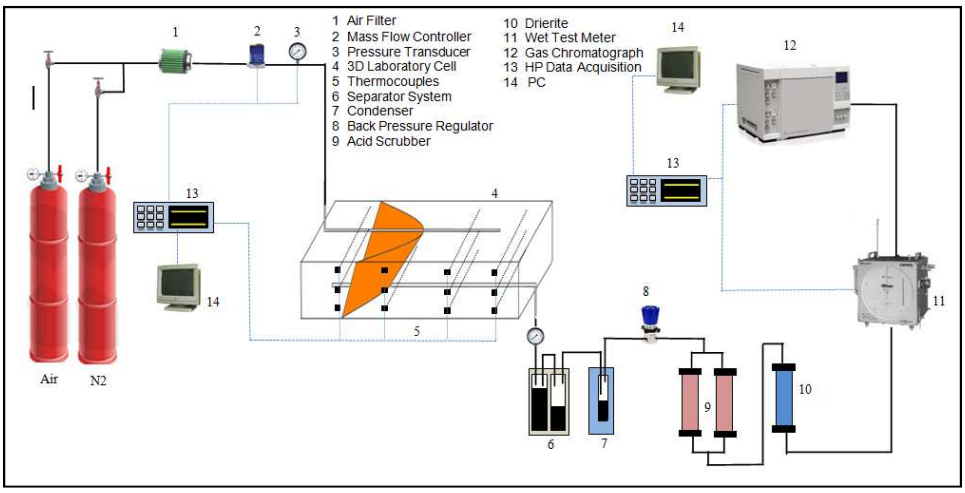

Fig. 6- Schematic view of the CAGD experimental setup. Injection control panel, CAGD cell, fluid production, data acquisition and gas chromatograph are the main parts of the laboratory setup.

3.1.1 Injection control panel

Different air injection rates were required to conduct the experiments. Injection rates was between 3 to 12 L/min. High pressure air cylinder was the source of air during the experiment. Also, a second air cylinder was reserved for cases were experiment might run out of air supply. The pressure control panel (Fig. 7) consisted of a mass flow controller, backpressure regulator, gauges and valves. This set of equipment controls the

injection and production schemes. Operational parameters such as injection pressure, injection rate, and production pressure were manually controlled.

At the end of the experiment, air injection was gradually decreased, followed by N_2 injection to flush the laboratory model and terminate the combustion reactions. Post-experiment N_2 injection last for 4 hours. In addition, N_2 was used for pressurizing the laboratory model before the start of the experiments.

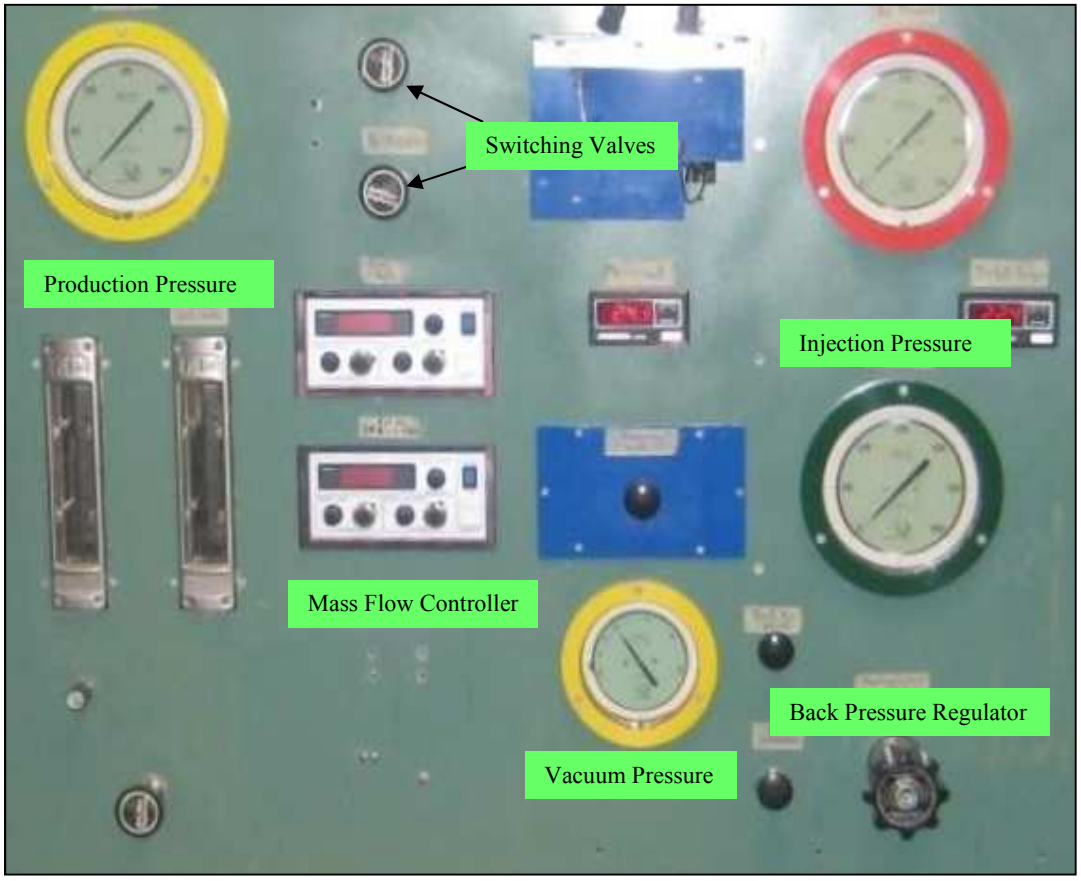

Fig. 7- An overview of the injection control panel. A mass flow controller was used for measuring and controlling the injection gas rate. In the production end a backpressure regulator was set up to maintain constant pressure inside the system.

3.1.2 3D laboratory cell

A rectangular stainless steel combustion cell with dimensions of 0.62 m length, 0.41 m width, and 0.15 m height was used to conduct the CAGD experiments. These were placed at the three different distances of 1.3, 5, and 11 cm from top of the cell. Fig. 8 shows the well configuration and well spacing inside the cell. The CAGD cell is shown in Fig. 9.

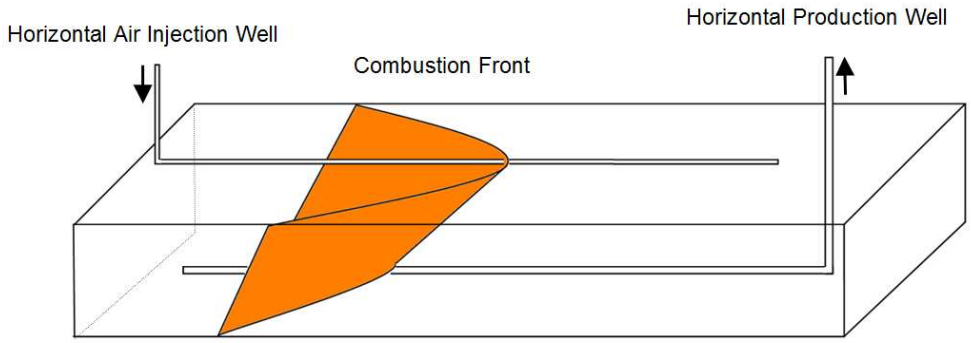

Fig. 8 - Concept of CAGD process. The combustion front initiates near the heel of injection well and follows the path of injector. Mobilized oil is drained to the lower horizontal producer.

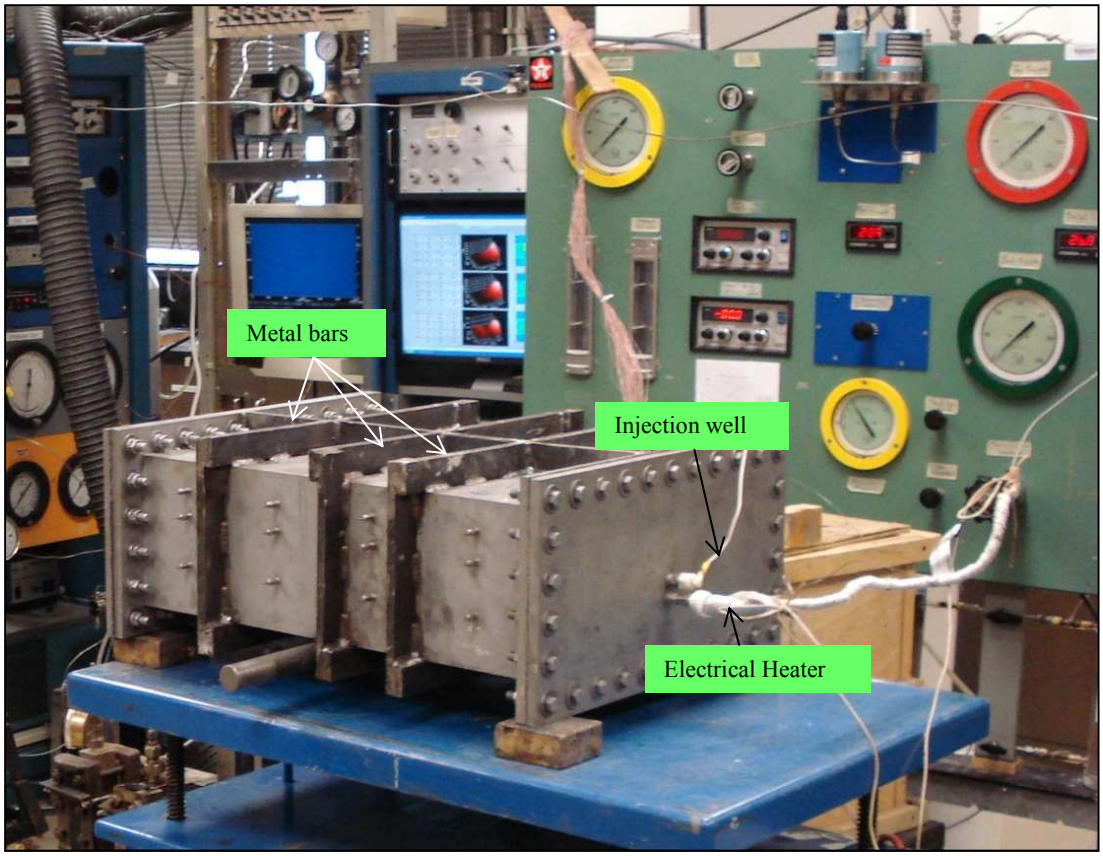

Fig. 9- The 3D CAGD cell, injection well and electrical heater. Metal bars were welded around the cell to increase the operating pressure of the cell up to 1723 kpa (250 psi).

3.1.3 Fluid production

The system's outlet pressure of the system was controlled by a backpressure regulator. This pressure was set at the beginning of the experiment. Production fluids were sampled through two visible stage separators. Samples were taken every 30 minutes. Samples volumes varied between 2 and 30 cc. The next step was to extract condensates from hot gases out of the separator. This was done by using condenser unit. Gases were scrubbed of acid (permanganate column) and dehydrated (calcium sulfite column) before flowing to the gas chromatograph (Fig. 10).

a) b)

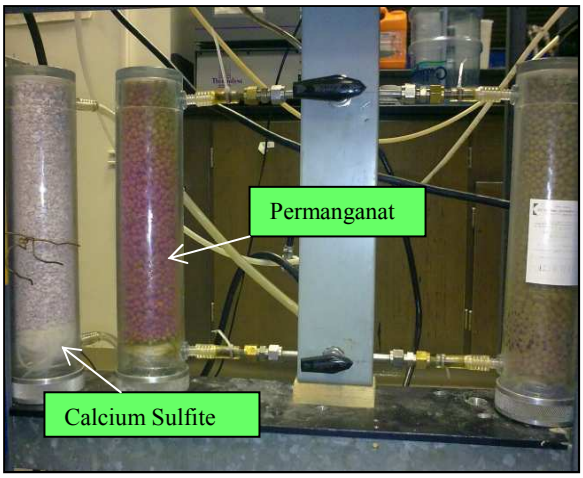

c)

Fig. 10- Production fluid system including; a) Two-stage separator, b) Ice condenser and c) gas dehydration columns

3.1.4 Gas chromatograph and wet test meter system

Scrubbed and dehydrated gas flowed to the wet test meter, where the volume of produced combustion gas was measured and recorded by using data logger/PC.

Produced gas was analyzed for carbon dioxide, oxygen, nitrogen, and carbon monoxide using an HP 5890 Series II gas chromatograph (Fig. 11). The rate of production gases, which ranges between 3 and 12 L/min was measured by using wet test meter equipment (Fig. 12).

Fig. 11- Laboratory gas chromatograph. Produced gas was analyzed for carbon dioxide, oxygen, nitrogen, and carbon monoxide.

Fig. 12- Wet test meter equipment.

3.1.5 Data acquisition

The following variables were recorded during each experiment; time, fluid injection rate, temperature, injection pressure, production pressure, gas production rate, and produced gas composition. These variables were recorded every 30 seconds. A LAB-VIEW program was developed for recording laboratory data during each run. Fig. 13 shows the interface of the LAB-VIEW program. Temperature measurements inside the sand pack were recorded by using an array of thermocouple rods inserted through the

porous media. The combustion cell was fitted with 48 thermocouples to measure the temperatures inside the model and to monitor the combustion front propagation. These thermocouple positioned in 12 thermo-well recorded the temperature profile inside the porous media. Fig. 14 and 15 describe the location of thermocouples inside the CAGD cell. Also, the rate of produced gas is recorded by using a HP data Logger (Fig. 16).

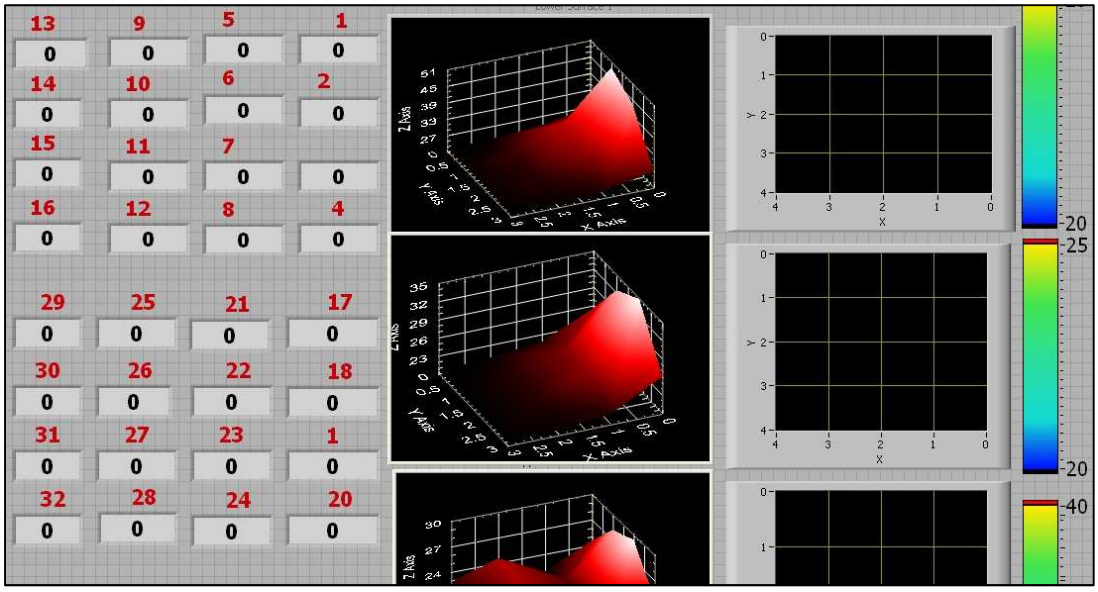

Fig. 13- Lab-view interface used for monitoring temperature of 48 thermocouples. These data were recorded every 20 seconds to have sufficiently refined temperature records.

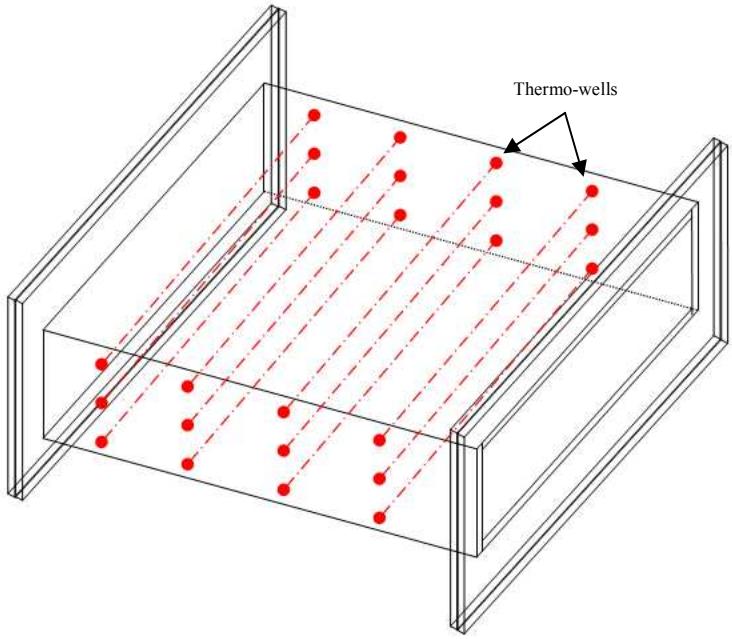

Fig. 14- Thermo-wells were fitted inside the model in 12 locations with 4 thermocouples in each thermo-well (48 thermocouples in total).

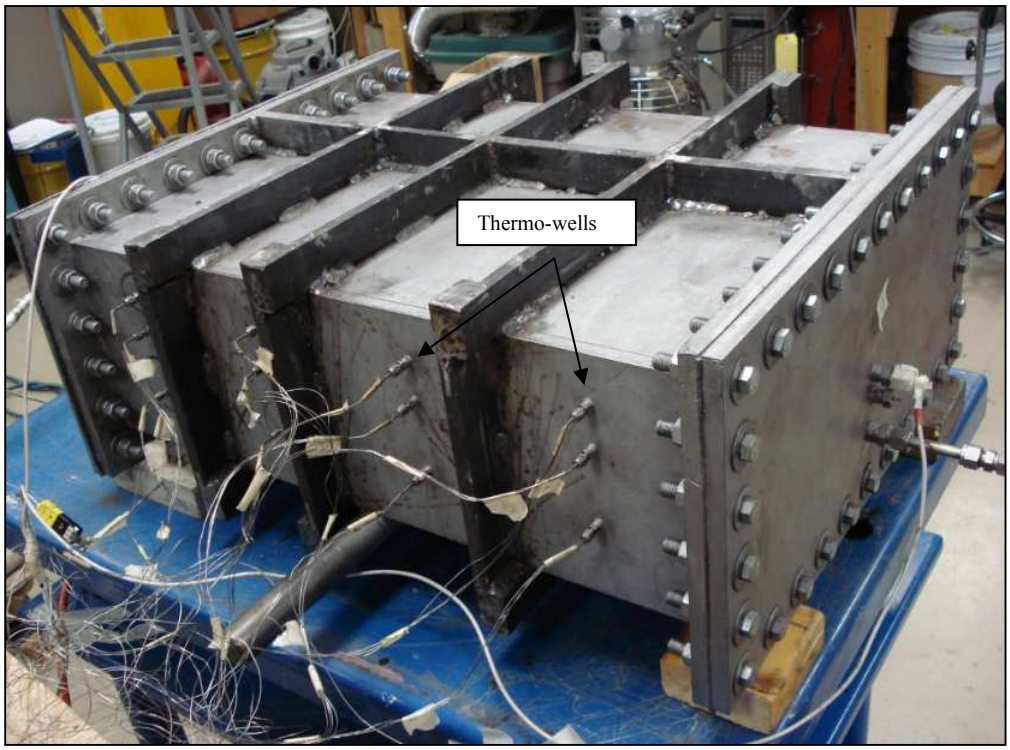

Fig. 15- A view of the thermo-wells inside the model. The location of the thermo-wells was designed in such a way that injection-well temperature could be closely monitored during the experiment.

Fig. 16- Production data logger. Cumulative gas production was recorded by using this data logger

3.2 Scaling

Table 1 presents the scaled conditions between the field prototype and the laboratory model according to the scaling methodology developed by Islam and Farouq Ali (1992). In this study field prototype properties are based on the Peace River heavy oil reservoir in Canada. The scaling technique ensures that the gravity drainage is the main recovery mechanism and also maintained the geometric similarity. However, scaling leads to unscaled variables such as relative permeability, fluid/solid interactions, and capillarity pressure. For very viscous crude oil in a high permeable formation, capillarity can be neglected. But in general satisfying all the scaling criteria is impossible. Therefore, some scaling parameters should be relaxed to honor others. Appendix A provides the detailed geometric and heat-loss scaling calculations.

Table 1: Field prototype and laboratory model parameters.

Reservoir Parameters	Prototype	Model
Width, m	72	0.41
Height of the Reservoir, m	27	0.15
Well Length, m	108	0.62
Permeability, D	5.23	942
Porosity (%)	19.5	39
Oil saturation	72	72
Water saturation	0	0
Gas saturation	28	28
Airflux, $m^3/(hr\text{-}m^2)$	0.71	0.71
Air injection rate, m^3/day	50,000	4.32
Reservoir temperature °C	30	30
Pressure drop, kpa	13.78 (2 psi)	2482 (360 psi)
Oil viscosity@ 25°C, cp	25,000	25,000 c
Oil density@ 25°C, ºAPI	9.15	9.15

3.3 Thermal insulation

The laboratory model was made of stainless steel, which has higher thermal conductivity than wet crushed sand (16 w/m.k vs. 2 w/m.k). This difference in thermal conductivity alters the temperature front movement in the model. In other words, generated heat at the combustion zone will be transferred to the downstream porous media through the cell body which causes an abnormal temperature rise in the sand pack. To minimize this issue, installing internal isolation was a necessity. The inside of the model was covered by a waterproof ceramic insulation with thermal conductivity of 1.13 KJ/Kg.K and 1.28-cm thickness. To have a nearly adiabatic condition at the preheating

stage of the experiment the outer surface of the cell was wrapped with four heating tapes connected to the computer-controlled electrical resistance. The goal was to accelerate the preheating period. The adiabatic condition was maintained during the preheating period, and band heaters were switched off as soon as the air injection was started. The preheating period is not scaled in this study.

The outer insulation consisted of a 2-cm thick ceramic fiber blanket wrapped around the cell. The outer insulation significantly reduced the preheating period. When the hot nitrogen was injected for preheating the injection well, the temperature was increased substantially and the maximum recorded temperature did not exceed 120ºC along the injection well. However, using electrical heater right above the injection well resulted in a faster preheating period and higher temperature up to 250ºC. Downhole heating devices are frequently used in ISC processes for starting the combustion (Baibakov et al. 1989). Similar approaches can be utilized in field application of the CAGD process to increase the temperature of the injection well. The electrical heater does not necessarily need to cover all the length of the horizontal injection well; it could be placed near the heel of injector. In laboratory experiments, the preheating period took about 4 hours, and the electrical heater was switched off after maximum temperature in the injection well reached near 357ºC. The setup was heated using band heaters up to 30°C, which is considered the initial reservoir temperature. Although the typical initial temperature of the target reservoir is about 16.7°C. Laboratory limitations prevented decreasing the temperature of physical model. However, based on oil viscosity dependency on temperature, oil has very low mobility at these two temperatures, and it

is a valid assumption that the initial temperature difference has negligible effect on the experimental results.

3.4 Experimental procedure

The 3D laboratory cell was packed with a heavy oil sample and crushed sand. The combustion cell packed in the vertical position beginning from the production side by tamping a thin layer of oil and sand. Thermo-wells were placed into the cell as packing progressed. During packing, the total weight of the sand, oil and water mixture was measured. High-temperature graphite sealant was used to seal both caps of the cell. Then, outer insulation was placed around the cell. Injection lines were connected for a pressure test. Laboratory cell was pressure-tested at 1723 kpa (250 psi) for 4 hours. N_2 is used for the pressure test, and after successful leakage inspection; the cell was depressurized to atmospheric conditions.

Before the start of the experiment, the mass flow-meter was calibrated for different injection rates. The gas chromatograph also was calibrated. This was done by using a standard gas calibration sample. The experiment was started by pressurizing the cell with N_2 up to 1378.9 kpa (200 psi). The voltage of the electrical heater was gradually increased using a variable power transformer. After 30 minutes it reached to it maximum output. The preheating stage took about 4 hours. During this time, the temperature profile inside the model was constantly monitored using LAB-VIEW program and N_2 was injected at a rate of 3 L/min to minimize the low-temperature oxidation on the sand grain surfaces. The backpressure regulator was adjusted to

maintain outlet pressure at 1378.9 kpa (200 psi). When the maximum temperature of the injection well reached 250°C, the injection stream switched to a low rate (3 L/min) of air. A sharp increase in the injection well temperature was a clear indication of ignition inside the model. At this stage the electrical heater was still powered on and air was continuously injected. After about 3 to 4 hours, the electrical heater was turned off and enriched air was injected at a predetermined rate. A second rise in the injection well temperature indicated the initiation of the combustion process.

Every 5 minutes a sample from the gas production line was flushed into the gas chromatograph to measure the composition of flue gases. Produced fluids were collected in pre-weighted glass flask bottles at regular time intervals. Once the production well temperatures outside of the cell exceeded 200°C, air injection was terminated and N_2 was injected for 4 hours. This killed the combustion and cooled down the system. The fluid samples were kept in an oven at a temperature of 50°C for 48 hours to remove the dissolved gases, and then water was separated by using a centrifuge.

4. EXPERIMENTAL RESULTS*

4.1 Experimental study

Five types of experiments were done in this research. Repeatability of each experiment has been confirmed. In all of these experiments crushed sand with 100 US mesh size was used for packing. The combustion process was tested for Athabasca as well as Peace River heavy oil. Table 2 and 3 summarize the packing information and experimental conditions for each run.

Vertical well spacing, initial crude oil viscosities, partial pressure of oxygen, and injection pressure were the variables that selected for this study. During each experiment, different properties were measured such as; oil recovery, air-to-oil ratio, fuel consumption, air requirement, location of the combustion front, temperature profile, combustion front velocity, oxygen consumption, and oil physical properties. Moreover, the recovered sand pack was analyzed to measure the volumetric sweep efficiency, shape of the coking zone and the residual oil saturation in unburned areas. In the following sections, each of these experimental runs is discussed and compared in detail.

* Part of the data reported in this section is reprinted with permission from "Dual Horizontal Well Air Injection Process" by Rahnema, H., Barrufet, M.A., Martinez, J.A., Paper SPE-153907 Presented at the Western Regional Meeting, 21-23 March, Bakersfield, California, Copyright 2012 by SPE and "Self-Sustained CAGD Combustion Front Development; Experimental and Numerical Observations" by Rahnema, H., and Mamora, D., Paper SPE-154333 Presented at the Improved Oil Recovery Symposium, Tulsa, Oklahoma. Copyright 2012 by SPE.

Table 2: Summary of packing data. In all of the experiments sandstone crushed sand was used for packing the laboratory model.

RUN NO.	1	2	3	4	5
Porosity	0.39	0.39	0.39	0.39	0.38
So,%	72	63	61	63	74
Sw,%	0	0	17	21	0
Sg,%	28	27	22	16	26

Table 3: Experimental specification, vertical well spacing, initial crude oil viscosities, partial pressure of oxygen and injection pressure were investigated through this research.

Run No.	1	2	3	4	5
Vertical well Spacing, m	0.03	0.13	0.13	0.13	0.13
Injection Pressure, kpa	345 (50 psi)	345 (50 psi)	1379 (200 psi)	1379 (200 psi)	1379 (200 psi)
Permeability, md	5,230	5,230	5,230	5,230	5,230
Porosity, %	39	40	38	39	41
Preheating, hr	4	6.8	7.1	5.6	5
Injection Gas, O_2 Mole fraction,%	100	100	50	50	50
Injection Gas, N_2 Mole fraction,%	100	100	50	50	50
Oil Sample	Peace River	Peace River	Peace River	Athabasca	Peace River
Oil Viscosity@ 25°C, cp	24,800	24,800	24,800	27000**	24,800
Oil Density@ 25°C ,°API	9.15	9.15	9.15	9.15	8.24**
Injection rate, L/min	3	2.5	3	3	10

** This value measured at 60 °C

4.2 Results and discussion

4.2.1 Run 1

In this experiment the vertical distance between pair wells was 3 cm, corresponding to 5 m at the field scale, similar to typical SAGD process. Fig. 17 shows the schematic of combustion cell and location of horizontal wells.

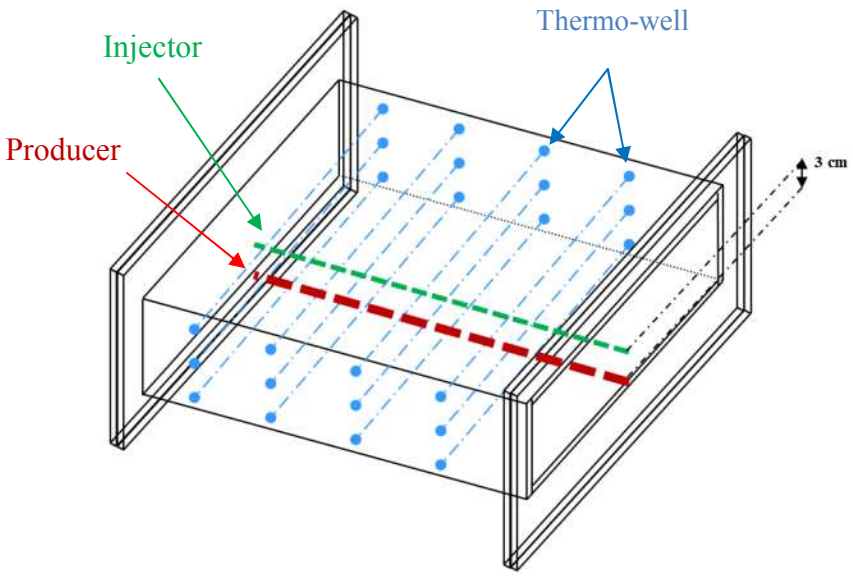

Fig. 17- 3D combustion cell and location of horizontal wells. The well configuration is similar to the SAGD process. Vertical well spacing corresponds to 5 m in the field scale (Run 1)

Fig. 18 shows the maximum recorded temperature along the injection well and the composition of the flue gases. The temperature data shows that a self-sustained combustion front was achieved for about 2 hours and then its temperature gradually declined until it dropped below 200ºC. This observation indicated a failure in combustion reactions at later stages of the experiment. This might indicate the lake of

sufficient oxygen at the combustion zone. To investigate this possibility, the same experiment was repeated using enriched air (50% O_2) and pure oxygen (100% O_2). However, similar results were observed in these experiments, too.

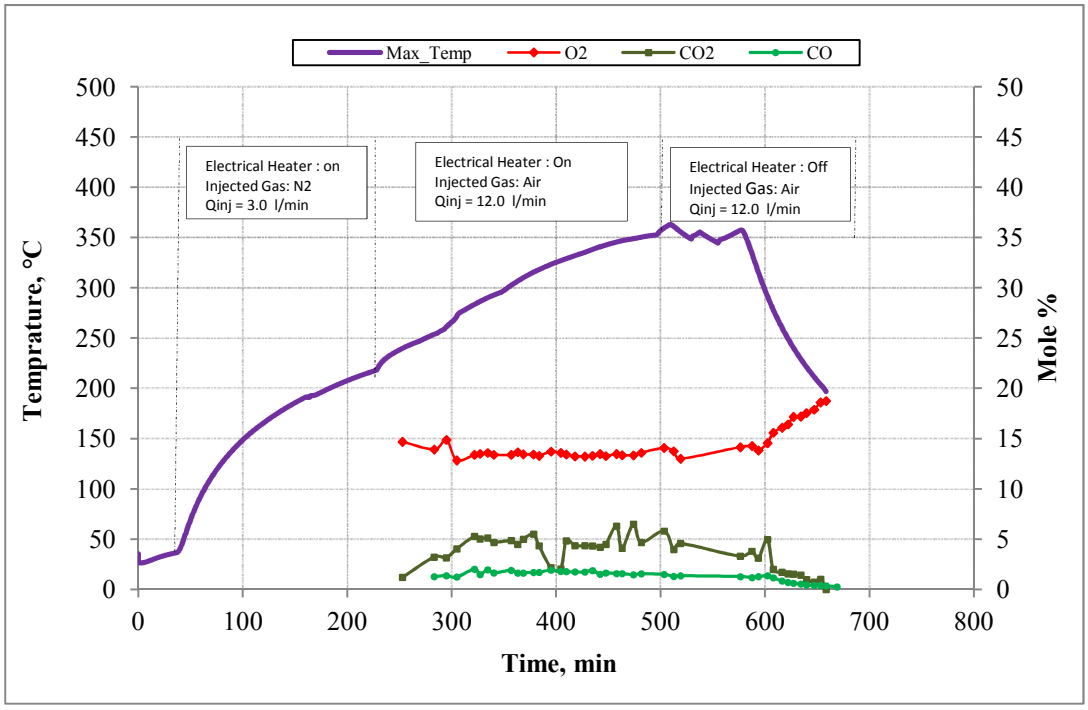

Fig. 18- Maximum temperature along injection well and produced gas composition. Self-sustained combustion front was achieved for about 2 hours and then its temperature gradually declined until it dropped below 200°C at 680 minutes (Run 1)

Fig. 19 shows a post-experiment analysis of the sand pack at the inlet face of the laboratory model. The electrical heater was right above the injection well. The injection well was a little bent when the cell was opened. The electrical heater was touching the injector all along the length of the model. A cylindrical coke layer with thickness of about 3 cm was observed around the injector. Clear sand inside the cylindrical coke zone indicated that good ignition was achieved at early time. However, the shape of the deposited coke showed that when the combustion front developed, a layer of coke

reached to the production well, and plugged the producer and terminated the process. This is consistent with experimental observation, which showed zero oil production rates near the end of the experiment.

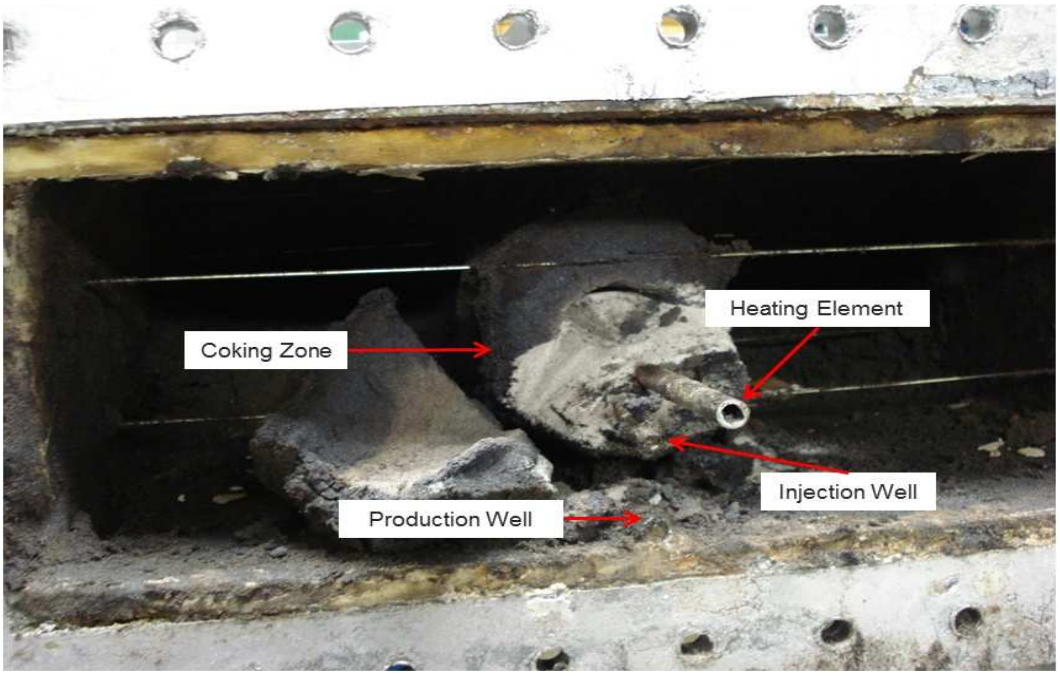

Fig. 19- Post-experiment sand-pack analysis. A cylindrical shape coke zone with thickness of about 3 cm formed around injector and the electrical heart. (Run 1)

In close-spaced horizontal well air injection (Run 1), coke deposition created a major problem and plugged the production well. Coke deposition is unavoidable in a combustion process and it occurs on the sand grain surface. Coke is generated from thermal cracking of the heavy oil. In front of the combustion zone, crude oil is heated by conduction and in the absence of oxygen, a series of thermal cracking reactions convert the heavy fractions of crude oil into coke. This solid carbon forms on sand grain surfaces

and then reacts with oxygen at the combustion zone. To develop a self-sustained combustion front, oxygen must pass through the deposited coke layer.

In the close-spaced experiment, combustion occurred while the coke layer was between the injector and producer, but when coke reached the producer all injected oxygen bypass the production well and did not react with the fuel (coke). In fact, in this type of well configuration, coke deposition caused two major problems that stopped the process: restriction of air circulation in the limited area between the injector and producer and plugging of the production well. In the next experiment, these two major problems were resolved by moving the injection well to the top of the model. Similar result can be expected in the field operations, when vertical well spacing is 5 meter (SGAD well spacing). But CAGD process is not feasible as a primary production method with close vertical well spacing.

4.2.2 Run 2

To study the effect of larger vertical well spacing on CAGD process and to minimize the problems related to the coke layer development, the horizontal injection well was moved to the top of the laboratory cell with 13 cm distance from the production well (Fig. 20)

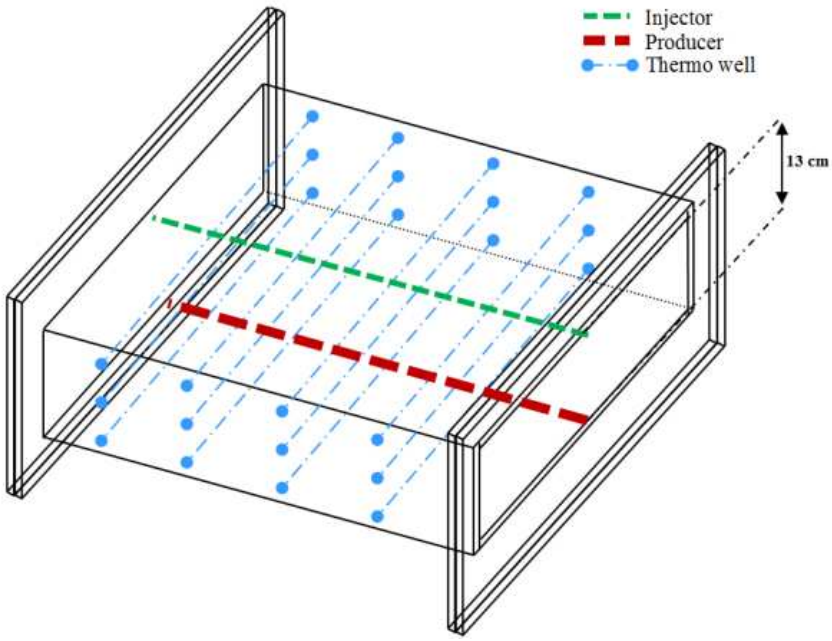

Fig. 20- 3D combustion cell and location of horizontal pair well. (Run 2)

Early preheating provided vertical communication between the injector and producer. Produced gas composition indicated that the injected gas circulated inside the combustion chamber and reacted with the coke deposits. Combustion gases (flue gases) and hot oil drained to the production well. Air was not a suitable gas for injection due to its low operating pressure of 345 kpa (50 psi). To ensure a combustion reaction would take places after turning off the electrical heater, pure oxygen was selected as injection gas. In this way the partial pressure of oxygen was high enough to create a self-sustained combustion front.

Fig. 21 shows the temperature along the injection well at four different points after the start of the experiment. Preheating took about 5 hours. After switching to pure O_2, the combustion began and the maximum-recorded temperatures increased to about

620°C near the heel position of horizontal injection well. The combustion front propagation stabilized when the electrical heater was turned off and thereafter it was self-sustained during rest of the experiment. Clearly, the combustion occurred near the heel of the injection well and most of the injected O_2 was consumed in this area. Fig. 22 shows the produced gas composition of far-spaced experiment. Most of the produced gas consisted of CO and CO_2, confirming the effectiveness of the combustion performance. For safety, the experiment was stopped after the combustion front reached near 15 cm of the production side.

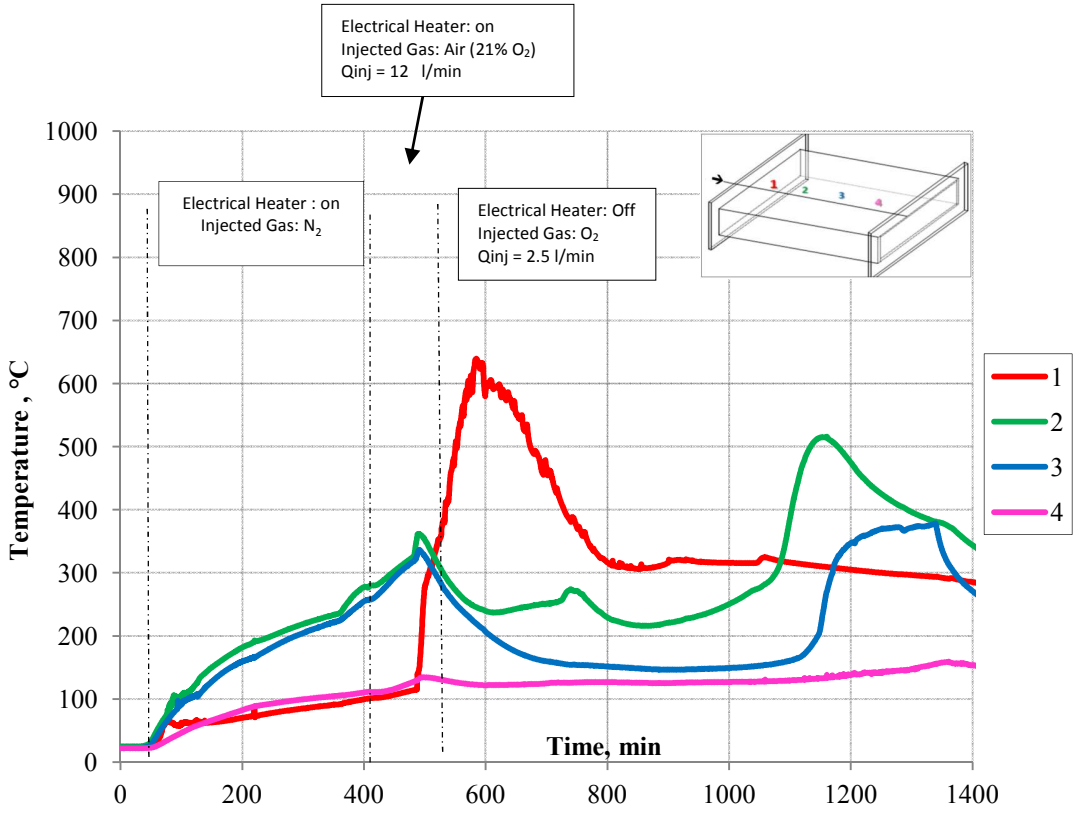

Fig. 21- Temperature vs. time along injection well of four different locations. After switching to pure O_2, the combustion began and the maximum-recorded temperatures increased to about 620°C near the heel position of horizontal injection well. Combustion front moved along the injector. (Run2)

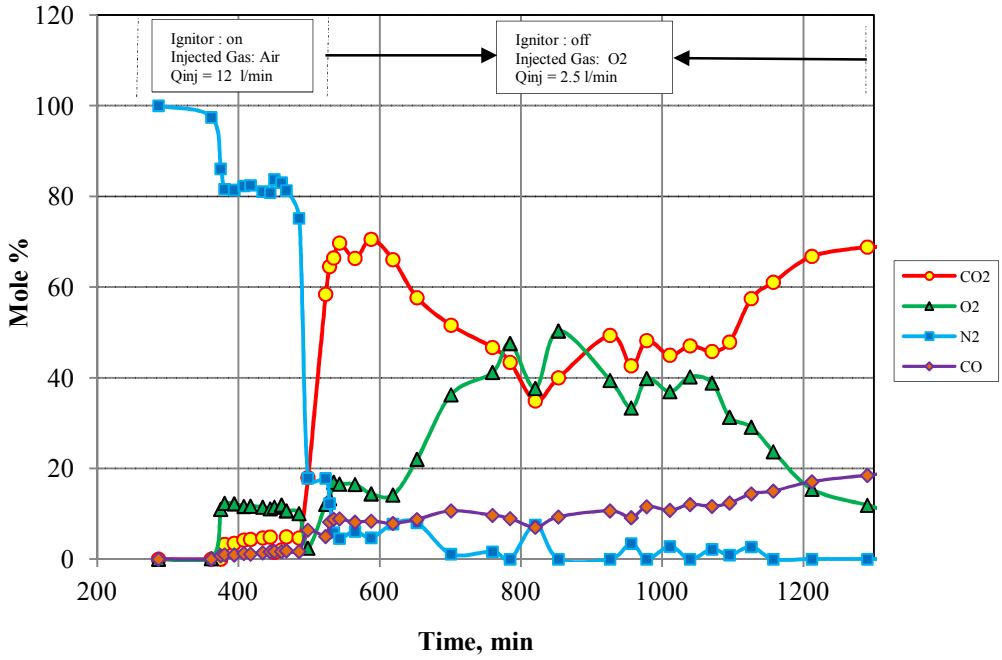

Fig. 22- Produced gas composition vs. time. Most of the produced gas consisted of CO and CO_2, confirming the effectiveness of the combustion performance. (Run 2)

Fig. 23 depicts the temperature profile inside the model at different snapshots. The temperature of the points between the thermocouples was interpolated by using a Kriging interpolation scheme. The selected temperature surface of 350°C demonstrates propagation of the combustion chamber in the cell. After combustion was initiated (at about 580 minutes), combustion chambers developed in both the lateral and forward directions with temperature of about 620°C.

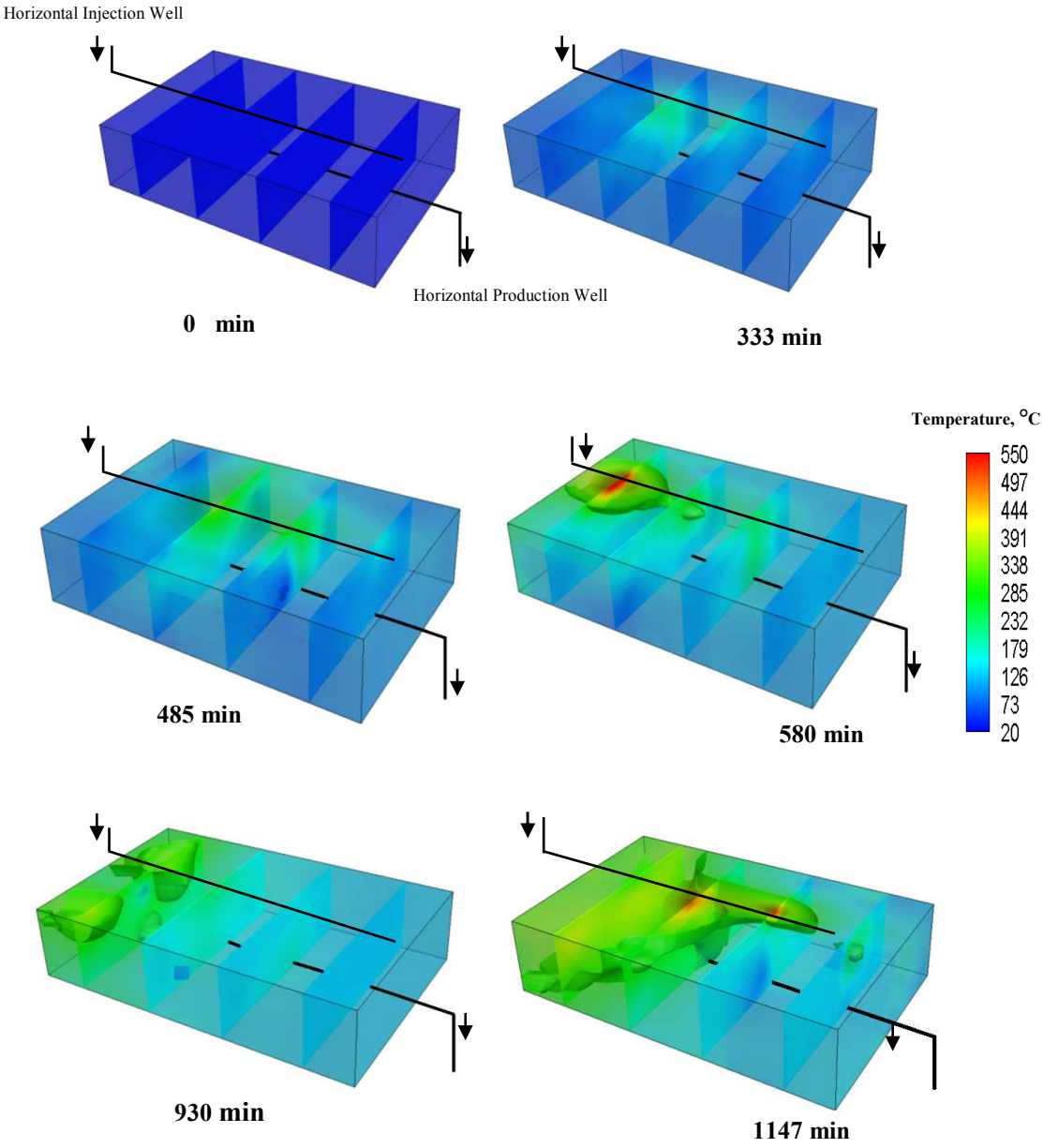

Fig. 23- Iso-surface temperature of 350°C demonstrates the propagation of the combustion front. (Run 2)

High volumetric sweep is shown by the post-experiment analysis of the combusted sands (Fig. 24). Based on this picture, porous media is divided into three main parts;

Clean sand: The burned part of the coke zone, which is completely saturated with gases and is visible as clean sand.

Coke zone: Hard, dark shell, which has lower permeability. The coke zone occupied half of the area near the heel of injector. Coke zone formed around the horizontal injection well and its concentration declined toward toe section of the well.

Unburned area: Oil saturation in the area near the toe of production well was not completely drained and less affected by combustion heat. This suggests that the heat conduction to these areas can be enhanced by using wet combustion.

Increasing the vertical spacing not only eliminated the coke-plugging problems, but the coke layer also created a gas seal inside the cell. That is the coke deposits formed a seal layer between the injector and the producer and improved the circulation of the injected oxygen in the combustion chamber. Based on the front temperature and the oil properties, the gas seal may be partial or total, but is more developed near the toe of production well. Coke formation is a dynamic process and involves formation ahead of the combustion front, and then burning as the combustion front approaches.

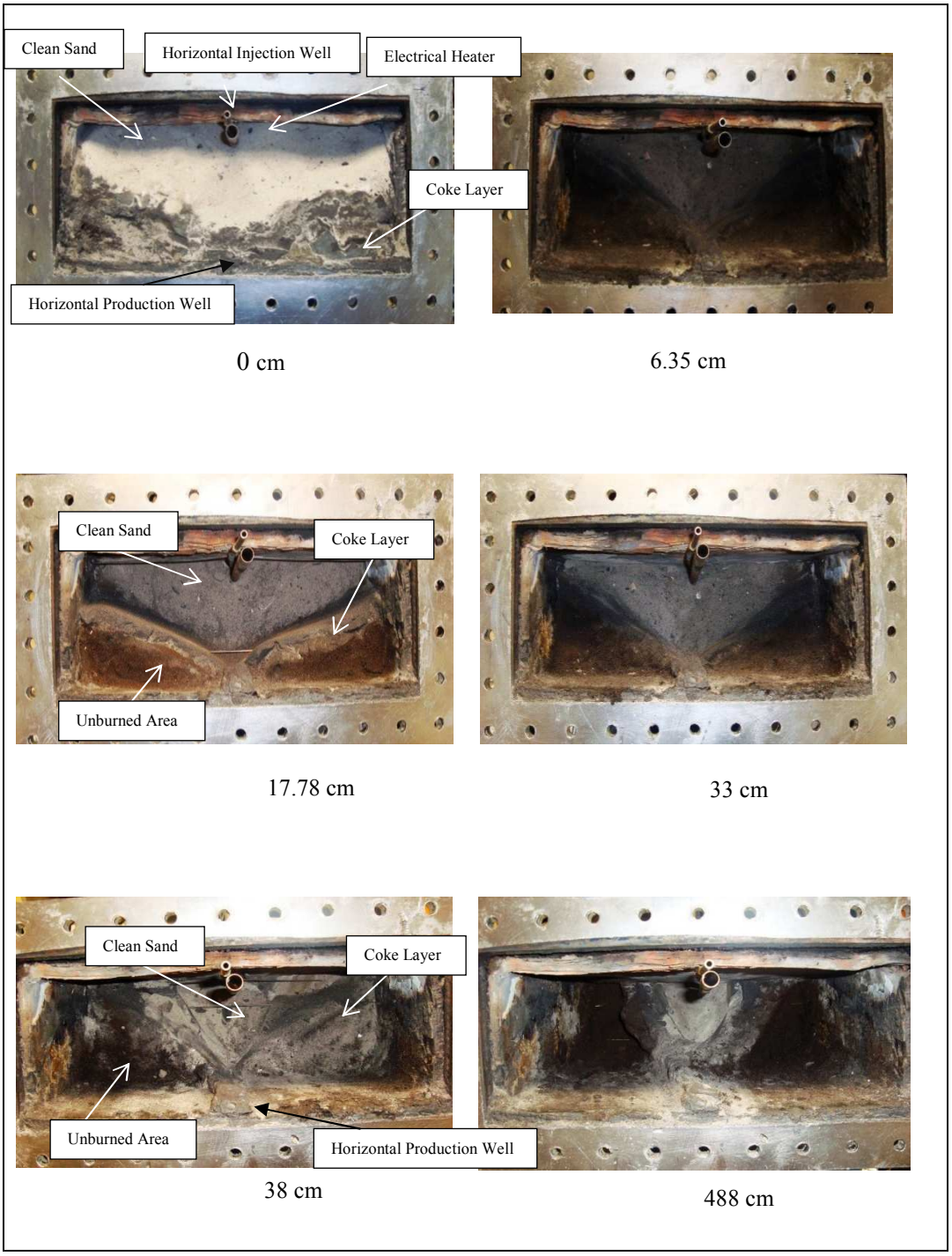

Fig. 24- Post-experiment pictures of coke deposition inside the CAGD cell. Three different distinct zones can be identified; clean sand, coke zone, and unburned area (Run 2).

In Run 2, the combustion front velocity was estimated about 3.8 cm/hr within the range that was reported for conventional ISC processes in the field (Greaves et al., 1996; Glatz et al., 2011). Fig. 25 shows the cumulative oil production. Oil recovery of 82% OOIP was recorded at the end of the experiment.

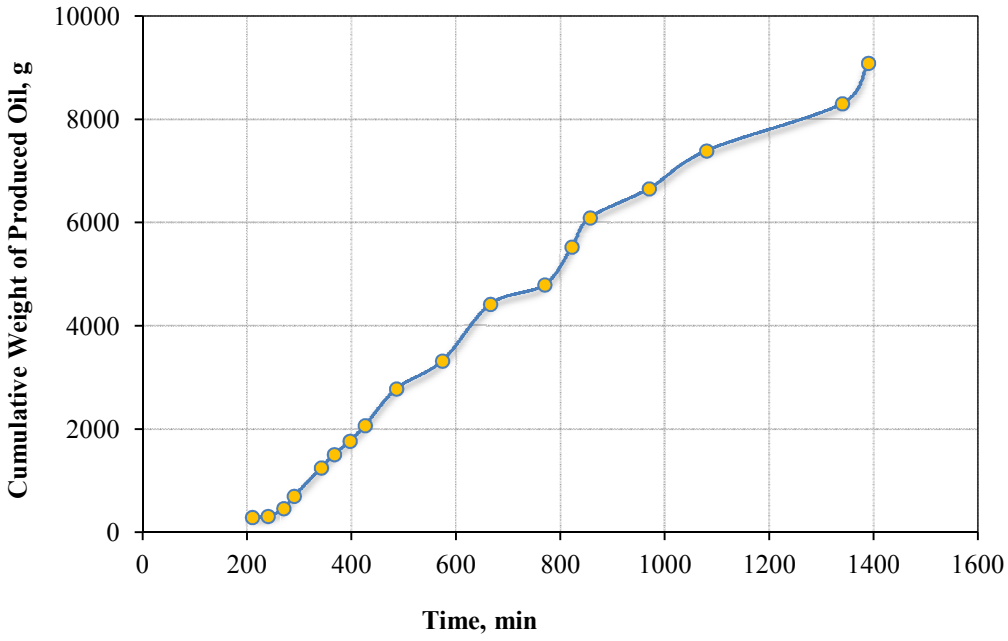

Fig. 25- Cumulative oil production on a mass basis. Oil recovery of 82% OOIP (mass basis) was recorded at the end of experiment (Run2).

Substantial thermal upgrading was observed at the end of the experiment. Ultimate density of the produced oil was enhanced to about 14.37ºAPI, compared to the initial value of 9.15 (Fig. 26). Typically in ISC, thermal upgrading is not significant. In this process, the mobilized oil should pass through the cold oil bank in front of the combustion zone to be produced; as a result upgraded oil is mixed with initial crude oil. However, in the CAGD process, upgraded oil directly drains to the production well and

thermal cracking is preserved. The thermal upgrading is shown in Fig. 27, where the viscosity reduction is about two orders of magnitude. In the early time, combustion took place in a small portion of the cell, most of the produced oil was from those parts that are not directly in contact with the combustion front, and LTO reactions were dominant. In LTO reactions, an oxygen molecule will be added to the structure of the crude oil and increases the oil density and viscosity (Fassihi et al., 1984b; Mamora., 1995; Hanson et a., 1991). LTO occurs where oxygen is present at the lower temperature. Generally in all of the experiments, LTO was observed as the dominant reaction mode at the early stages of the combustion process. When the combustion chamber develops, produced oil was drained from the high temperature narrow mobile zone where high temperature oxidation reactions was more dominant and led to substantially upgrading produced oil. Fig. 28 provides visual comparison of the viscosity for the initial and the final upgraded oil.

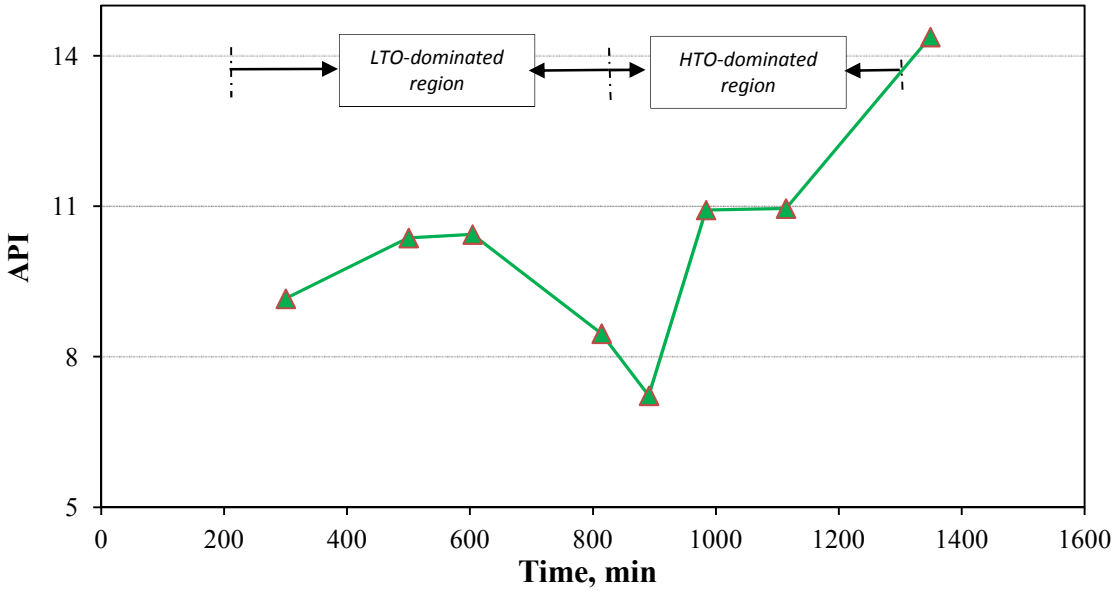

Fig. 26- Measured density of produced oil at 25 °C versus time indicates substantial thermal upgrading in CAGD process (Run 2).

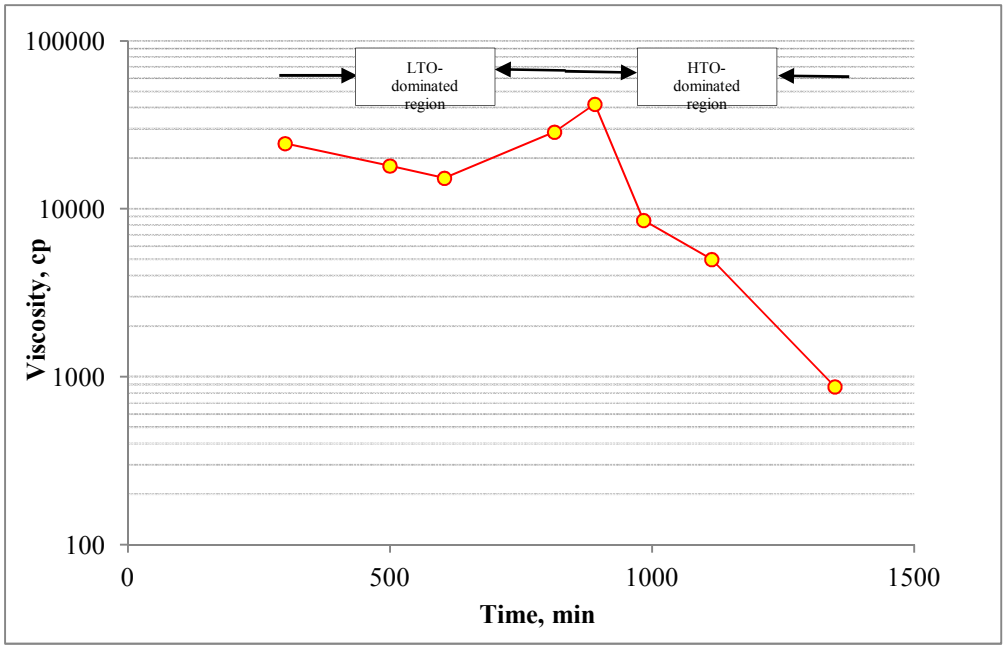

Fig. 27- Produced oil viscosity as a function of time. Viscosity of produced oil clearly shows the type of combustion reaction (Run 2).

Initial Oil – 24,800 cp

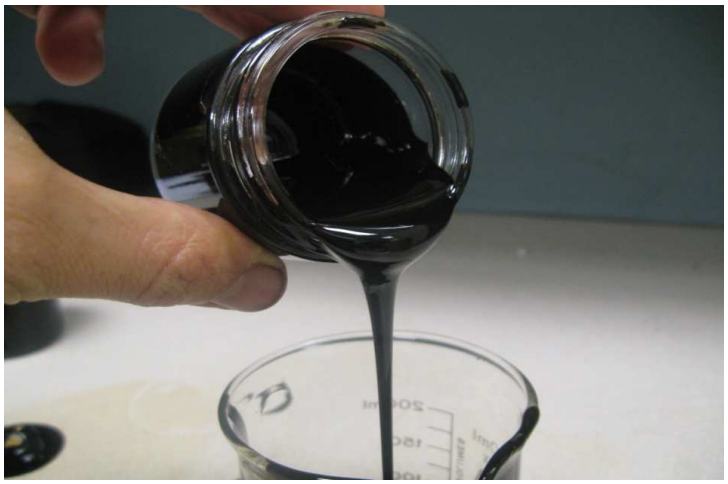

Upgraded Oil – 873 cp

Fig. 28- Visual comparison of initial and upgraded oil viscosity. Final upgraded oil viscosity was enhanced to 873 cp (Run 2).

4.2.3 Run 3

In the third experiment injection pressure was increased to 1379 kpa (200 psi) and injected oxygen concentration was reduced to 50%. Fig. 29 shows the temperature at four different points along the injection well. First 420 minutes were allocated for preheating. At this time, nitrogen was injected to minimize low-temperature oxidation inside the model. The injection stream was switched to air (21% O_2 and 79% N_2) after the maximum recorded temperature reached about 200°C. Vigorous combustion started when enriched air was injected, and the maximum temperature of the injection well increased to 530°C. The combustion front remained steady and its forward movement was recorded by thermocouples along the horizontal injection well.

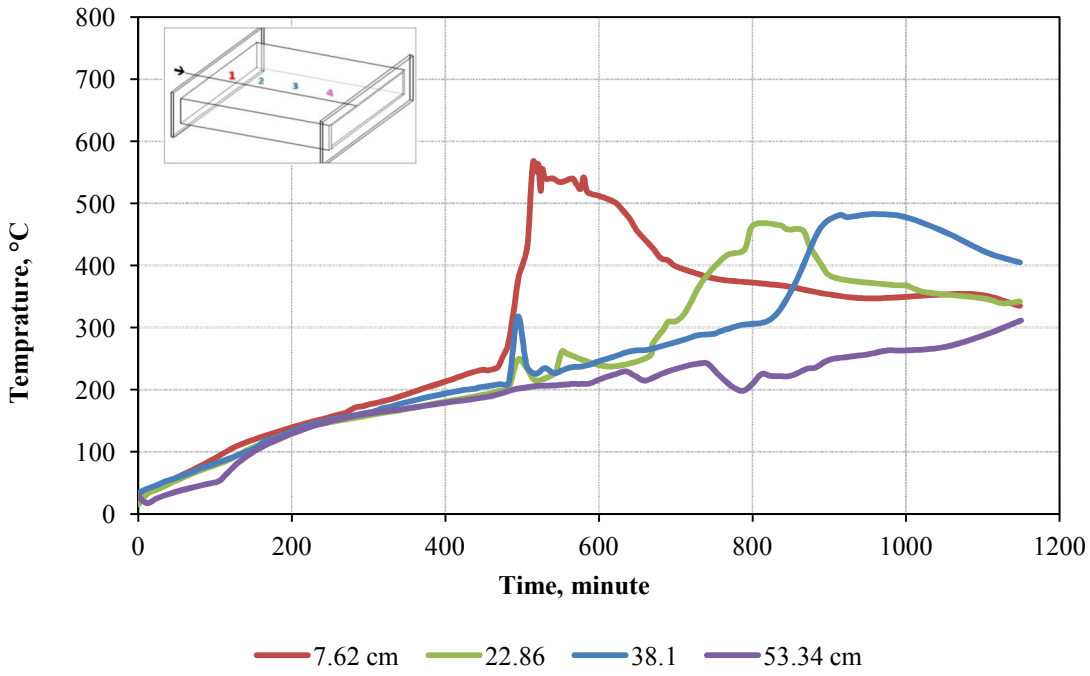

Fig. 29- Temperature vs. time at four different points along the injection well. Vigorous combustion started when enriched air was injected and the maximum temperature of the injection well increased to 530°C (Run 3).

Fig. 30 shows the temperature profile in both the top horizontal and mid vertical plane inside the cell. At 550 minutes, the combustion started around the injection well near injection side. The temperature profile at 710 minutes indicated that combustion developed in the vertical direction. When coke deposition reached to the production well, it apparently plugged the perforations. This was the main reason that the injection and production sides were placed in opposite directions. At time 825 minutes the combustion front reached to the bottom of the model in the first 20-cm interval and the maximum recorded temperature reached to 480°C. A mobile oil zone immediately ahead of the combustion front developed in a wider area as process progressed. The temperature profile shows that the combustion front was developed laterally in the top layers. This was favorable for the process: it minimized the accumulation of flue gases at the top layer and prevented uncontrolled gas override. The combustion front did not move away from the injection point but always stayed in close contact with the injector perforations and followed the path of the injection well. This led to highly efficient oxidation reactions and better control of the direction of the combustion front movement.

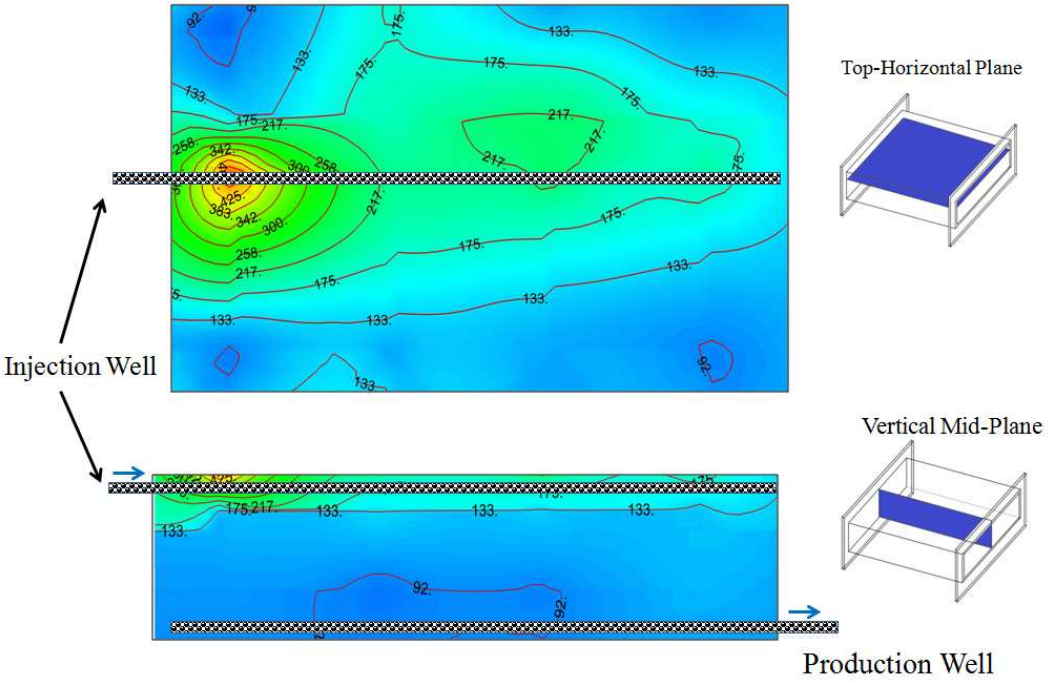

a) Time = 550 minute

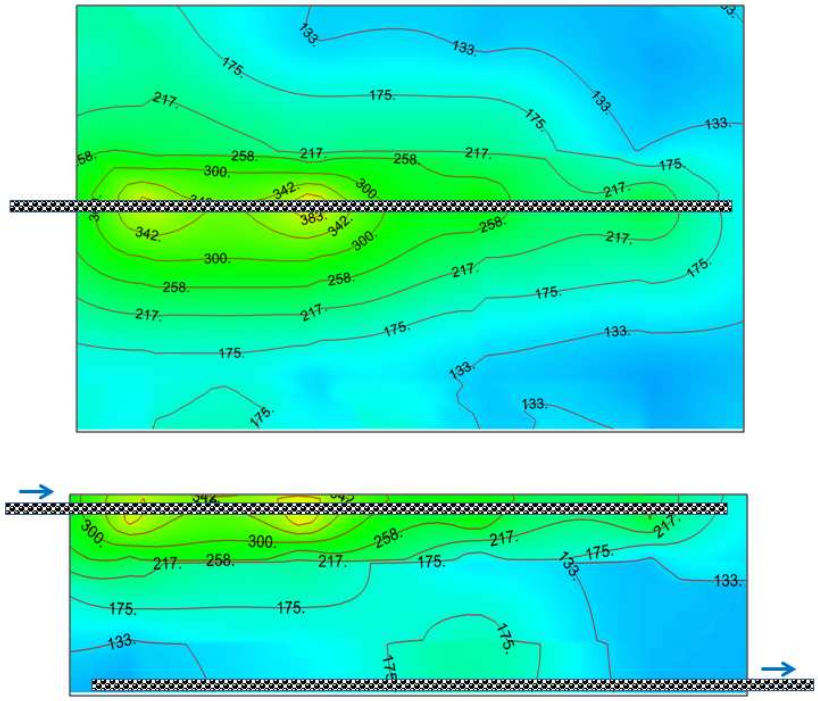

b) Time = 710 minute

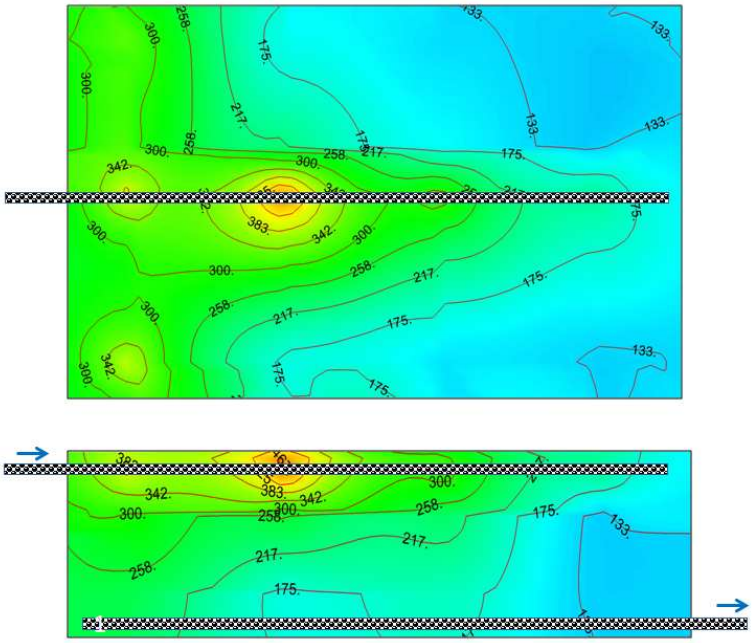

c) Time = 8250 minute

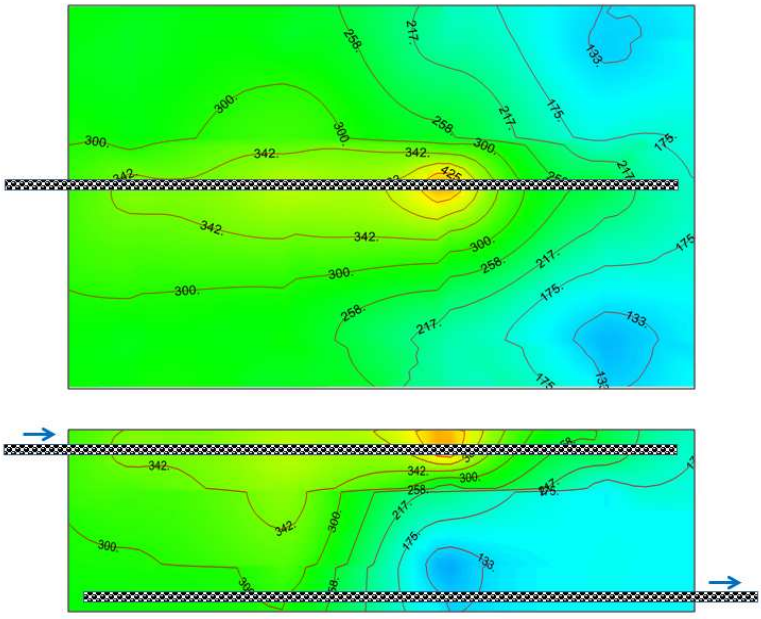

d) Time = 1000 minute

Fig. 30- Temperature profile in different snapshot. The combustion front developed laterally in the top layers. This was favorable for the process and minimized the accumulation of the flue gases at the top layer, and prevented uncontrolled gas override condition (Run3).

Oxygen consumption was close to 67%, and at the early stage, nearly all of the injected oxygen was consumed (Fig. 31). This value decreased as the process continued, while the oxygen concentration in the production stream increased and reaching 20%. As combustion propagates and moves forward, coke deposition plug the perforations completely or partially. The overall impact is positive and minimizes the amount of oxygen that can bypass; however, some of injected oxygen may pass to the producer through unplugged perforations. Lower differential pressure and optimum air injection rate may help to minimize the rate of bypassed oxygen.

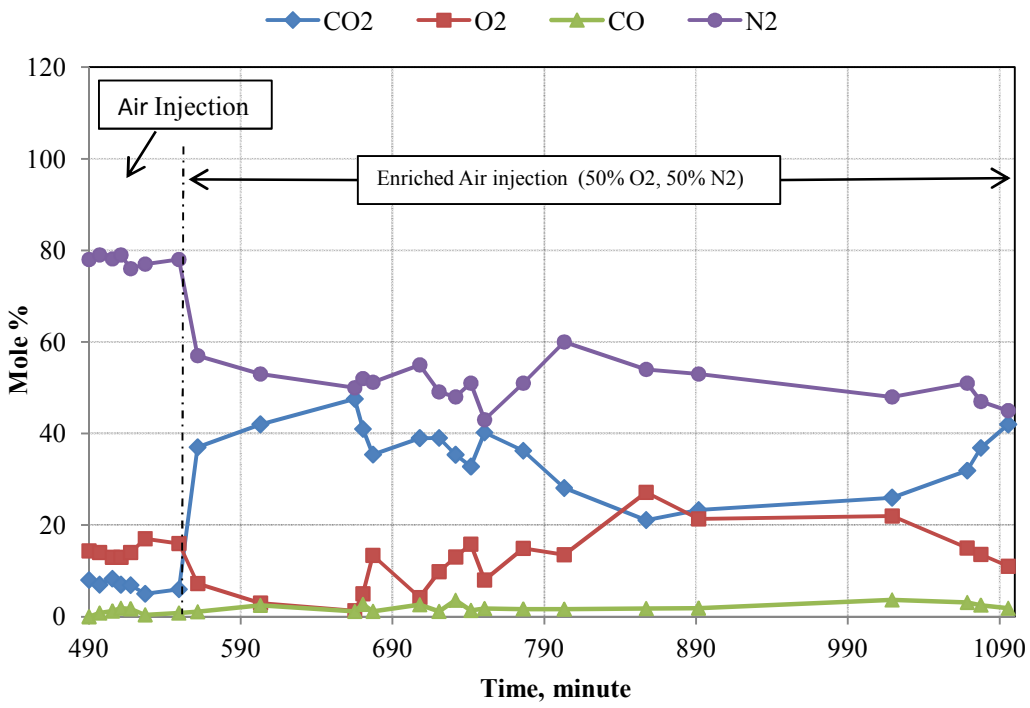

Fig. 31- Produced gas composition vs. time during the test. In early stages of the experiment, all of the injected oxygen was consumed, but this value decreased as combustion progressed. A fraction of the injected oxygen bypassed through the already swept part of the production well. Coke plugging minimized the oxygen bypass rate (Run 3).

The samples of produced fluid were taken at regular time intervals during the experiment. Oil sample volumes varied between 2 and 30 cc. The oil production rate (Fig. 32 and Fig. 33) peaked at about 625 minutes. This peak is related to the production of mobilized oil during preheating. After this stage, oil product remains steady at the level of 12 g/min. last peak before end of experiment was achieved by pressure depletion if the system. Overall recorded oil recovery was about 73% of OOIP. Because the produced oil density changed during the experiment, oil samples were reported on a mass basis. Fig. 34 shows the maximum oil saturation in the unburned zone. Maximum oil saturation never exceeded 18% which implies that the combustion front effectively drained the oil in a narrow zone ahead of the combustion front.

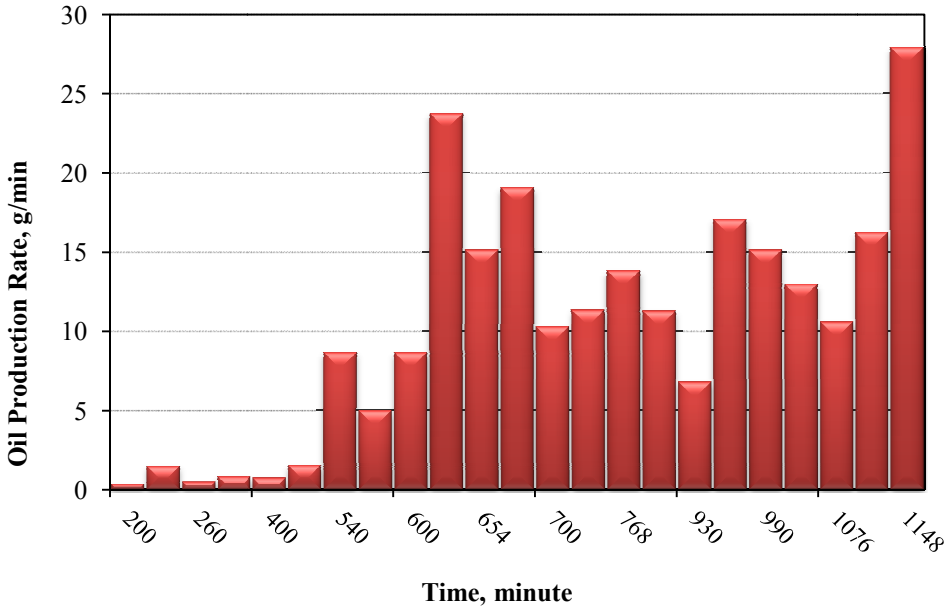

Fig. 32- Oil production rate of CAGD experiment after separation of water and dissolved gases. oil product remains steady at the level of 12 g/min after the first peak. Overall recorded oil recovery was about 73% of OOIP (Run 3).

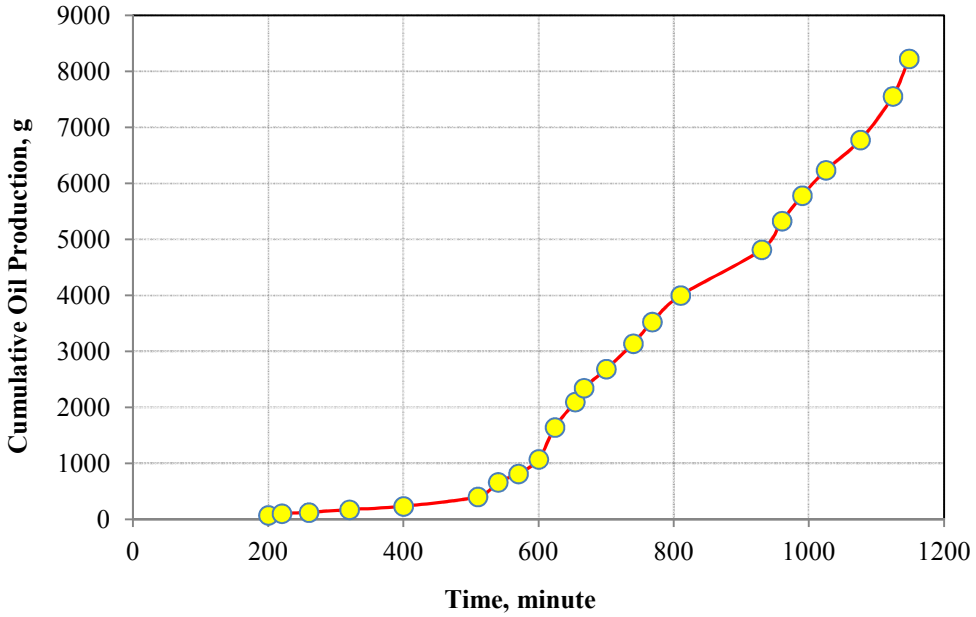

Fig. 33- Cumulative oil production of the CAGD experiment. Oil recovery of 73% OOIP (mass basis) was recorded at the end of the CAGD operation (Run 3).

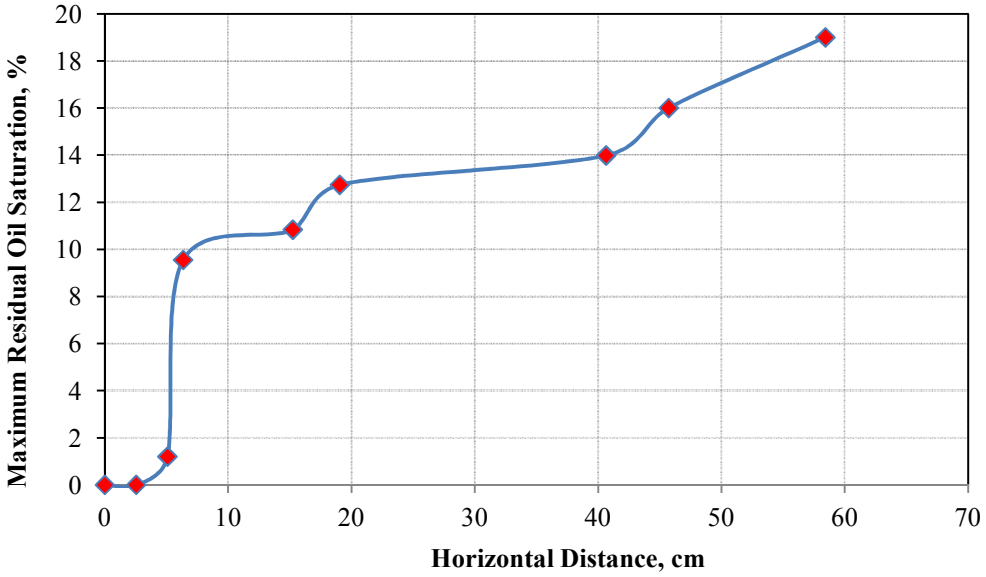

Fig. 34- Residual oil saturation vs. horizontal distance. Maximum oil saturation is below 18%, which indicates the effectiveness of the combustion process (Run 3).

In Fig. 35, the produced oil density changed significantly during the experiment. The initial oil density was about 9.15° API; this value decreased at the early stages of the test, where it dropped to about 8°API. In this stage, the combustion front was not fully developed and most of the produced oil was drained for those areas that had lower temperature (below 250°C). This condition favors LTO type of reactions and leads to crude oil downgrading. After the combustion front became fully stable and more developed, the higher temperature of narrow mobile oil zone cause significant upgrading, and the produced oil density reached about 12°API.

Runs 1 and 2 showed that the vertical spacing between horizontal injection and production wells is very critical in the horizontal well air-injection process. A close distance can have a negative effect on the process by early plugging of production well by coke deposition. On the other hand, a larger distance can postpone the pressure communication between the paired wells and cause air injectivity problems as shown in Fig. 36 where the pressure difference is near 552 kpa (80 psi) at the beginning of the test. Initial crude oil mobility is a key factor in designing the vertical spacing between the wells. However, other preheating approaches like hydraulic fracturing or steam preheating may be feasible and accelerate the pressure communication between paired wells.

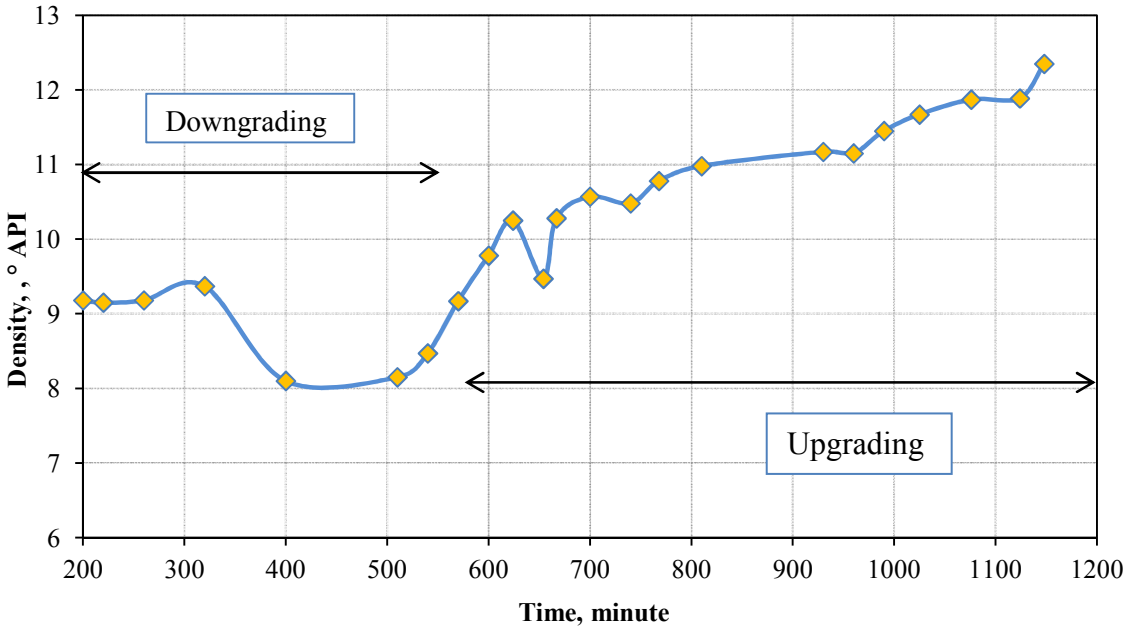

Fig. 35- Upgrading of the initial oil during CAGD process. Initial crude oil downgrading and later upgrading were observed in this experiment. Crude oil density was increased up to 12.35°API at the end of the experiment (Run 3).

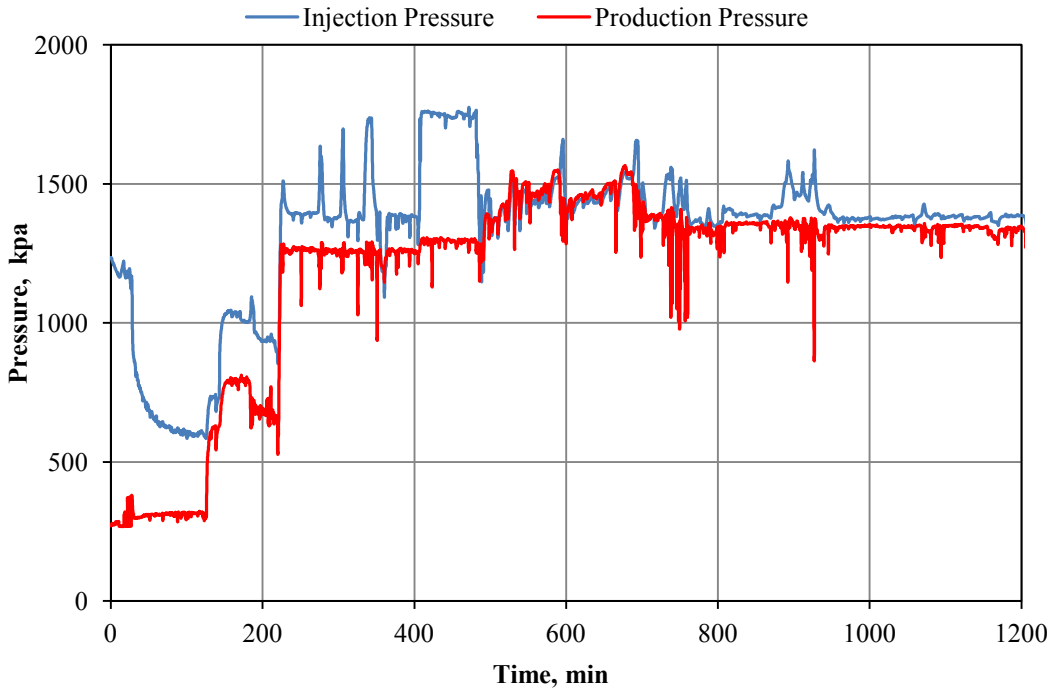

Fig. 36- Injection and production pressure during the experiment. Significant initial pressure drawdown (932 kpa) was required to establish pressure communication between paired wells (Run 3).

4.2.4 Run 4

In all of the previous experiments, Peace River oil sample (24,800 cp) was used for packing the experimental model. In Run 4, it was tried to test the CAGD process with lower initial viscosity and completely immobile oil at standard conditions. For this reason the Athabasca oil sample was considered the initial crude oil. Similar experimental procedure was implemented for this run. Fig. 37 shows the produced gas composition during the experiments. N_2 mole fraction is excluded from these data. To accelerate the preheating period, air was injected between times 4 to 5.3 hours. During this period self-sustained combustion front was not observed. As a result, enriched air ($50\%O_2$, $50\%N_2$) was selected as injection gas. After this switch, the CO_2 mole fraction peaked near 48%. During this stage the electrical heater was off and the combustion front showed sustainability for the rest of the experiment. Nearly stable CO_2 composition (35 %) has been observed at the production outlet. This indicates the robustness of the process for initially immobile crude oil.

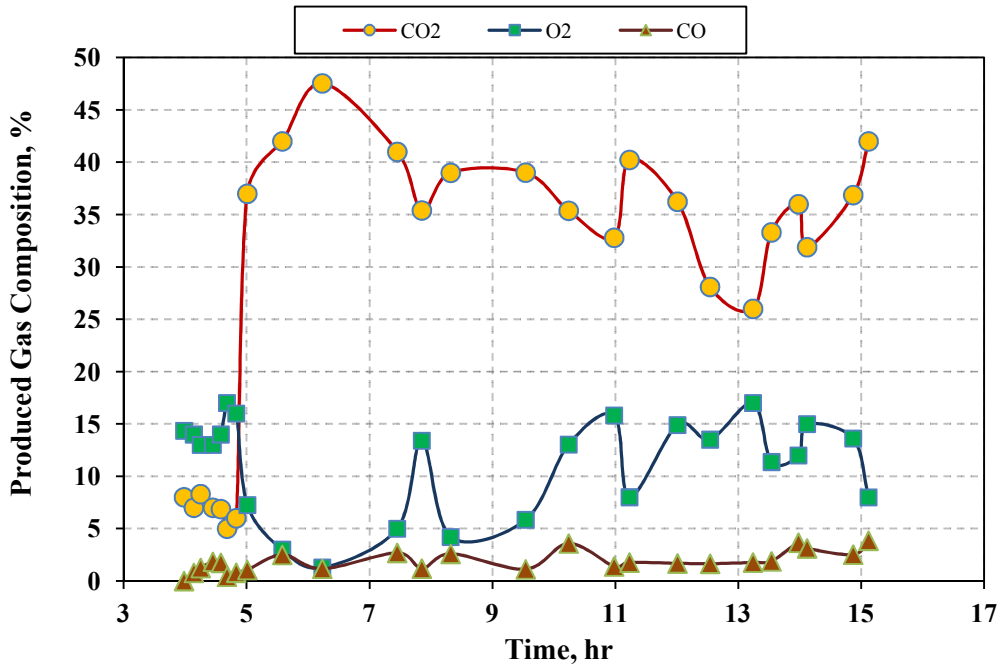

Fig. 37- Produced gas composition during the experiment. Fairly stable oxygen consumption and flue gas production were observed (Run 4).

Cumulative oil production is illustrated in Fig. 38. At the end of the experiment, recorded oil recovery reached about 65% of OOIP. During the experiment, several well plugs caused pressure fluctuation (69 to138 kpa) in the system. This plugging was mainly due to condensation of water and gases inside the production vessels. The ratio of burned area to total area varied along horizontal distance (Fig. 39). For example, the combustion front is more developed near the heel of the injection well. Experimental observation showed that at the first 3.6 cm, the sand pack was completely burned leaving only the remaining coke layer and clean sands with zero oil saturation. Coke layer thickness varied along horizontal distance from 6 cm in the heel to 1 cm in toe of the injection well.

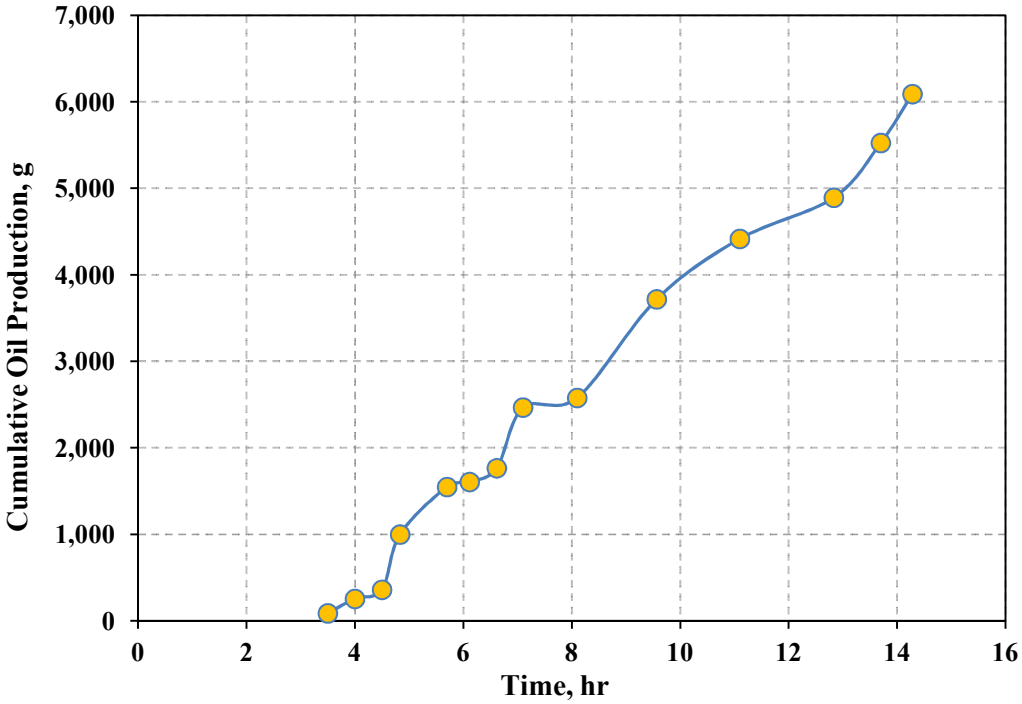

Fig. 38- Cumulative oil production of CAGD experiment. At the end of the experiment, recorded oil recovery reached to about 65% of OOIP (Run 4).

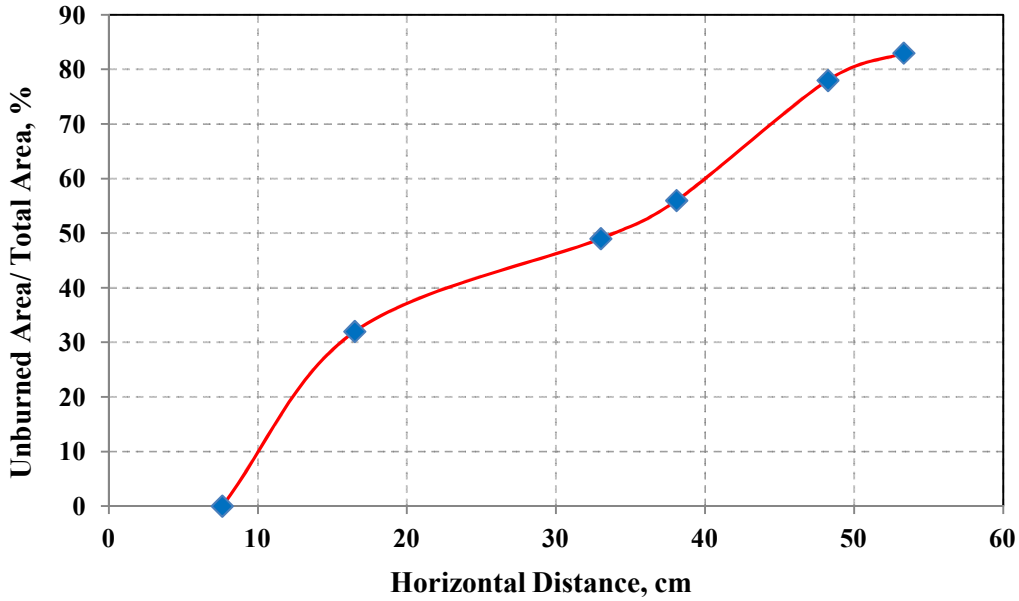

Fig. 39- Ratio of unburned area to total area along horizontal paired wells. The combustion chamber was more stable in the heel part of the injection well. (Run 4).

Density of the produced oil samples is show in Fig. 40. Water and dissolved gases were separated from oil samples before this measurement. At the early stages of the process, produced oil was downgraded to about 7ºAPI due to vaporization of lighter components. Crude oil density was enhanced more than 2ºAPI at the later stages of the experiment.

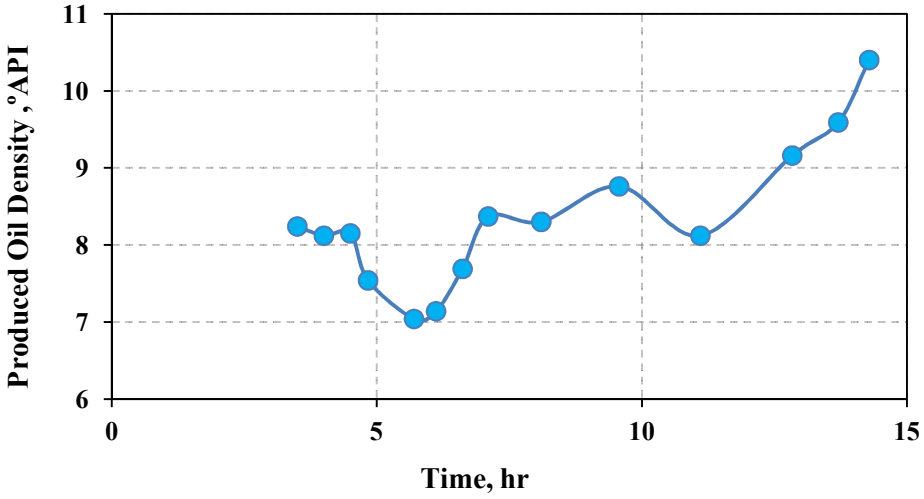

Fig. 40- Thermal upgrading of produced oil during the CAGD experiment (Run 4).

Fig. 41 shows the temperature profile inside the CAGD laboratory model. An Isosurface of 350°C was used for better illustration of the hot temperature region inside the porous media and the propagation of the combustion front. Combustion front initiated near the heel of injection well and developed in lateral and forward directions. As shown in this temperature profile, the combustion front followed the path of the injection well. Sustainability of the combustion front depends on removing flue gases out of the system and maintaining high oxygen partial pressure in the combustion zone. In comparison to Run 3, the combustion front was more stable and swept the formation uniformly.

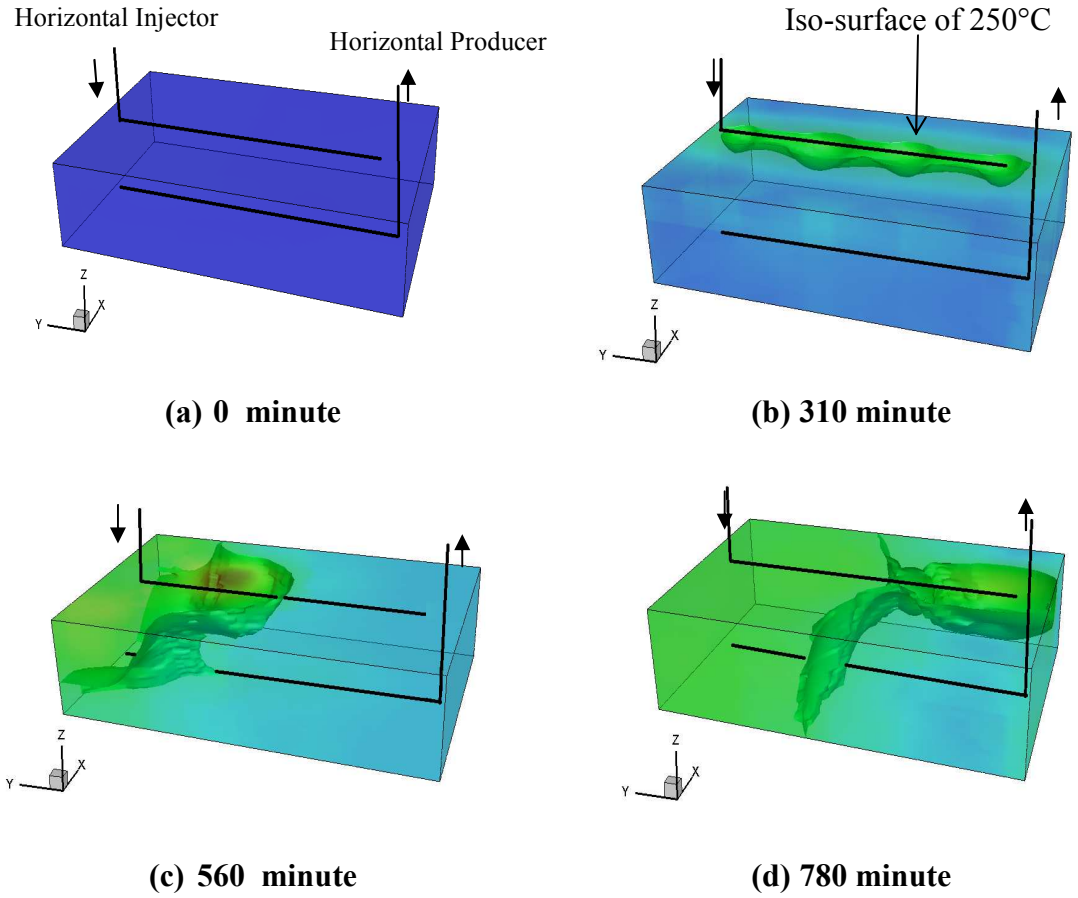

Fig. 41- Temperature profile inside the CAGD laboratory cell. The combustion front was more stable and swept the porous media uniformly. The maximum recorded temperature reached 560°C (Run 4).

4.2.5 Run 5

This experiment investigated the potential of post-SAGD in-situ combustion. The packing procedure was slightly different from previous experiments, and the SAGD pair was modified: the injection and production sides were set in opposite directions. No extra well was implemented for venting, so the flue gases produced through the production well. Two porous media with different fluid saturation were used for packing. An aluminum cylinder with thickness of about 0.3 mm was used to separate the

two sand pack zones and the thermo-wells were placed into the cell as packing progressed. Fig. 42 shows the oil, gas, and water saturation in these two regions. The inner region (Region 1) represented the mature SAGD chamber, after cooling down and steam condensation. Residual oil saturation was about 25% and water saturation about 32%. Table 4 summarizes the fluid saturation in both regions. Region 2 was considered an untouched region that was not produced during the SAGD operation. Measured initial crude oil viscosity versus temperature is summarized in Table 5.

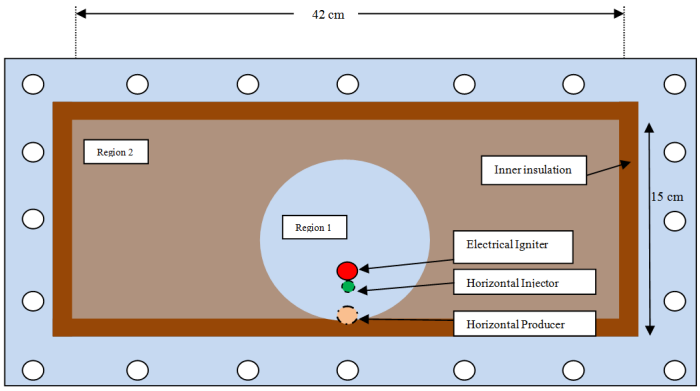

Fig. 42- Schematic view of the two different sand pack regions and position of wells and igniter in the middle plane of the model. (Run 5)

Fig. 43 illustrates the temperature of four different points along the injection well. For preheating, a heating element was placed in the first 15 cm of the injection well. Preheating took about 5 hours and was terminated when saturated steam temperature was achieved in this area (190°C @ 1379 kpa). At this condition, steam was in two phases in the SAGD chamber. Enriched air was injected with the rate of (3 L/min). Combustion was initiated in the first 15 cm of the injection well. The igniter was turned off after one hour of enriched air injection.

Table 4: Fluid saturation for two different zones (Run 5).

Property	Region 1	Region 2
S_w	**0.00**	**0.32**
S_o	**0.72**	**0.25**
S_g	**0.28**	**0.43**
Sand Grain Size	**100 US Mesh Size**	**100 US Mesh Size**

Table 5: Viscosity and density measurement for Pease River oil sample.

Temperature ºC	Density Kg/m3	Viscosity, cp
25	**1006.43**	**24500**
50	**995.52**	**10145**
75	**991.18**	**435**
100	**984.98**	**105**

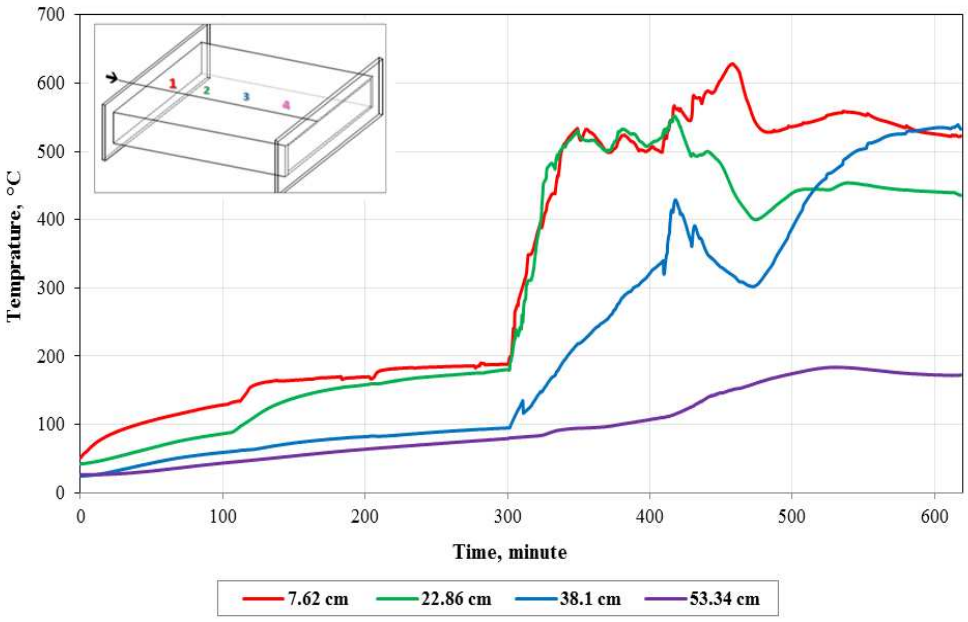

Fig. 43- Temperature vs. time along injection well in four different points. The combustion front moved along the injection well, and temperature behind the combustion front stays relatively high. (Run 5)

Combustion front temperature increased to about 550 °C and developed in

forward direction. Combustion chamber reached to 38.1 cm distances from the injection side at 430 minute after starting the experiment. During this period, maximum-recorded temperature was about 614 °C. Temperature profile shows that virgin oil zone was also affected by combustion heat and its temperature increased to about 150°C, which led to some oil production from this area. Fig. 44 shows temperature profile in the mid-vertical plane along the horizontal pair during the combustion process. The combustion front was clearly limited inside the mature SAGD chamber and did not sweep the area beyond this region. This behavior may be related to the low concentration of oxygen on the boundary of the SAGD chamber. At this region, the oil saturation is higher (72%) compared to SAGD than in the (25%), the coke deposited layer apparently formed a dense shell with low permeability. Gas flow restriction could be the reason for not burning the fuels that already had deposited at the SAGD chamber boundaries. Since in this experiment oil was produced in the opposite direction from enriched air injection, combustion started near the end of the production well, and even if these segments were plugged by coke deposition, the rest would remain open to flow (Fig. 44).

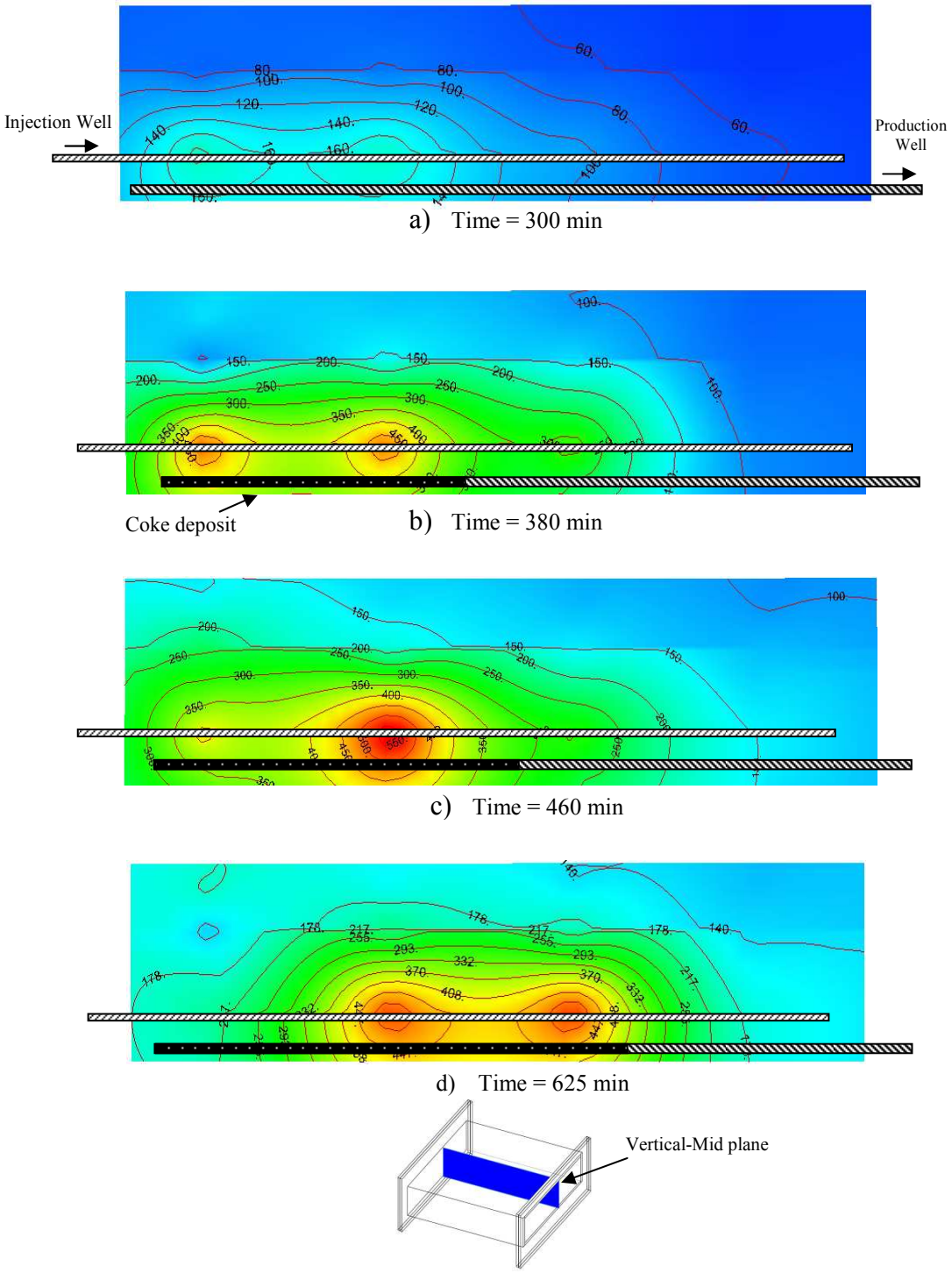

Fig. 44- Temperature profiles at the vertical mid-plane of the laboratory cell. The combustion front is limited inside the mature SAGD chamber and does not sweep the area beyond this region. This behavior may be related to low concentration of oxygen on the boundary steam chamber (Run 5).

Fig. 45 shows produced gas composition during the experiment. In early time, oxygen was completely consumed. However, as combustion advanced forward, oxygen concentration in the production stream increased continuously until it reached the level of 40%, which is 20% consumption of injected oxygen at the latest period. Production well plugging was not as effective as in previous experiments. This is because of lower oil saturation and as a results lower coke concentration on the sand grain surfaces. The rate of bypassed oxygen was higher for this experiment.

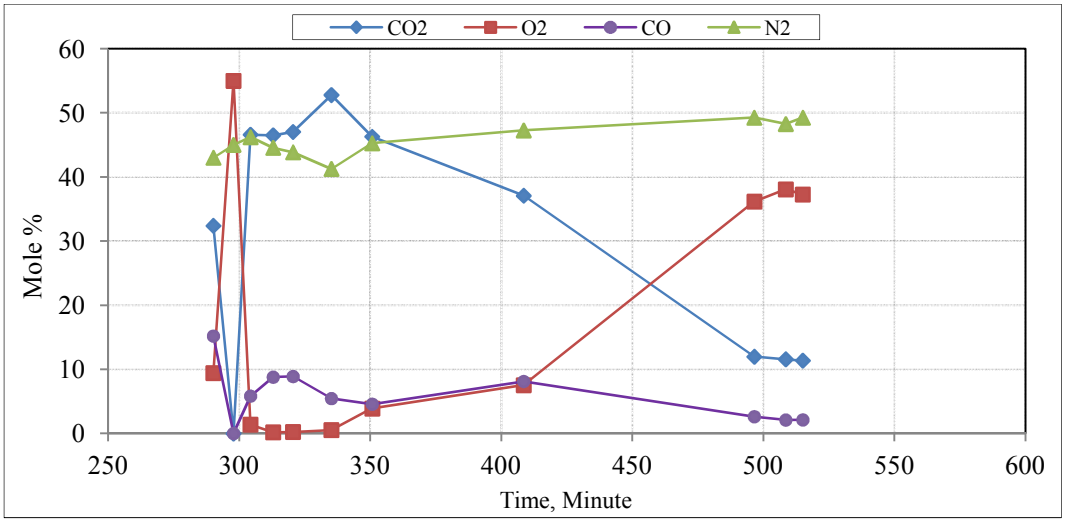

Fig. 45- Produced gas composition versus time. At early time nearly all injected, oxygen is consumed. This amount is decreased as combustion progressed (Run 5).

In-situ combustion resulted in production of 1,075 gram oil after about 5 hour's air injection which corresponded to recovery of nearly 12% OOIP. Fig. 43 shows the cumulative oil production after stabilization of the combustion front. The oil production rate increased slowly to about 530 minute. The temperature profile (Fig. 44) indicated that at early time, only the SAGD chamber was heated up, and oil production came from residual saturation inside the SAGD chamber. However, at later time, the virgin zone

beyond the SGAD chamber was also affected by combustion heat. At this point (after 550 minutes) an increase in oil production was observed. However, at a larger scale, such oil production is not feasible due to the temperature gradient and lower heat transferred by conduction. This is a valid point, but the main purpose of SAGD air injection is to produce the residual oil inside the SAGD chamber and create an insulating barrier around the SAGD chamber.

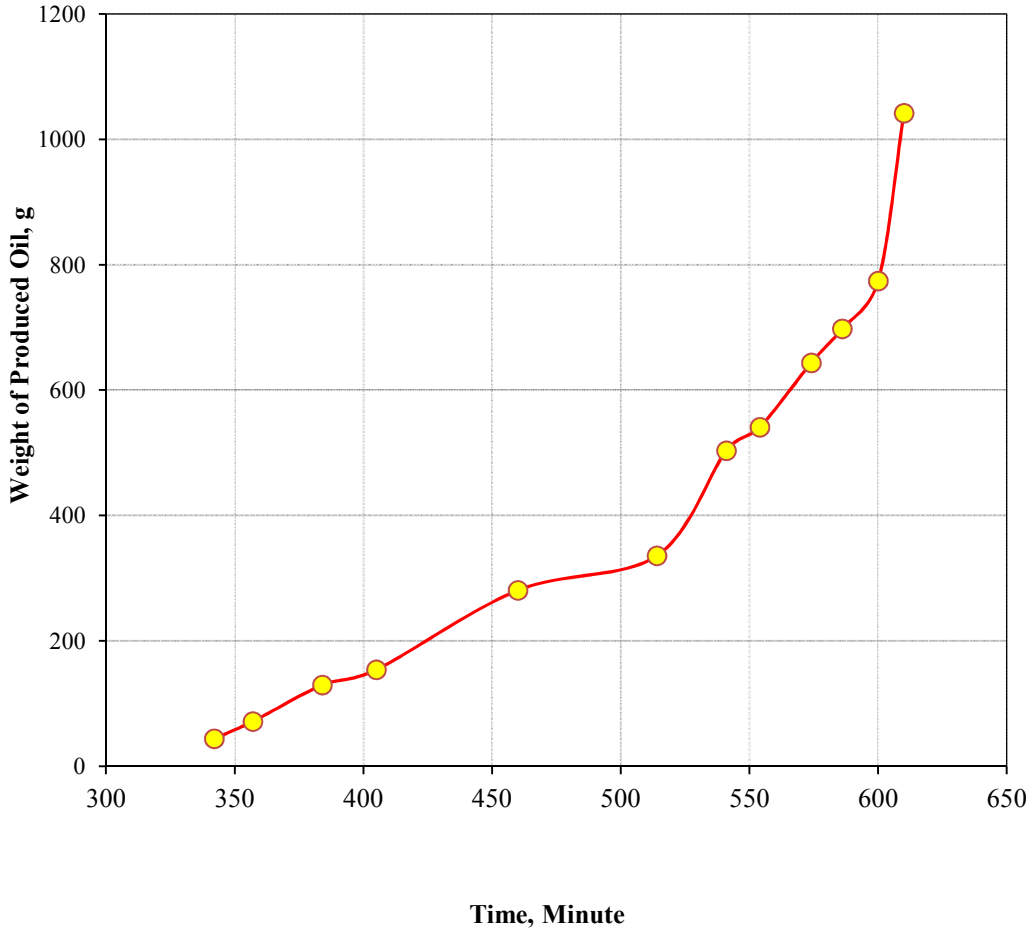

Fig. 46- Cumulative oil production on mass basis. Oil recovery of 12% OOIP (mass basis) was recorded at the end of the experiment (Run 5).

Fig. 47 shows the measured produced oil viscosity at 25ºC. Two different parts

can be identified in this graph. At early time, viscosity gradually increased; the same trend also can be seen in Fig. 48, which illustrates the produced oil density versus time. In this period, low- temperature oxidation reactions are more dominant. In the ISC process both LTO and HTO take place alongside each other at different temperature. This is visible in first half of experiment, when the produced oil viscosity increased to about 41,000 cp. In the second part of the graph, produced oil viscosity declined and reached to about 3150 cp. The HTO mode was more dominant which led upgrading of the initial oil and increasing oil API gravity from 9.15ºAPI to near 12ºAPI. Lower crude oil upgrading was observed than in previous experiments.

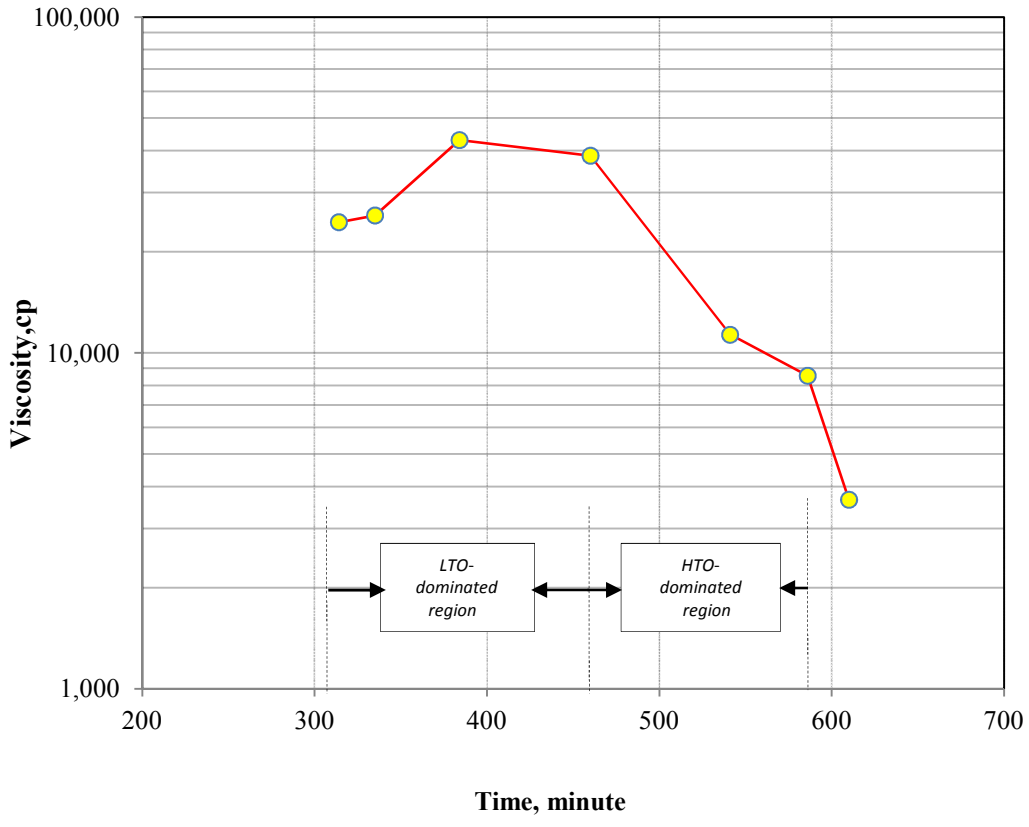

Fig. 47- Measured viscosity of produced oil at 25°C over time indicates substantial in-situ upgrading is taking place (Run 5).

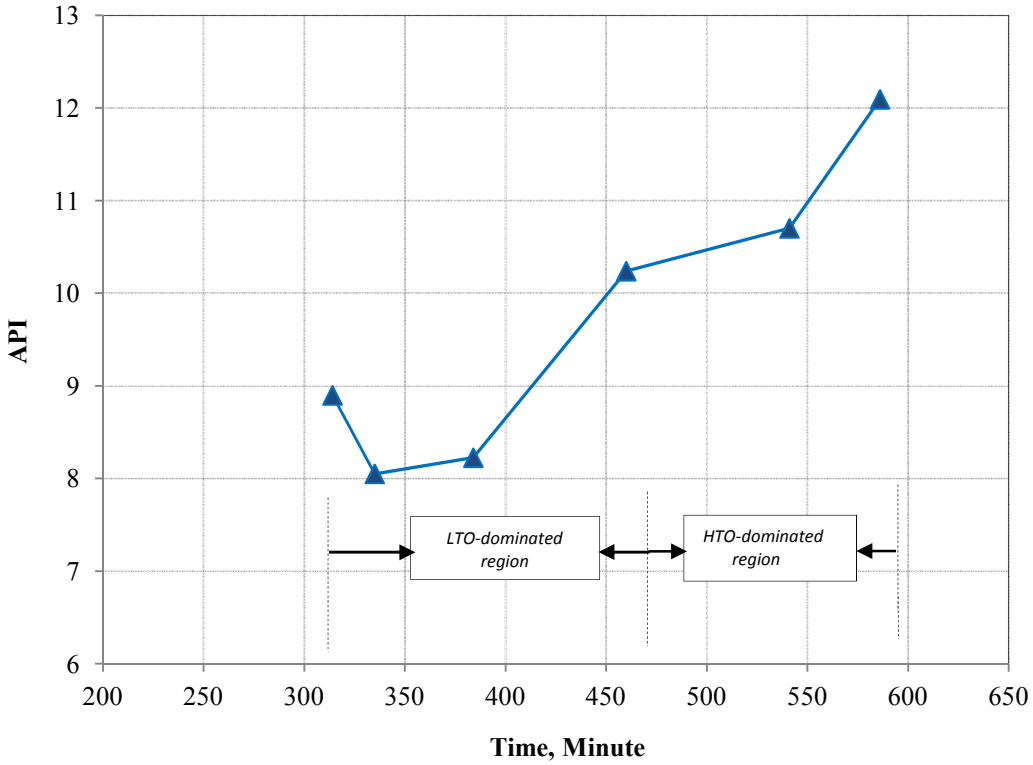

Fig. 48- Produced oil density as a function of time. Oil gravity was enhanced by 3ºAPI (Run 5).

5. SIMULATION RESULTS*

5.1 Simulation study

A commercial thermal simulator (CMG's STARS) was used for history matching experimental results and further study of the main mechanisms of the CAGD process. This section first provides the specifications of the numerical model and later on compares the simulation data and experimental results. Final part of this chapter investigates the performance of the CAGD process in comparison to two other thermal methods; THAI and SAGD.

5.2 History matching

5.2.1 Simulation model

The simulation model has a rectangular configuration with 8,000 total grid blocks uniformly distributed in the X, Y and Z directions. The simulation model is homogeneous and based on properties of the laboratory model. Fig. 49 shows the schematic of the numerical model and the location of the horizontal well pair.

* Part of the data reported in this section is reprinted with permission from "Experimental Study of Air Injection in SAGD Chamber" by Rahnema, H., and Mamora, D., Paper SPE-149195 Presented at the Canadian Unconventional Resources and International Petroleum Conference, Calgary, Alberta, Canada, Copyright 2011 by SPE and "Combustion Assisted Gravity Drainage (CAGD) Appears Promising" by Rahnema, H., and Mamora, D., Paper SPE-135821 Presented at the Canadian Unconventional Resources and International Petroleum Conference, Calgary, Alberta, Canada, Copyright 2010 by SPE.

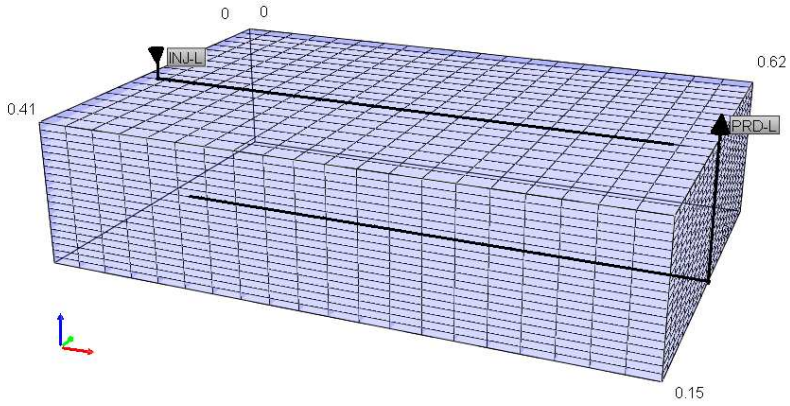

Fig. 49- Schematic of the simulation model and the horizontal wells pattern.

5.2.2 Fluid model

Athabasca bitumen was characterized into pseudo-components: maltenes, asphaltene, and coke. Other components like water, oxygen, carbon dioxide, carbon monoxide, and nitrogen were added to the simulation model, their properties were extracted from a chemical handbook (Perry et al. 1997) or the STARS^{TM} library (CMG. 2008). In total, 8 components were used in the simulation model. Also, temperature dependent viscosity of Athabasca bitumen was modeled by using the Arrhenius formula (Eq.3).

$$\mu_{oi} = Ae^{\left(\frac{B}{T}\right)} \quad \text{.....} \quad (3)$$

Where A and B are the adjusting coefficients and were determined by regression of experimental measurements. It is assumed that initial bitumen consists of asphaltene and maltenes. This assumption is based on the SARA fraction lumping method. Bitumen viscosity is calculated by the logarithmic mixing rule (CMG. 2008).

$$\mu_{bitumen} = (\mu_{maltenes})^{X_{mal}} . (\mu_{asphaltens})^{X_{aspl}} \quad \text{.....} \quad (4)$$

Fig. 50 shows the measured viscosity of the Athabasca bitumen sample at different temperatures. Viscosity correlation parameters were extracted by curve fitting of measured viscosity data. (Table 6)

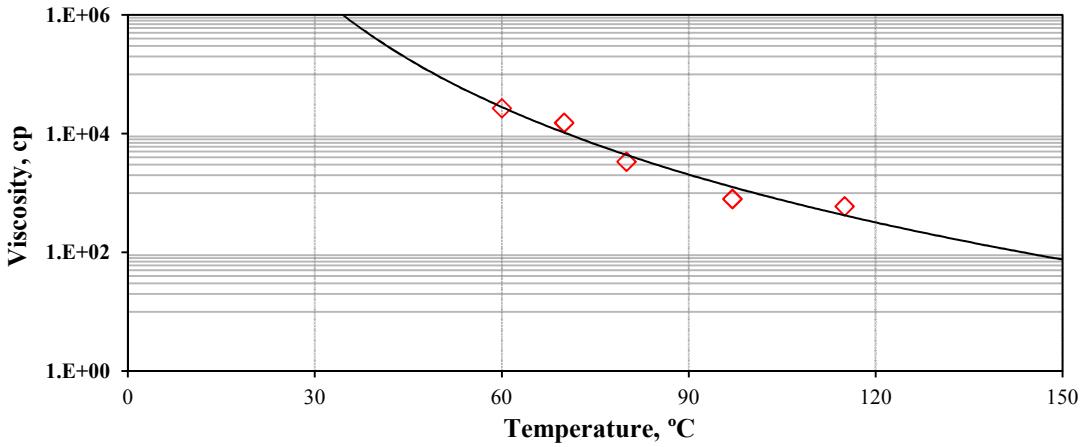

Fig. 50- Measured viscosity of Athabasca bitumen.

Table 6: Viscosity correlation parameters for Athabasca oil sample

Oil Phase Components	A	B
maltenes	1.94E-05	6.89E+03
asphaltens	1.62E-13	2.98E+04

5.2.3 Kinetic model

Kinetic reaction data was extracted through the Belgrave et al. (1993) reaction model for Athabaska bitumen. Table 7 summarizes the reaction kinetics which were considered irreversible and on a mass balance basis. Appendix C listed the properties of the pseudo-components and an example of mass balance between the reactions. In CMG STAR, three controlling parameters (activation energy, frequency factor and reaction

enthalpy) were set for each reaction. These parameters were used in the regression procedure. Five sets of reactions were used for modeling the combustion reactions. In total, 15 matching variables of the kinetic model were used in the regression. The table on page 128 lists the properties of each component.

In the history matching work flow, it was tried to match the produced gas composition, cumulative oil, and water production. Timing of temperature elevation inside the model was the first matching goal rather than peak temperature. The location of thermocouples was in the form of discrete points inside the model and the maximum recorded temperature was not necessarily the peak temperature. The next matching criteria were the produced gas composition, such as N_2, CO_2, O_2, and CO. Among these components, CO_2 and O_2 were assigned higher weights. Because the amount and the ratio of these gases at the outlet represented the oxidation reaction characteristics.

Table 7: Bitumen reaction scheme (Belgrave et al. 1993)

Reactions	Reaction #	Kinetics
Thermal Cracking	1	maltenes → 0.372 asphaltens
	2	asphaltens → 83.223 Coke
	3	asphaltens → 37.683 Gas
Low Temperature Oxidation (LTO)	4	maltenes + $3.431O_2$ → 0.4726 asphaltens
	5	asphaltens + $7.513O_2$ → 101.539 Coke
High Temperature Oxidation (HTO)	6	(Coke)$CH_{1.13}$ + 1.232 O_2 → Cox + 0.5635 H2O

End-point relative permeability information was extracted from the Belgrave et al. (1993) experimental data. In thermal processes especially in ISC, relative permeability shows temperature-dependent behavior (Kumar et al. 1985; Pratt 1986). Temperature dependencies of end points were also used as regression variables. Table 8

and 9 summarized the most important regression parameters that have been used in tuning and their values.

Table 8: Summary of kinetic data used in the tuning procedure and their final values.

Reaction	Frequency Factor, A	Activation Energy, Ea, J/mol	Reaction Enthaly , J/mol
1	3.154e+10 day^{-1}	2.06E+06	0.00E+00
2	3.815e+5 day^{-1}	6.49E+04	0.00E+00
3	3.201e+14 day^{-1}	3.03E+04	0.00E+00
4	3.506e+5 day^{-1} $kPa^{-0.4246}$	2.59E+06	2.96E+04
5	4.115e+5 day^{-1} $kPa^{-4.7627}$	3.24E+07	4.12E+05
6	2.319 day^{-1} kPa^{-1}	6.34E+05	9.31E+05

Table 9: Summary of end-point relative permeability data in low and high temperature.

Curve Endpoints	15°C	700°C
S_{wirr}	0.15	0.04
S_{orw}	0.21	0.272
S_{gc}	0.08	0.18
S_{org}	0.11	0.03
k_{rorw}	0.84	0.78

5.2.4 Variable permeability

Permeability of the porous media is dynamical changing due to deposition of solid coke layer around the sand grain surface. In this simulation study it was tried to model this process. When the coke layer forms on the sand grain surface it will reduce the pore through size. Permeability of porous media can be related to the porosity using carman-kozeny correlation (Eq. 5)

$$K(\varphi) = \mathrm{K_{initial}} \times \left[\frac{\phi}{\phi_{\mathrm{initial}}}\right]^{\theta} \times \left[\frac{1-\phi}{1-\phi_{\mathrm{initial}}}\right]^{2} \quad \text{..... (5)}$$

Where $K_{initial}$ and $\phi_{initial}$ are the initial permeability and porosity of porous media (without coke) and, θ is the tuning exponent. The lower limit of θ is 0, and the upper limit is 10.

For this history matching the value of 5.12 was obtained for θ. Using this correlation assumes that coke layer forms homogeneously around the sand grain.

5.2.5 Matching results

Produced gas composition in Fig. 51 shows acceptable matches for the produced O_2 and CO_2. Moreover, the simulation model was able to match the timing of combustion initiation, where a CO_2 mole fraction increased to near 50% of the outlet stream. Another point is the gas composition at the later stages of the experiment: there is a mismatch for CO_2 and O_2 concentration, where laboratory results showed higher CO_2 production. The accumulation of flue gases especially CO_2 at the combustion chamber and later production of these gases apparently causes a difference between the numerical model and the laboratory data. The simulator was not able to capture this behavior because of the homogeneous assumption of the numerical model.

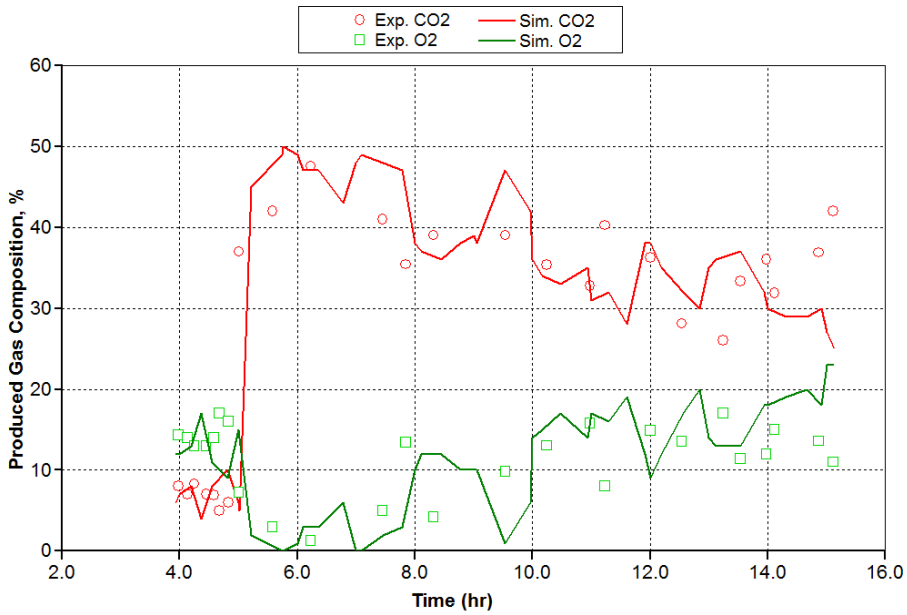

Fig. 51- Produced gas composition. A fair match was obtained between experimental and simulation data. The rise in CO_2 concentration at the end of the experiment is due to production of accumulated flue gases inside the combustion chamber.

Fig. 52 compares the cumulative produced gases. A fair match was obtained between the simulation and experimental data. When similar timing was tried for gas breakthrough, the simulation showed a very good match for O_2 production, but it had a higher rate of CO_2. This can be due to inaccurate CO_2 solubility and diffusivity modeling in the water and crude oil. The cumulative oil and water production match is illustrated in Fig. 53. While good matching was obtained, there is mismatch at early stages where the experimental model shows higher fluid production and the timing of the oil and water production are not preserved. This is because of porous media heterogeneities that were created during packing.

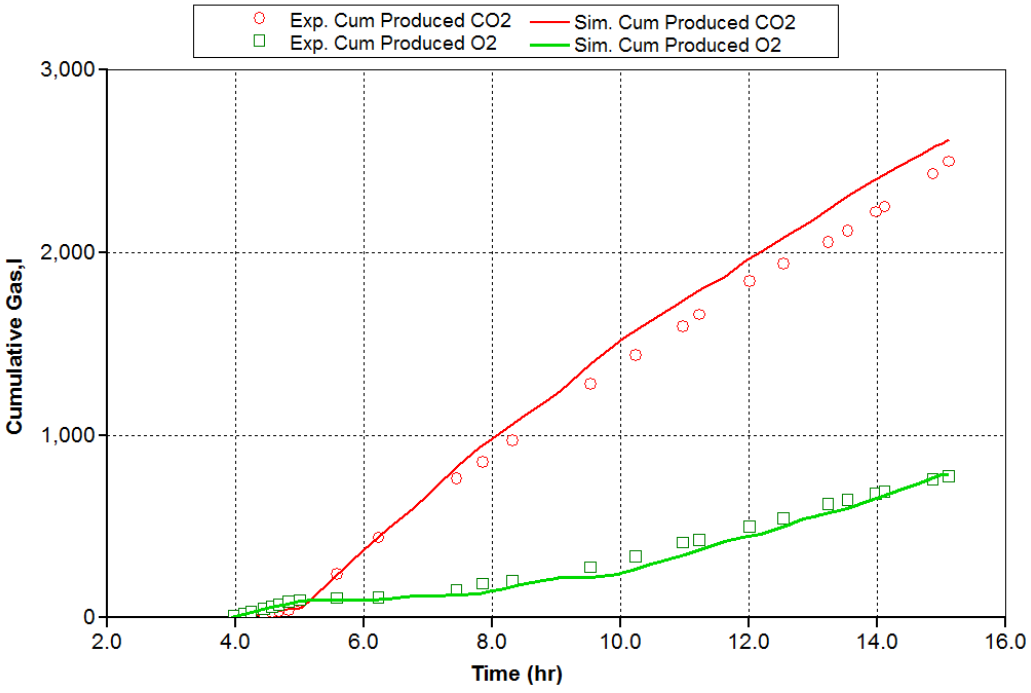

Fig. 52- Cumulative gas production. The simulation model was able to follow the trend and timing of the experimental data.

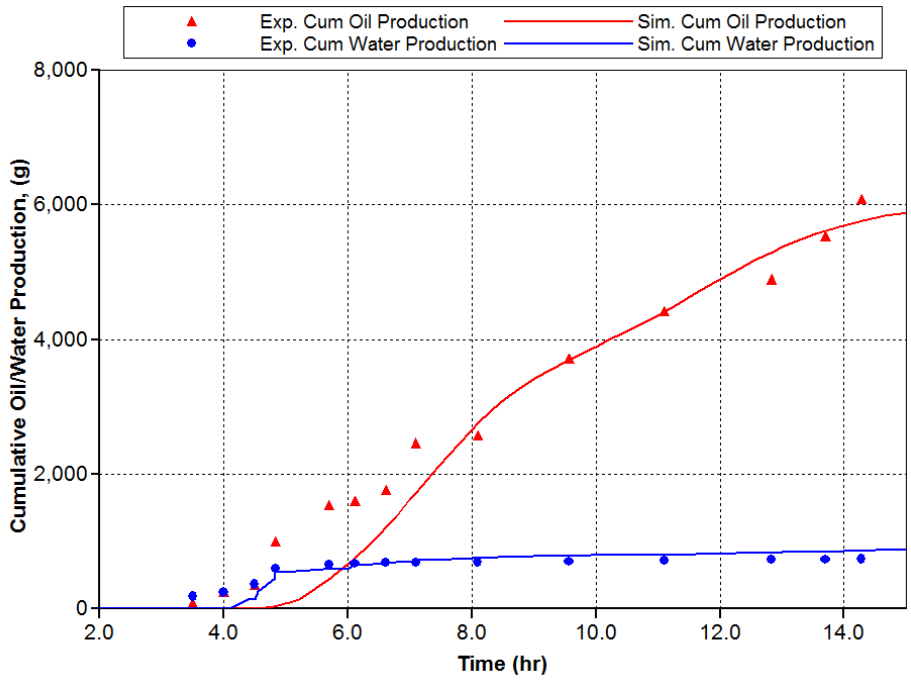

Fig. 53- Cumulative oil and water production. Sand pack heterogeneity was the main reason for the early mismatch of simulation and experimental data.

Fig. 54 shows the temperature of the injector at 7.62 cm form the injection side. Numerical results show a good match with experimental data during the preheating period (first 5 hours). However, it shows higher temperature at later stages when combustion front moved away from this point (7.62 cm). This is directly related to the difference between the heat losses in the numerical model and the experimental apparatus. In the numerical model, constant values were used for heat capacity and heat conductivity for the overburden formation, while in the experimental apparatus, heat conductivity of the inner insulation varied with temperature. Consistent trends were obtained in both cases in terms of preheating, timing of combustion initiation, and temperature decline at a later time.

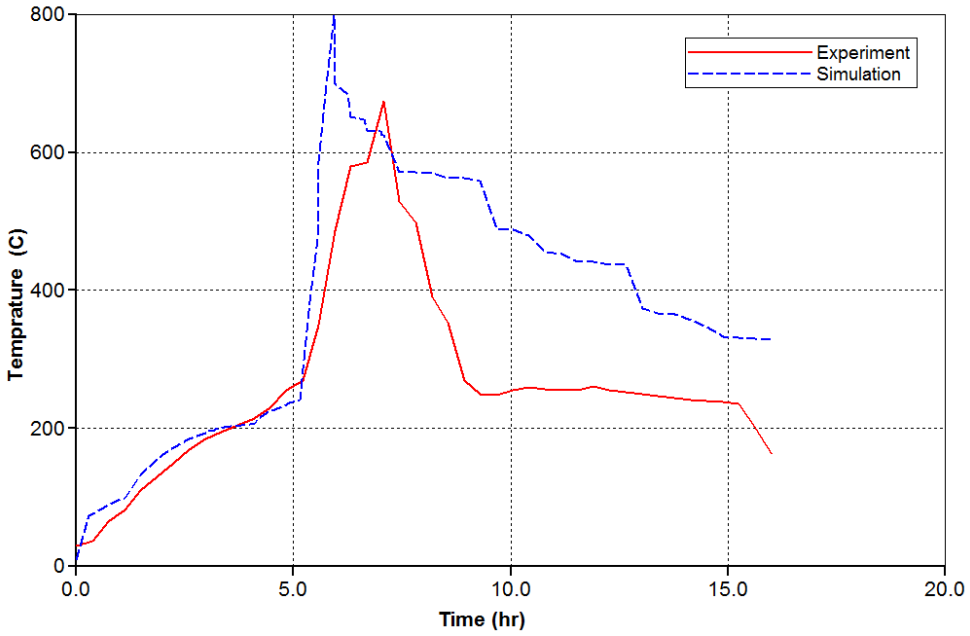

Fig. 54- Comparison between simulation and experimental results: temperature profile of injection well at 7.62 cm.

5.3 Comparison of CAGD with other thermal process

Field scale numerical simulations of SAGD, THAI, and CAGD methods were conducted, and their performance has been evaluated in terms of oil production rate and cumulative energy–to-oil ratio.

5.3.1 Field scale simulation mode

A three-dimensional (3D) Cartesian grid configuration was used to the represent reservoir model. The model showed is half symmetry along the horizontal well pair and consists of 32 grid blocks in the horizontal direction (total length of 72 m), 30 grid blocks in the vertical direction (total net pay of 36 m) and 10 grid blocks along the horizontal production well (total length of 500 m). In both CAGD and SAGD case the production well was located near the bottom of the reservoir and the injection well was

placed 6 m above the production well. The THAI model consisted of a horizontal producer positioned in line drive in the reservoir, and air was injected through a vertical injection well. Grid blocks were sufficiently refined near the injection vertical well to minimize computational time. Fig. 55 depicts the well configurations for these processes.

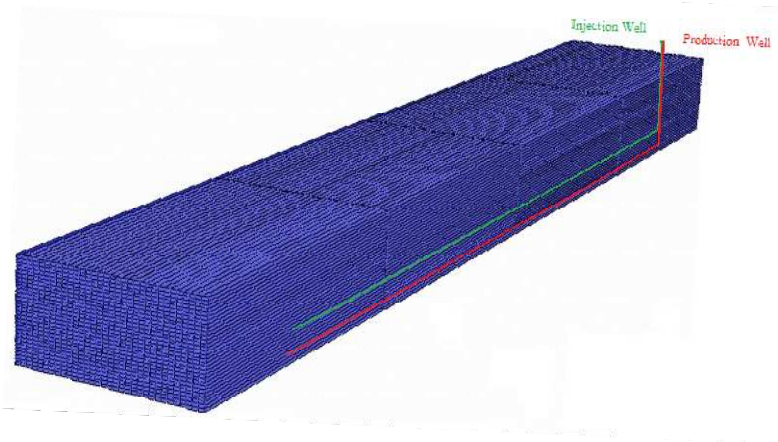

(a)

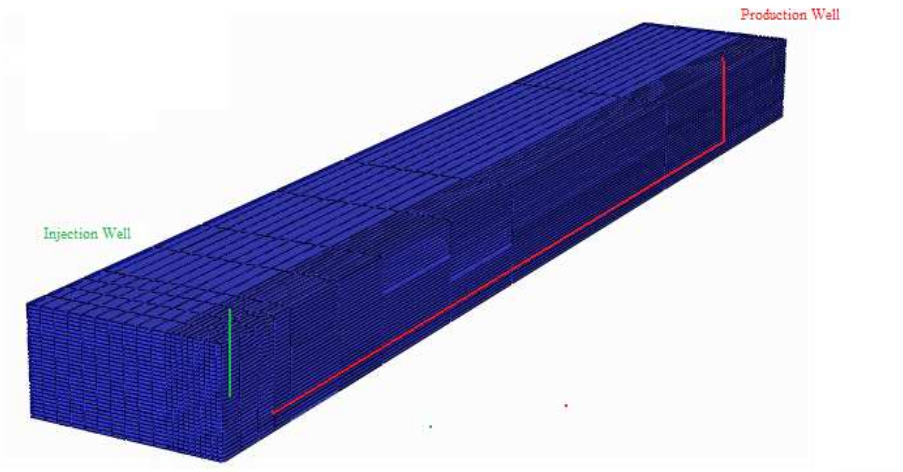

(b)

Fig. 55-Well configuration for (a) SAGD and CAGD, (b) THAI. In total 9600 grid block were used to represent the field scale model. Grid blocks were sufficiently refined near the injection vertical well to minimize computational time.

All simulation cases ran for 10 years. In first 3 months, steam was injected to preheat and increase oil mobility around paired wells and accelerate thermal communication between them. Moreover in the THAI and CAGD models, temperature around the injection well was increased to 350°C to ignite the combustion after switching to air injection. Igniters were simulated by adding heat to the grid blocks near the injection well. For this purpose, constant heat flux was assigned to the injection well grid blocks in such a way that after the preheating period (3 months) the temperature of the injection well increased to 250°C. This value was based on laboratory data. In a combustion override split production horizontal well (COSH), Coats et al. (1995) reported 2.8 m^3/m^2-hr air injection rates. Bagci et al. (2000) used a similar value (2.56 m^3/m^2-hr). Greaves et al. (1998; 2003) reported higher air requirements for the THAI process (5-22 m^3/m^2-hr). For the sake of simplicity in both the CAGD and THAI maximum air flux was set at 3 m^3/m^2-hr, which corresponds to 2.0E+7 m^3/day. The main features of the numerical model are listed in Table 10. In addition, the simulation model included heat losses to the overburden and underburden formations.

Table 10: Simulation model parameters in the range of Athabasca heavy oil reservoirs.

Reservoir Parameters	Value
Pay; h (m)	36
Porosity (%)	35
Horizontal Permeability	3000
Permeability Ratio, Kv/Kh	0.7
Oil Saturation, So (%)	0.7
Water Saturation, Sw (%)	0.26
Reservoir Pressure, (kPa)	2500
Operating Pressure, (kPa)	4000
Reservoir Temperature, (^{o}C)	18
Horizontal Well Length (m)	500
Well Spacing (m)	150
Vertical Spacing (m)	6

Fig. 56 and Fig. 57 show the oil production rate and oil cumulative production for the three processes. Simulation results indicated that the production rate for both SAGD and CAGD peaked in the first 2 years of operation. CAGD oil production rate exceeded SAGD oil rate after 3.5 years of operation when the combustion front was fully developed inside the model. Two factors should be considered in comparison of oil production rate for these two processes: first, the quantity of the heat created or injected in the formation, and second, heat delivery to the crude oil. Saturated steam has a higher ability to transfer heat to the oil than to hot combustion gases have. In the first 3.5 years of operation, SAGD showed higher production rate, but for the longer period of time, high temperature within the CAGD chamber led to a stable oil production rate. In the THAI process, a high-temperature gas chamber formed in a small portion of the

reservoir, and oil production rate (10 m^3/day) was relatively lower than for two other methods.

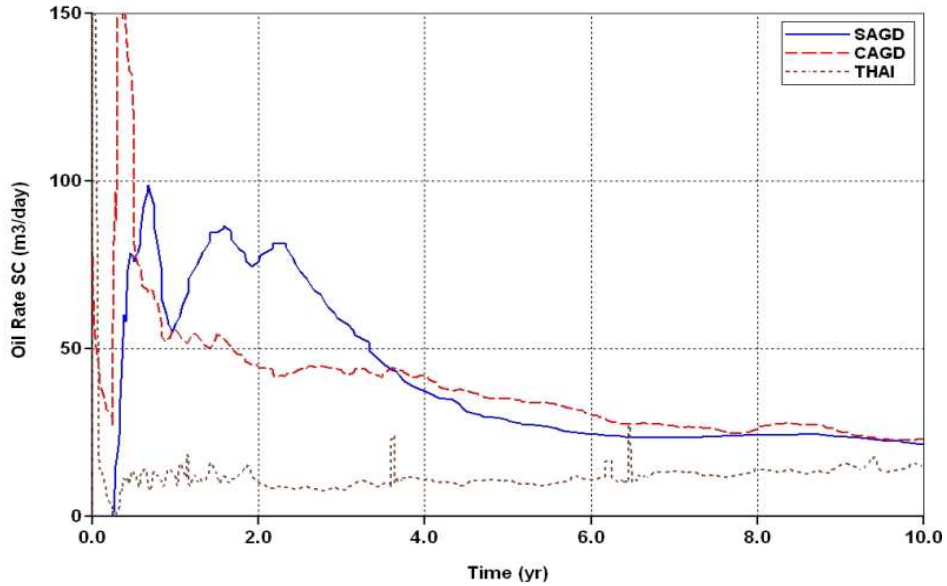

Fig. 56- Comparison of oil production rate for SAGD, CAGD, and THAI. CAGD has comparable oil production to SAGD after 3.5 years of operation. THAI has the lowest oil production rate.

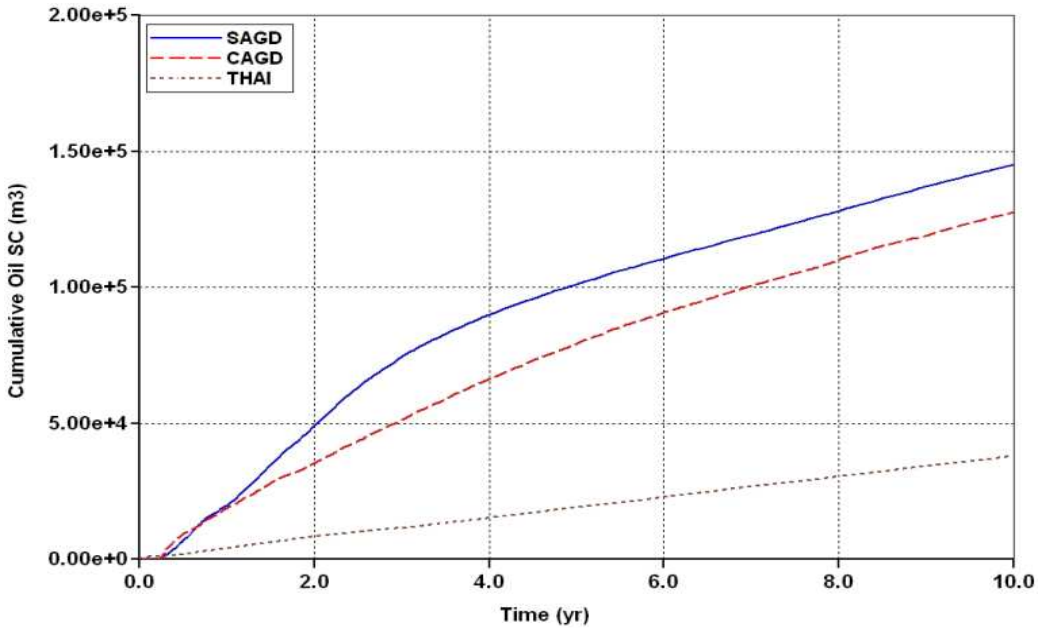

Fig. 57- Cumulative oil rate production for SAGD, CAGD and THAI.

Fig. 58 shows the temperature profile for three cases. Inside the steam chamber (SAGD), temperature was about 250°C given an injection pressure of 4000 kpa, while in CAGD the temperature near the combustion zone reached to 550°C and stabilized at this level. In the THAI process, initially, this number was about 500°C but gradually declined as the combustion front moved away from the injection point, where it reached to 350°C at the end of 7 years of air injection. Similar behavior was observed with the THAI file pilot test. When the combustion front moved far away from the injection well, it was difficult to provide oxygen to the combustion zone so most of the injected oxygen bypasses into the previously swept segments of the production well and did not participate in the oxidation reactions. As a result temperature declined. However in the CAGD process the distance between injection well and combustion front is relatively short, the combustion front is always provided with fresh air and temperature stay high. In addition, the CAGD well configuration has the advantage to use the full length of production well which led to a higher oil production rate.

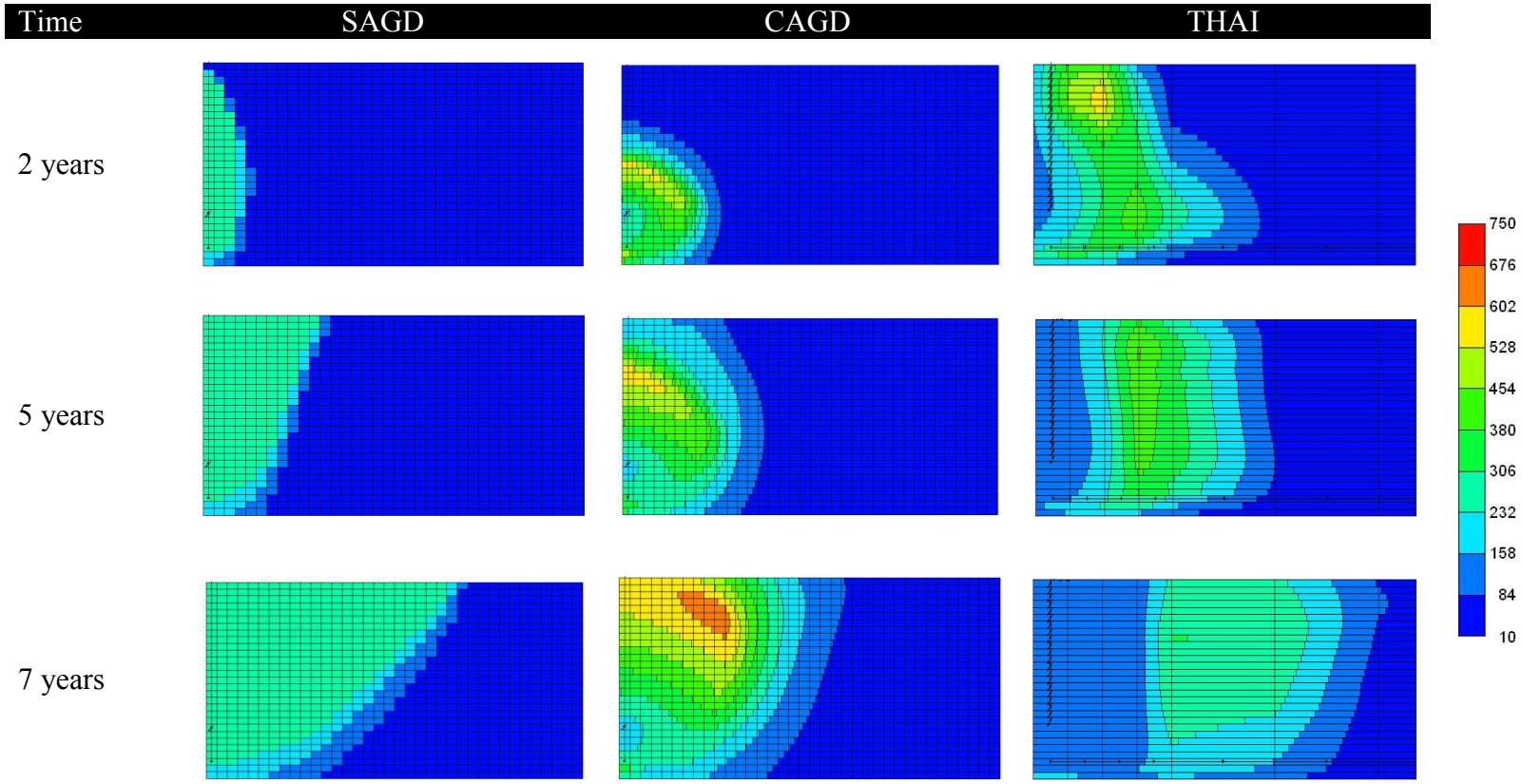

Fig. 58- Temperature profile (°C) comparison for SAGD, CAGD and THAI after 2, 5, and 7 years of operation. The THAI process cannot sustain high temperature inside the formation. In the CAGD process, the front temperature remained high even after 7 years of air injection.

5.3.2 Energy efficiency

Fig. 59 shows cumulative energy-to-oil ratio (cEOR). cEOR includes enthalpy of injected steam (SAGD) or energy required for compressing air (THAI and CAGD) and shows the energy efficiency for these processes. Appendix B summarized the energy calculations for steam and air injection process. This comparison indicates that CAGD process is significantly more energy efficient method compare to SAGD. CAGD process reduces the cEOR about 73% respects to SAGD while it shows a comparable oil production rate. The cEOR value for THAI stabilized at 3.14 GJ/Sm3 which is also lower than for SAGD. Table 11 summarizes the cEOR for these processes and the average of cEOR reduction respect to SAGD.

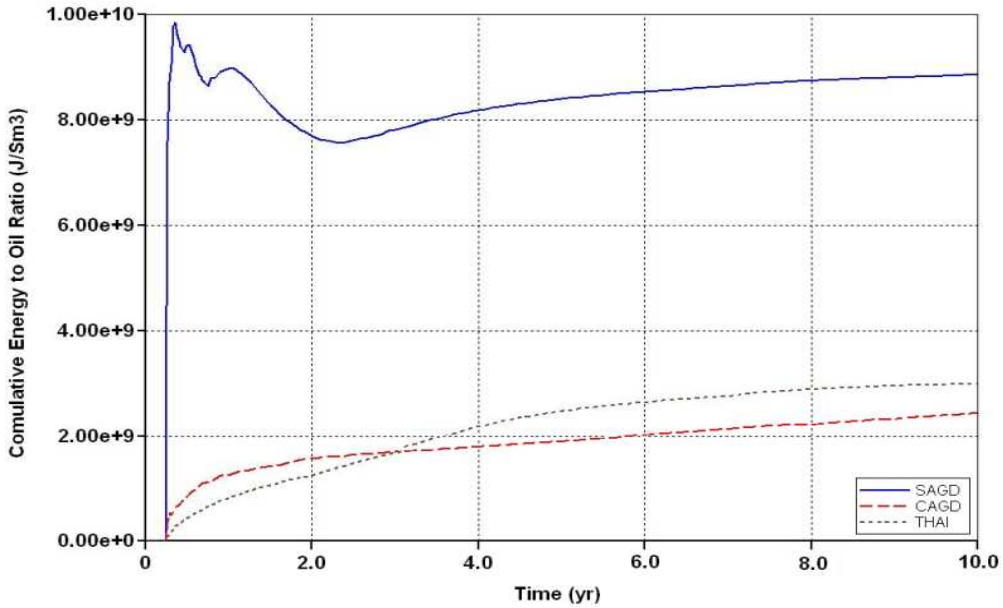

Fig. 59- Comparison of cumulative energy to oil ratio (cEOR). CAGD is the most energy efficient process compared to other two methods.

Table 11: Summary of cumulative energy to oil ratio. CAGD reduced the required energy by 72.8% compared to SAGD.

Process	cEOR, J/Sm^3	cEOR reduction respect to SAGD
SAGD	8.17E+9	0.0 %
THAI	3.14E+9	61.5 %
CAGD	2.21E+9	72.8 %

5.3.3 Flue gas emission

In the SAGD process, most flue gas emission is related to the burning of natural gas to produce steam. Fig. 60 compares cumulative CO_2 to oil ratio for the three processes. In the CAGD process, heavy fractions of oil were burned and more CO_2 was produced due to incomplete oxidation. However, generated flue gases were trapped inside the chamber at high pressure and decreased the overall CO_2 emission rate (Fig. 61). Flue gas emission reduced by 32% compared to SAGD. Furthermore, SAGD consumed on average about 37 m^3 (1,300 ft^3) natural gas and 0.1 m^3 of water per cubic meter of produced oil (0.9 bbl/bbl).

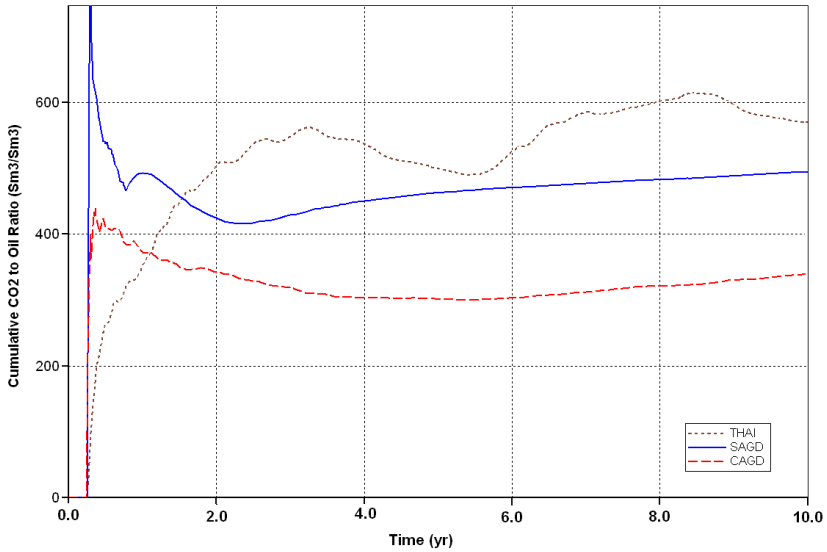

Fig. 60- Comparison of cumulative CO_2 to oil ratio (Sm^3/Sm^3). CAGD shows the lowest ratio compared of the three methods.

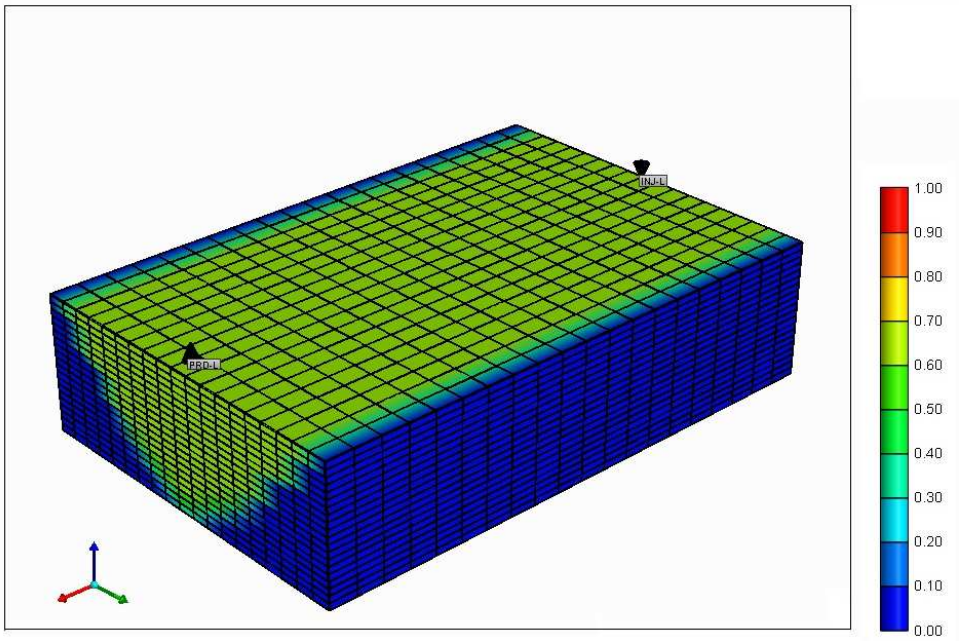

Fig. 61- Gas mole fraction (CO_2) in the CAGD combustion chamber after 10 years of air injection. The combustion chamber was filled by nearly 58% CO_2 gas. The flue gases that trapped inside the chamber at high pressure reduced the overall CO_2 emission.

Simulation results indicated that THAI well configuration causes serious drawbacks. First, this method is based on gravity drainage which itself is a slow process. Because combustion takes place in a small portion of the reservoir, the oil production rate is low. Second, as the combustion front moves inside the formation, the injection rate should be increased to push the air toward the combustion zone while most of the injected air bypasses through previously swept portions of the horizontal producer. Simulation results confirmed that the CAGD well configuration could be effective solution for these two problems. Horizontal well air injection provides wider area for air to combust and at the same time uses all portions of the horizontal producer. The combustion front is always near the injection point, and it is easier to deliver injected air to the combustion zone. This study did not involve economic analysis of these processes.

Although a detailed comparison of CAPEX and OPEX would provide a clearer indication of CAGD potentials.

Fig. 62 shows the oil saturation profile for the CAGD process after 6 years of air injection. Three distinct zones can be identified in this profile: the first zone, where oil saturation is zero, the water bank that was created by condensing of superheated steam in the low temperature area and finally, the initial oil bank. The pressure of the numerical model remained constant (4000 kpa) during the operation. The stability of the pressure was maintained by gravity drainage force.

Simulation results indicated that the oil production zone was in contact with hot steam. Heat generated by combustion created superheated steam inside the chamber; this steam delivered the heat to the crude oil and condensed. This created hot water bank ahead of the fire front (see Fig. 63). In other words steam plays an intermediate role to transfer the heat from combustion zone to the crude oil. This has a positive effect on the performance of the process due to the higher heat delivery of steam. Oil flux vectors confirm that most of produced oil is drained from those areas that are in contact with the steam.

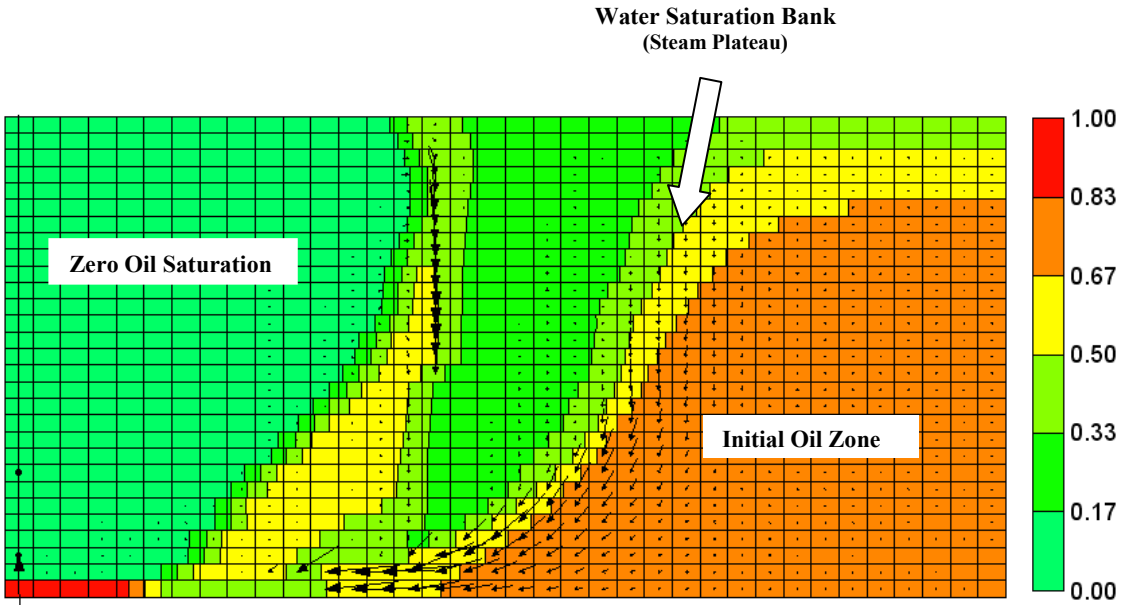

Fig. 62- Oil saturation profile after 10 years of air injection. Three distinct zones can be identified in this profile: The first zone where oil saturation is zero, the water bank that was created by condensing of superheated steam in the low temperature area and finally, the initial oil bank.

Fig. 64 depicts the temperature profile inside gas chamber at the end of the operation. The combustion front moved upward in the chamber due to density difference between injected air and initial crude oil. This created a hot temperature region at the top layer of the formation.

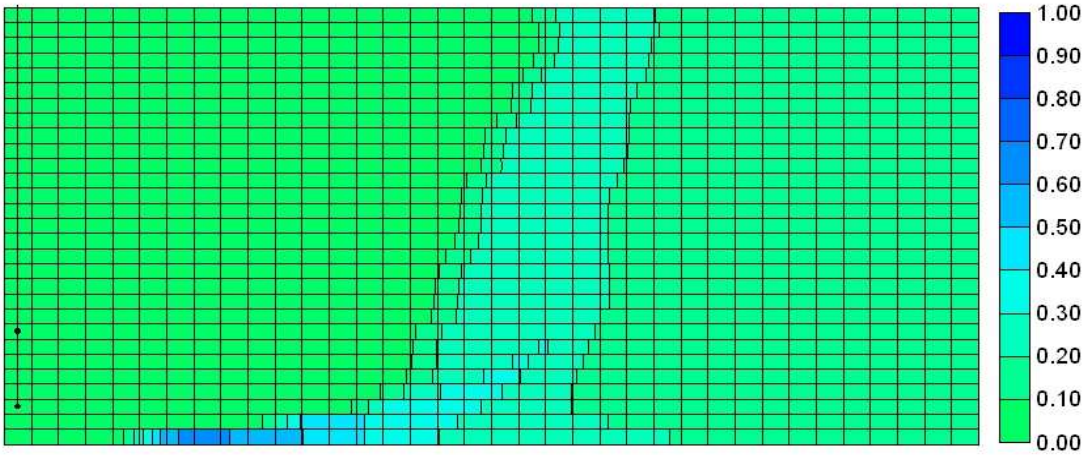

Fig. 63- Water saturation profile after 10 years of air injection. A water bank is created between the combustion front and initial crude oil. This water bank enhanced the heat transfer inside the model.

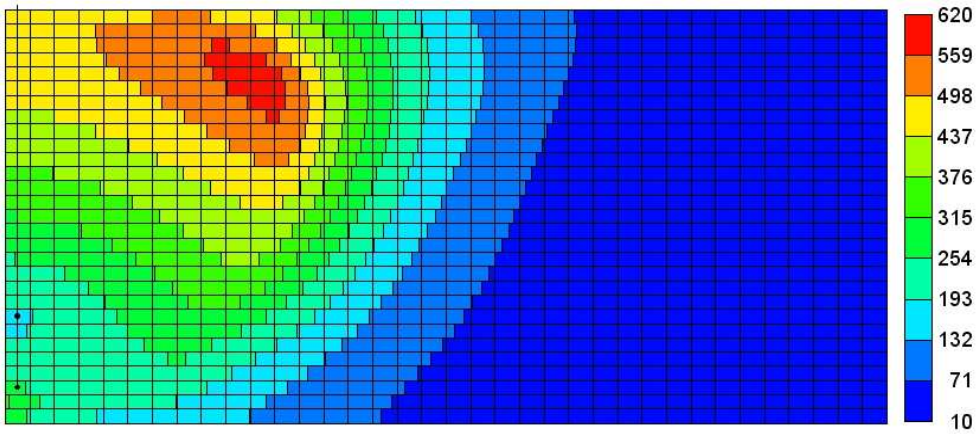

Fig. 64- Temperature (°C) profile inside the gas chamber after 10 years of gas injection.

5.3.4 Air injection rate

The effect of air injection rate and air enrichment on CAGD performance was studied. Fig. 65 shows the cumulative oil recovery for different air injection rates. Simulation results indicated that higher injection rates lead to the higher ultimate oil recovery.

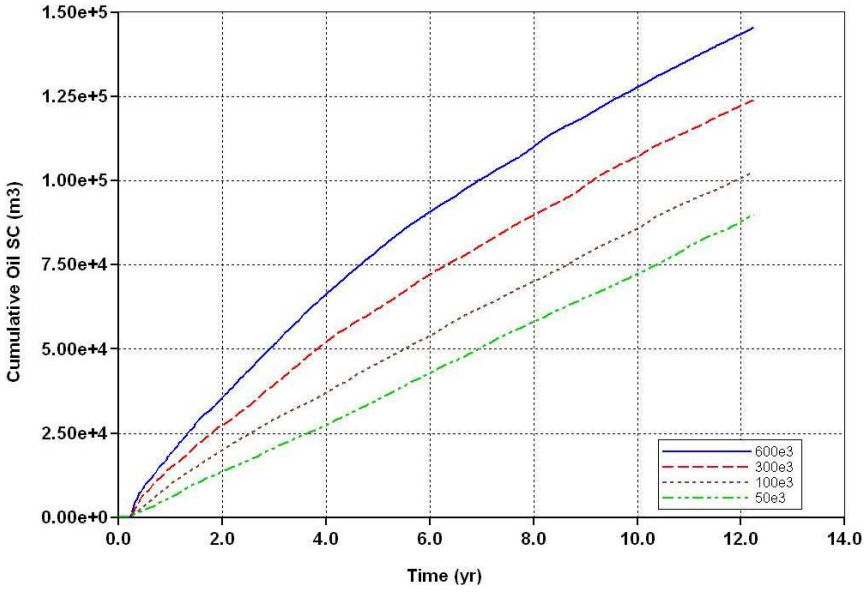

Fig. 65- Effect of air injection rate on the cumulative oil production.

Fig. 66 indicates that most of the injected air does not participate in the combustion reaction and just bypasses through the production well. In all cases, bypassed O_2 rate is stabilized.

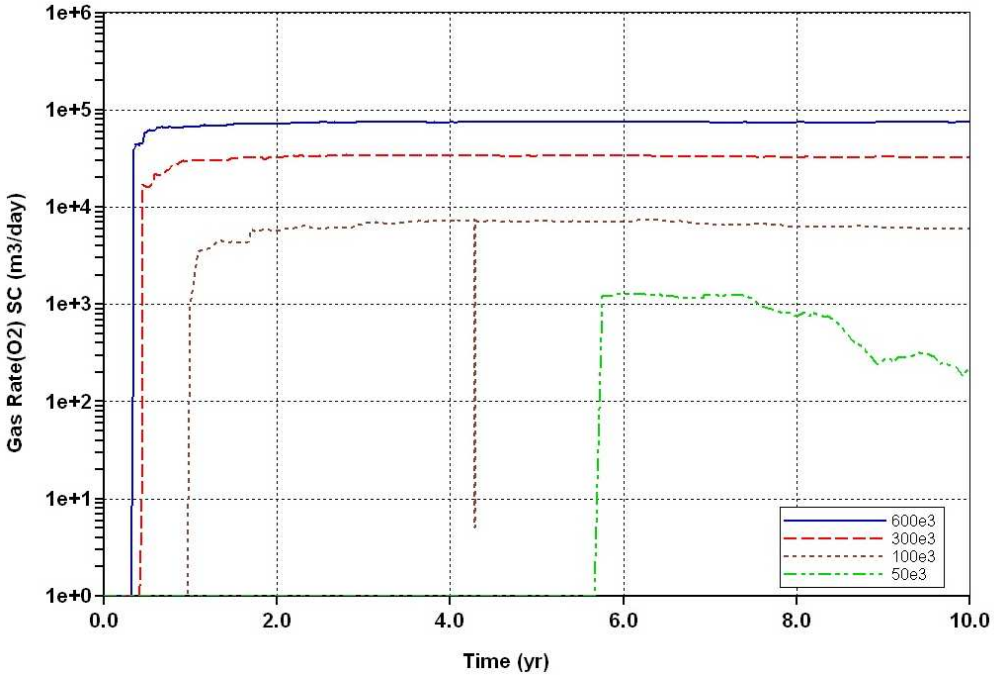

Fig. 66- Oxygen production for different rates of air injection. Higher air injection rates increased the bypassed oxygen but had a positive effect on gas circulation inside the chamber.

.

Higher air injection rates increases O_2 consumption and temperature inside the gas chamber. In general, the ratio of consumed O_2 declines air injection rate increases. This number decreases from 82% for 50,000 Sm^3/day to 40% for 600,000 Sm^3/day. In a typical air injection process the air to oil ratio is between 200 and 1200 Sm3/Sm3, while this value is higher for CAGD. The combustion front is not in the direction of the air flux, and just a portion of air flux circulates inside the gas chamber by gravity and reaches the combustion zone.

Fig. 67 shows the air flux vectors inside the gas chamber. Gas circulation is not perfect, and part of the flue gases will stay in the gas chamber and decrease the partial pressure of O_2. This flue gas accumulation has negative effect on the combustion process. Increasing the injection rate may improve the gas circulation.

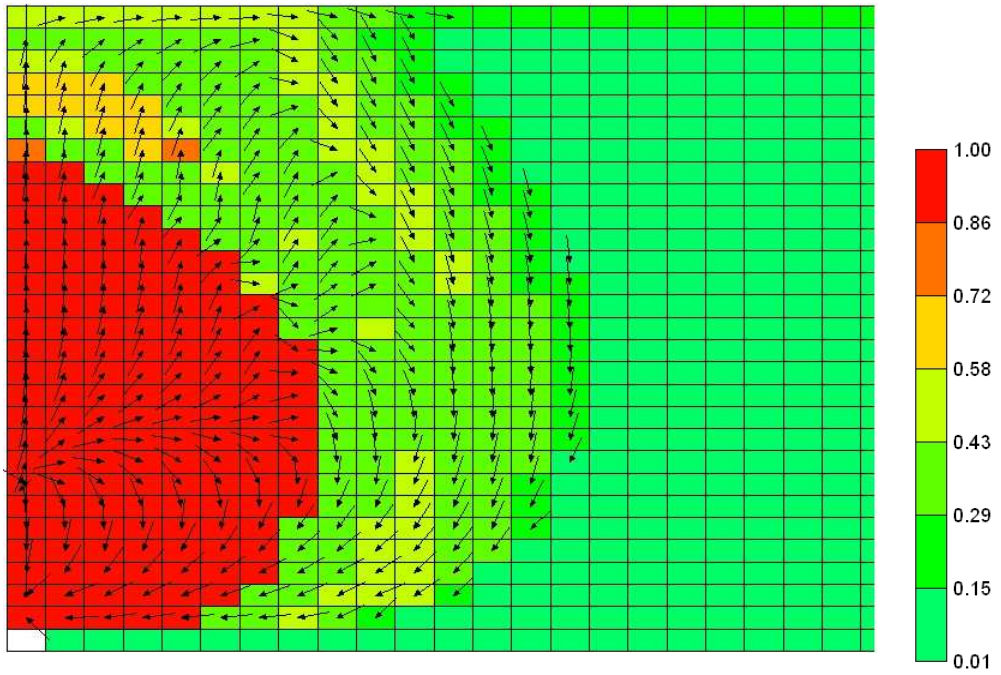

Fig. 67- Gas saturation profile and logarithmic-scale gas flux vector inside the chamber.

5.3.5 Air enrichment

Air enrichment is attractive option to lower the gas injection rate in the reservoir and consequently reduce the cumulative air-to-oil ratio. The effect of gas enrichment on oil production is shown in Fig. 68. In all cases, the gas injection rate is 100 Sm^3/day. The results indicated that high O_2 concentration can only slightly increase the cumulative oil

rate, and after 4 years of operation the oil production rate is more and less the same. Injecting 60% O_2 can improve the cumulative production rate by 20% compared to air injection; increasing injection rate is more effective than enriching the gas.

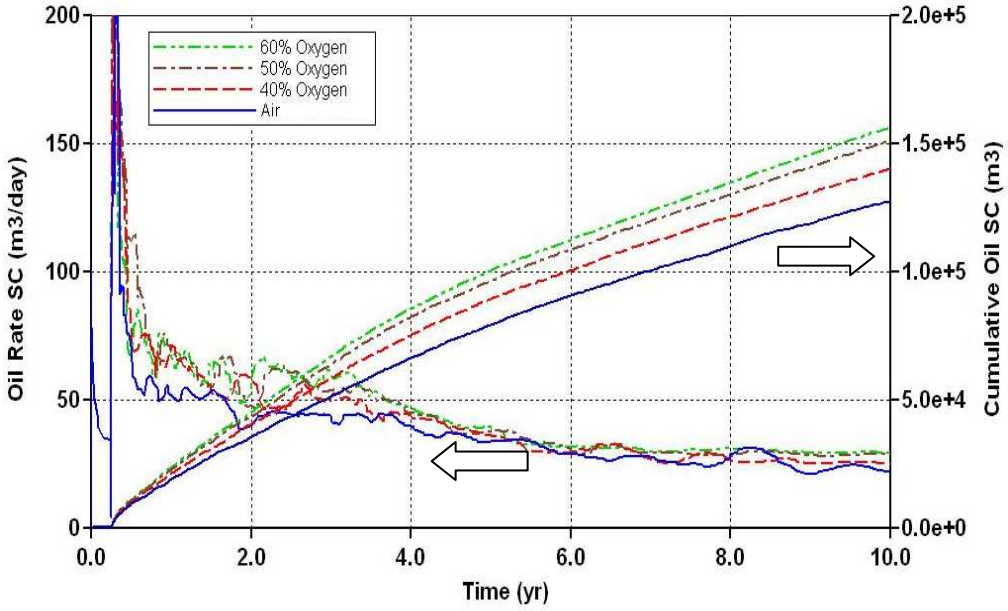

Fig. 68- Oil production rate and cumulative oil production for different concentration of O_2.

5.4 Single wellbore CAGD

Single wellbore CAGD helps to minimize the surface footprint and reduce the drilling cost. Fig. 69 shows the simulation model. In this model, two horizontal wells with vertical distance of 18.75 m were considered inside the formation (75% of net pay). A single wellbore was used for air injection and fluid production. Air was injected through the annulus, and downhole fluid was transferred to the surface through tubing, the simple wellbore design is shown in Fig. 70.

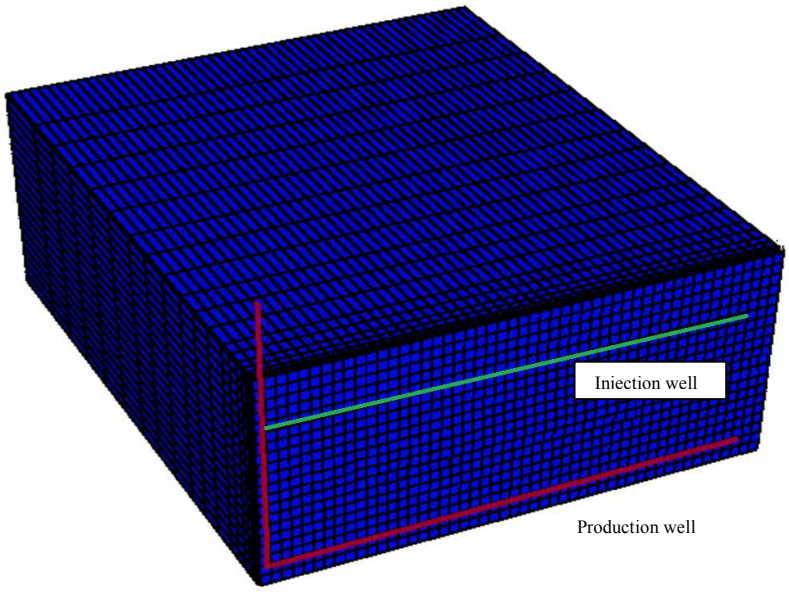

Fig. 69- Schematic of the half symmetry single wellbore CAGD numerical model.

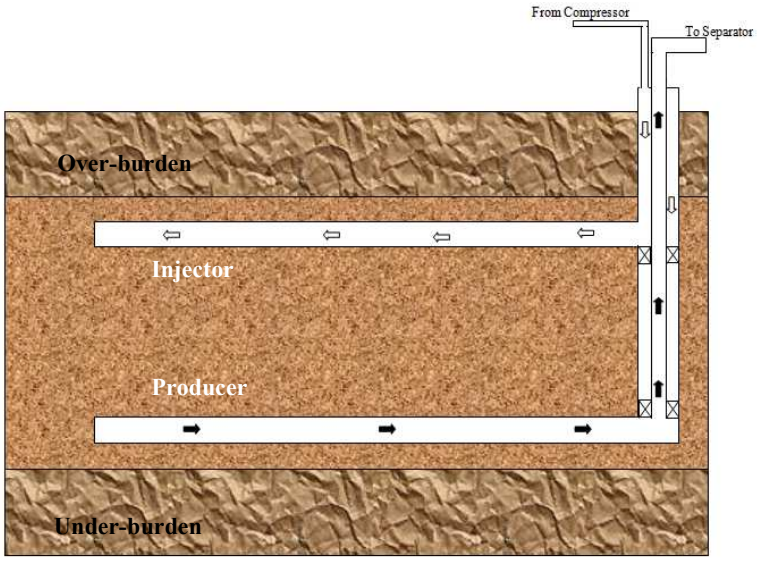

Fig. 70- Schematic of well structure in the single wellbore CAGD process. Air was injected through the annulus and downhole fluid was transferred to the surface through tubing

The length of the horizontal well was 50 m. An electrical heater was placed at the heel of the injection well. The goal was to initiate the combustion front from the end

section of the injection well and continuously advance it to the toe section. Fig. 71 depicts the temperature profile inside the formation at different time. Initially, the end section of the horizontal injector was heated up for 3 months. Target temperature was set at 400°C which can be achieved using downhole electrical heater in field operation. The combustion front initiated from heel section of the injection well and progressively developed in the lateral and forward directions. The injection well directed the path of the combustion front movement.

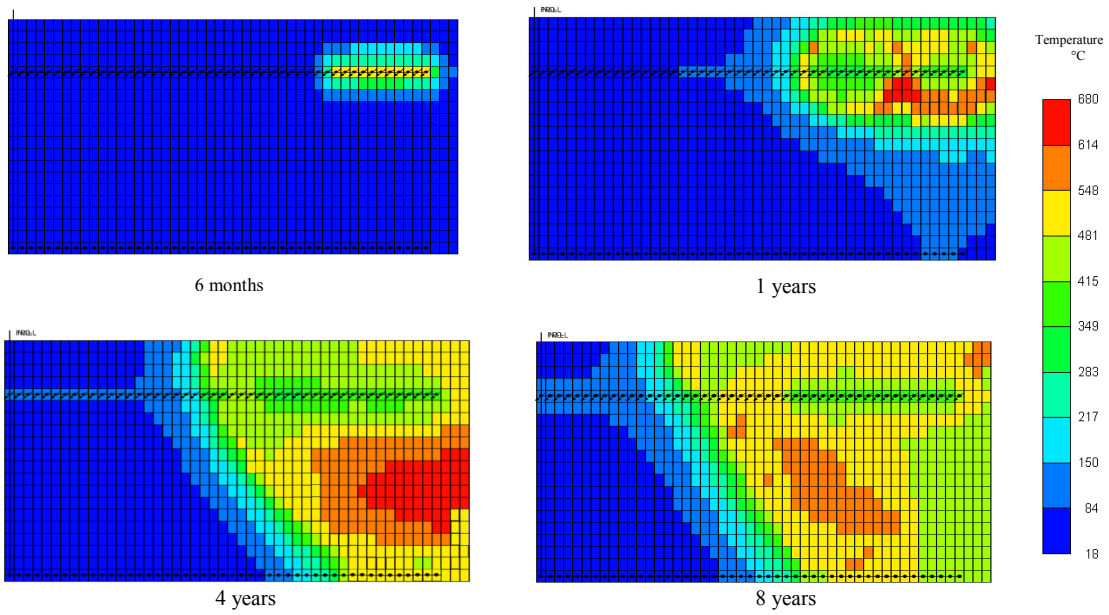

Fig. 71- Temperature profile of single wellbore CAGD process at different times. The injection well directs the path of combustion front movement.

Fig. 72, illustrates the oil saturation profile inside the model. Simulation results indicated that this well configuration can effectively sustain the combustion front inside the model. Stable oil sweep can be observed in this figure.

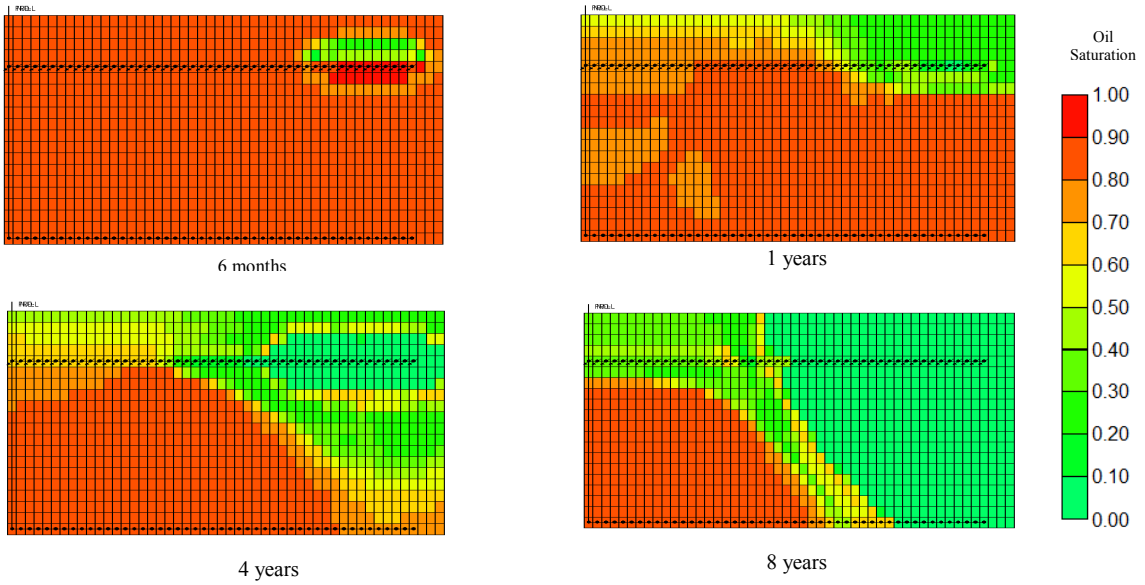

Fig. 72- Oil saturation profile for single wellbore CAGD process. Steady sweep was observed during air injection.

Fig. 73 shows the pressure profile in a vertical section inside the formation. At the early preheating period (first 3 month), pressure of the toe section of injector start to increase due to thermal expansion of rock and fluid where pressure increased up to 5,215 kpa (757 psi). Pressure communication between the horizontal wells help to stabilize the pressure inside the formation where it stayed between 4100 kpa (595 psi) to 4000 kpa (580 psi). Fig 74 depicts the coke saturation profile in different snapshot. Coke concentration moved from toe to heel section of injector. Coke saturation profile is an approximate of the combustion zone.

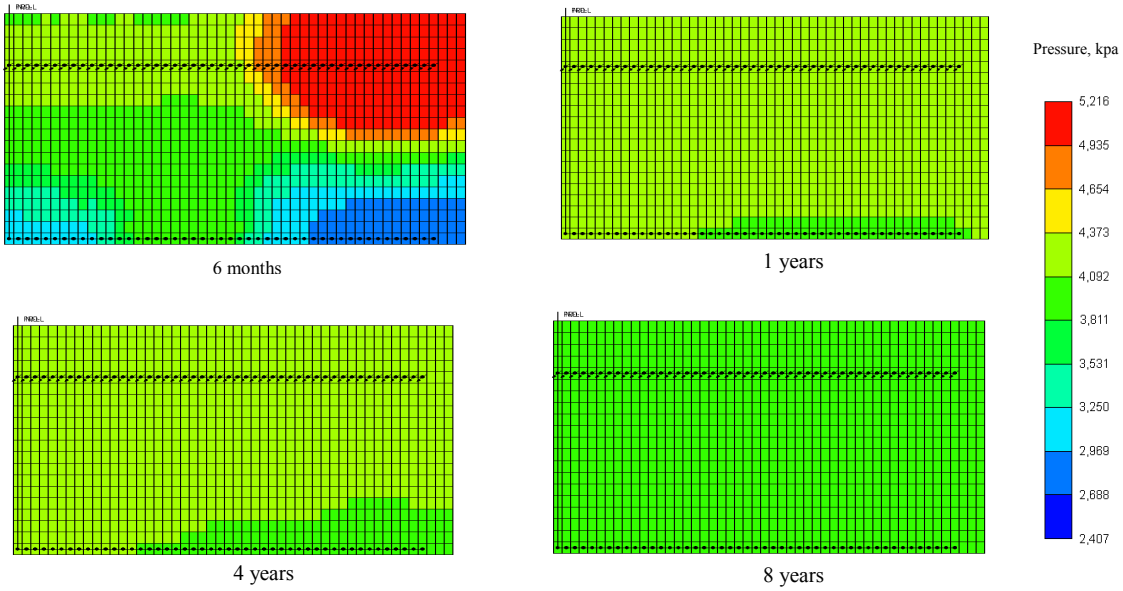

Fig. 73- Pressure profile for single wellbore CAGD process. At the end of preheating period, pressure of the toe section increased due to thermal expansion of rock and fluid.

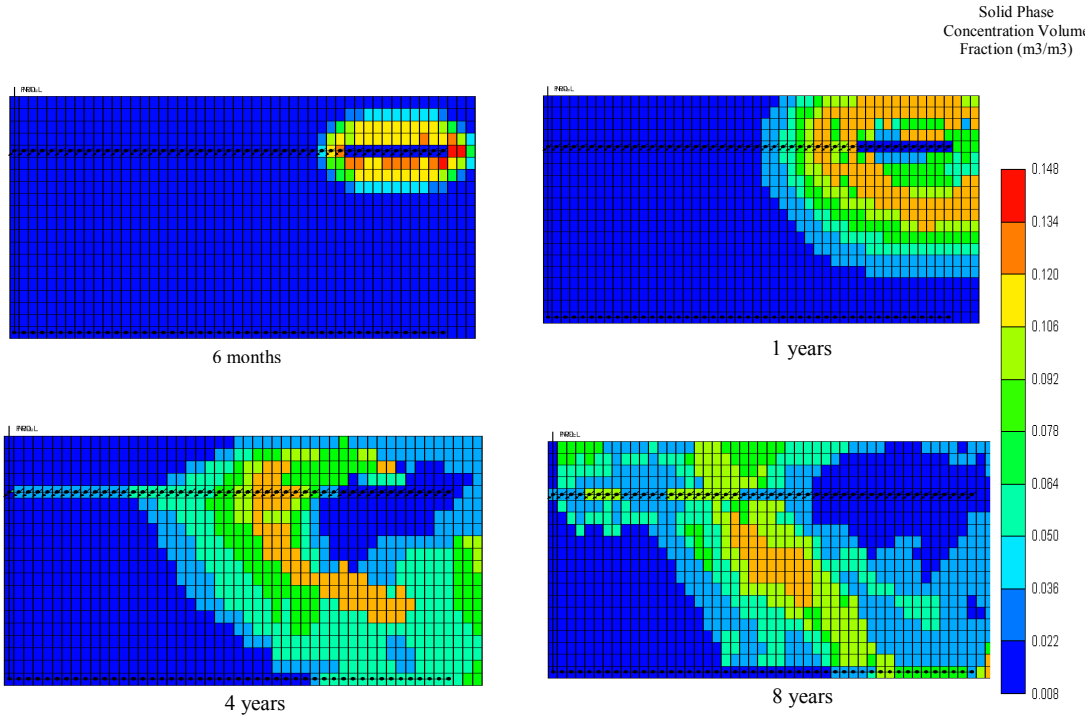

Fig. 74- This picture shows the concentration of deposited coke on the sand grain surface. The coke concentration moved from toe to heel section of injector. The coke saturation profile is an approximate of the combustion zone. Coke is the fuel for oxidation reactions.

Fig. 75 shows the cumulative and production rate for 10 years of air injection. The oil production rate peaked after 6 years and then continuously declined until it reaches to near 0.6 m3/day (3.18 bbl/day) at the end of the combustion process. This peak is related to break through of the mobilized oil. After this time, oil production declined as the combustion front swept the formation. Cumulative oil production was about 2,845 m3 (178,900 bbl), which corresponds to 78% OOIP recovery.

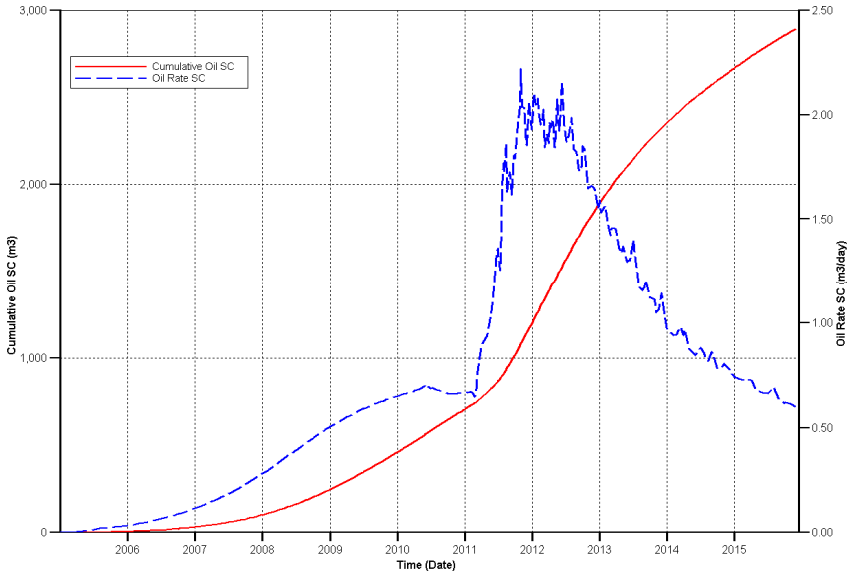

Fig. 75- Cumulative and oil production rate for the single wellbore CAGD process. Oil production rate peaks after 6 years of air injection (including 3 month of preheating). This peak is related to break through of the mobilized oil. After this time, oil production declined as combustion front swept the formation.

Fig. 76 shows the permeability variation in middle part of injection well as determined from simulation of single wellbore CAGD. At the preheating period (first 3 month) the porosity of the grid block increased due to pore pressure rise (thermal expansion) which resulted in permeability increase. Later on, coke formation reduced the porosity from 37% to below 32% which is translated to permeability reduction from 3,200 md to below 1,500 md. Coke formation is necessary for combustion process. Coke

provide fuel for oxidation reactions however unburned coke deposits reduce the permeability and as a result alter the fluid flow in the formation.

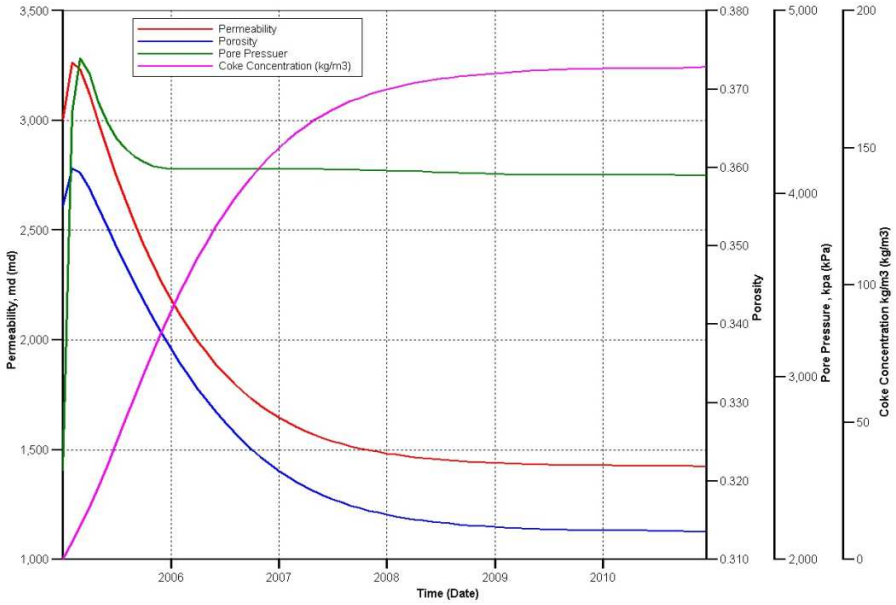

Fig. 76- Permeability variation in middle section of injection well.

5.4.1 Vertical well spacing

Vertical distance between the horizontal pair wells is very important in CAGD process. Larger spacing causes substantial delay in pressure and thermal communication between wells. This issue can be critical in the formation with low initial crude oil mobility. From other side, smaller well spacing increase the chance of production well plugging by deposited coke as it was discussed in experiment Run1. Fig. 77 shows the oil production rate for different vertical well spacing of 0.25, 0.5, and 0.75 of total net pay. Increasing well spacing from 0.25 to 0.5 and 0.75 of total net pay delayed the oil production peak for 2 and 5 years. Fig. 78 shows the comparison of oil recovery for different vertical well spacing. Larger well spacing leads to higher recovery.

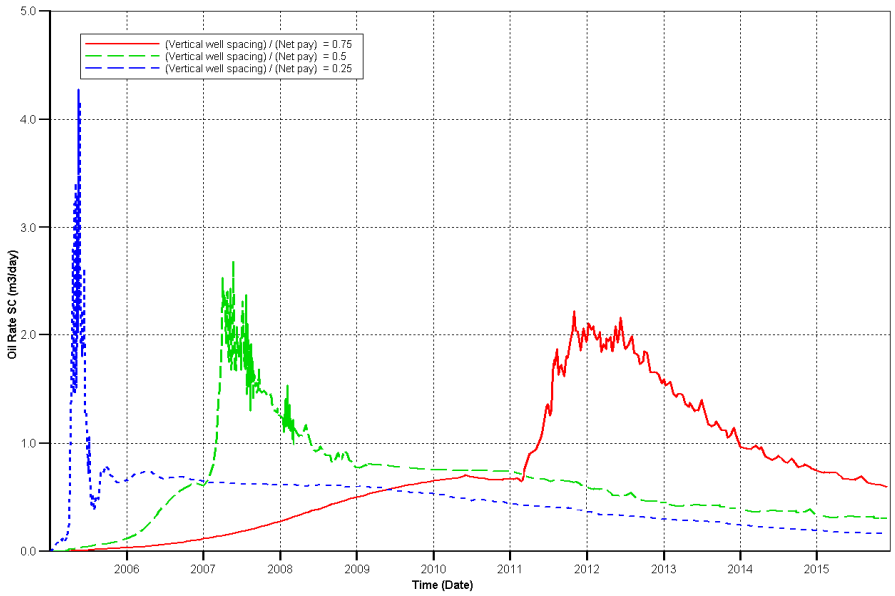

Fig. 77- Oil production rate comparison for three different vertical well spacing. Larger well spacing delays the oil production peak.

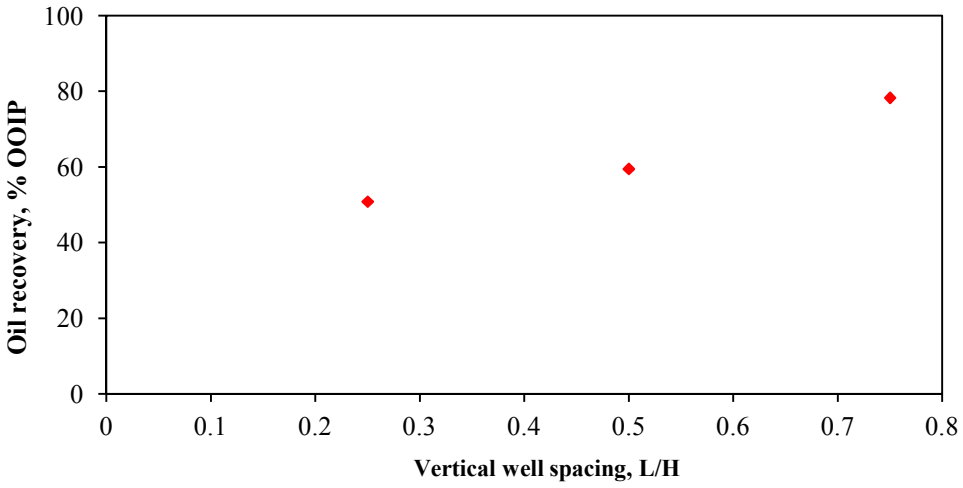

Fig. 78- Comparison of oil recovery for different vertical well spacing.

6. CONCLUSIONS AND RECOMMENDATIONS

6.1 Conclusions

Experimental and theoretical research through reservoir simulation has been conducted for better understanding of the CAGD process and combustion gravity drainage mechanisms. Vertical well spacing, initial crude oil viscosity, and oxygen partial pressure were the key variables that were selected for this study. A reservoir simulation model was used for history matching the laboratory data and to investigate the performance of the CAGD process at field scale. The following main conclusions can be drawn from this study:

1. Experimental evidences indicated that the CAGD process can effectively produce heavy oil by creating a hot region inside the formation. Stable sweep and high oil recovery identify CAGD as a high-potential recovery method for primary production.
2. Experimental observations showed that for the close vertical well spacing (Run 1), a cylindrical coke layer forms around the horizontal well pair and terminates the process prematurely by plugging the producer and restricting the gas circulation within a limited area. Increasing the vertical well spacing (Run 2) not only eliminated this problem, but also formed a gas-seal layer between the injector and producer, which enhanced the circulation of the injected oxygen inside the combustion chamber. This minimized the bypassed air rate. Similarly, the same behavior is expected at field scale, where a CAGD process with close vertical well spacing (Similar to SAGD) is not feasible.

3. The combustion front is fully stable due to the gravity drainage mechanism. Stable sweep results in oil recovery up to 82% OOIP (Run 2). However, this value is an optimistic recovery prediction in comparison to field scale, where there are no lateral boundaries for drainage volume.
4. Experimental data indicated that more than 60% of injected O_2 is consumed and most of the flue gases are continuously produced during the process, confirming the circulation of the injected O_2 inside the combustion chamber. The CAGD well configuration leads to better control of the moving direction of the combustion front. Since the combustion zone follows the path of the injection well it helps to deliver the sufficient oxygen to the oxidation zone and preserves the high-temperature oxidation mode (HTO).
5. The CAGD process with a bottom horizontal producer provides direct production of mobilized oil. In this way, upgraded oil drains directly to the producer and does not mix with the cold crude oil, thus preserving the thermal upgrading. Initial density of 9.15ºAPI was enhanced to 14.37ºAPI and correspondingly, the measured viscosity at 25 ºC, was reduced from 24,800 cp to 873 cp.
6. The CAGD process has been tested using the extra viscosity heavy oil (Athabasca bitumen). This test showed that lower mobility of the initial crude oil did not terminate the process. The combustion front is more uniform than to similar experiment with Peace River heavy oil, and ultimate oil recovery reached 72% OOIP. Also on average 70% of injected oxygen is consumed in combustion

zone. Athabasca tar sand bitumen was upgraded from its original value of 8.24 to 10.4°API.

7. A numerical simulation model was constructed based on physical properties for history matching of laboratory results. Simulation data showed fairly good matches with experimental data in terms of produced gas composition, cumulative CO2 and O2, and oil and water production rate.
8. In the THAI process, a small portion of the reservoir is affected by the combustion front and only a small part of the horizontal well is used, as a consequence, despite the high-temperature front inside the gas chamber, the oil production is lower than with CAGD. Moreover, by advancing the process and moving the combustion front moves away from the injection well decreases the average temperature of gas chamber.
9. A comprehensive study of CAGD, THAI and SAGD processes using a validated numerical model based on an Athabasca heavy oil reservoir indicated that CAGD improves the cumulative energy-to-oil ratio by 73% and reduces flue gas emissions by 33% compared to SAGD, while it has the same oil production rate.
10. Simulation results showed that in-situ steam generation in the CAGD process accelerates the heat convection inside the formation. Steam transfers the generated heat from the combustion zone to the cold regions.

6.2 Recommendations and future work

1. A high-pressure laboratory model is needed for further experimental study. Laboratory model should be able to maintain up to 4137 kpa (600 psi) pressure. This value corresponds to the typical heavy oil reservoir.
2. Mathematical modeling for the coke formation and oxidation reactions are recommended. Permeability reduction due to coke deposition is not addressed precisely in the literature and simulators. Detailed kinetic modeling can provide essential information for coke consumption and deposition. Simultaneous Thermo-gravimetric analysis (TGA) and differential scanning calorimetric (DSC) analysis is recommended to get better understanding of oxidation reactions.
3. Experimental study is required to investigate the effect of venting wells on the stability and performance of the CAGD process or minimizing the bypassed oxygen rate in the production well.
4. Further simulation and experimental study are required for optimum vertical spacing between paired wells.

REFERENCES

Abu-Khamsin, S.A., Brigham, W.E., and Ramey Jr., H.J. 1988. Reaction Kinetics of Fuel Formation for in-Situ Combustion. SPE Reservoir Engineering 3 (4): 1308-1316.

Abuhesa, R.H. and Hughes, R. 2009. Comparison of Conventional and Catalytic in Situ Combustion Processes for Oil Recovery. Energy Fuels 23 (1): 186–192.

Adegbesan, K.O., Donnelly, J.K and Moore, R.G. 1987. Low-Temperature Oxidation Kinetic Parameters for in-Situ Combustion Numerical Simulation. SPE Reservoir Engineering 2 (4): 573-582.

Akin, S., Bagci, S., and Kok, M.V. 2000. Dry Forward Combustion with Diverse Well Configurations. Paper SPE-62551 presented at the SPE/AAPG Western Regional Meeting, Long Beach, California.

Allen, J.C. and Shum, Y.M. 1976. Thermal Recovery Method. US Patent No. 3,991,828.

Ayasse, C., Bloomer, C. and Lyngberg, E. 2005. First Field Pilot of the THAI Process. Paper 2005-142 presented at the Canadian International Petroleum Conference, Calgary, Alberta.

Ayasse, C., Greaves, M., and Turta, A. 2002. Oilfield In-Situ Hydrocarbon Upgrading Process. Patent No. 6,412,557.

Bae, J.H. 1977. Characterization of Crude Oil for Fireflooding Using Thermal Analysis Methods. Society of Petroleum Engineers Journal 17 (3): 211-218.

Bagci, S. 1998. Estimation of Combustion Zone Thickness During in Situ Combustion Processes. Energy and Fuels 12(1): 1153-1160.

Barzin, Y., Moore, R.G. and Mehta, S.A. 2010. Role of Vapor Phase in Oxidation/Combustion Kinetics of High-Pressure Air Injection (HPAI). Paper SPE-135641-MS presented at the SPE Annual Technical Conference and Exhibition, Florence, Italy

Belgrave, J.D.M., Moore, R.G. and Ursenbach, M.G. 1993a. A Comprehensive Approach to In-Situ Combustion Modeling. SPE Advanced Technology Series 1 (1): 98-107.

Belgrave, J.D.M., Moore, R.G., Ursenbach, M.G. 1993b. A Comprehensive Approach to In-Situ Combustion Modeling. SPE Advanced Technology Series 1 (1)

Bhattacharya, R.N. and Chattopadhyay, S.K. 2007. Challenges in Workover Jobs During in-Situ Combustion Process in India-a Field Experience. Paper SPE-109906 presented at the Asia Pacific Oil and Gas Conference and Exhibition, Jakarta, Indonesia

Bousaid, I.S. and Ramy Jr., H.J. 1968. Oxidation of Crude Oil in Porous Media SPE Journal of Petroleum Technology 8 (2): 365-381

Brown, A., W. S., Huang and Shum. 1985. Thermal Injection and In-Situ Combustion Process for Heavy Oils. Patent No. 4,495,994.

Buxton, T.S. and Pollock, C.B. 1974. The SLOSS COFCAW Project-Further Evaluation of Performance during and after Air Injection. SPE Journal of Petroleum Technology 26 (12): 1439-1448.

Carcoana, A. 1990. Results and Difficulties of the World's Largest In-Situ Combustion Process: Suplacu De Barcau Field, Romania. Paper SPE-5865 presented at the SPE/DOE Enhanced Oil Recovery Symposium, Tulsa, Oklahoma.

Chien, S.-F., Shum, Y.-M., and Korstad, R.J. 1976. Numerical Simulation of Temperature Profiles and Oil Production During Dry or Wet in -Situ Combustion for an Inverted 5-Spot Pattern. Paper SPE-18751 presented at the SPE Symposium on Numerical Simulation of Reservoir Performance, Los Angeles, California.

Chu, C. 1982. State-of-the-Art Review of Fireflood Field. SPE Journal of Petroleum Technology 34 (1): 19-36.

Coates, R., Lorimer, S., and Ivory, J. 1995. Experimental and Numerical Simulations of a Novel Top Down In-Situ Combustion Process. Paper 30295-MS presented at the SPE International Heavy Oil Symposium, Calgary, Alberta, Canada.

Craig Jr., F.F. and Parrish, D.R. 1974. A Multipilot Evaluation of the COFCAW Process. SPE Journal of Petroleum Technology 26 (6): 659-666.

Cram, P.J. and Redford., D.A. 1978. Low-Temperature Oxidation Method for the Recovery of Heavy Oils and Bitumen. Patent No. 4,114,690.

Cristofari, J., Castanier, L.M., and Kovscek, A.R. 2008. Laboratory Investigation of the Effect of Solvent Injection on In-Situ Combustion. SPE Journal 13 (2): 153-163.

Dabbous, M.K. and Elkins, L.E. 1976. Preinjection of Polymers to Improve Oil Recovery by Subsequent Micellar Flooding. Paper PETSOC-7618 presented at the Annual Technical Meeting, Calgary, Alberta.

Dabbous, M.K. and Fulton, P.F. 1974. Low-Temperature-Oxidation Reaction Kinetics and Effects on the In-Situ Combustion Process. Society of Petroleum Engineers Journal 14 (3): 253-262.

Dart, J.C., Savage, R.T. and Kirkbride, C.G.,. 1949. Regeneration Characteristics of Clay Cracking Catalyst. Chemical Engineering Progress 45: 102-110.

Evans, E.B. 1937. The Viscosity—Temperature Relationships of Hydrocarbons. Paper WPC-2162 presented at the World Petroleum Congress, Calgary, Alberta.

Fassihi, M.R., Brigham, W.E., and Ramey Jr., H.J. 1984a. Reaction Kinetics of In-Situ Combustion: Part 1-Observations. Society of Petroleum Engineers Journal 24 (4): 399-407.

Fassihi, M.R., Brigham, W.E., and Ramey Jr., H.J. 1984b. Reaction Kinetics of In-Situ Combustion: Part 2—Modeling. Society of Petroleum Engineers Journal 24 (4): 408-416.

Freitag, N.P., Exelby, D.R., and Neate, C.J. 2006. A SARA-Based Model for Simulating the Pyrolysis Reactions That Occur in High-Temperature EOR Processes. Journal of Canadian Petroleum Technology 45 (3).

Freitag, N.P. and Verkoczy, B. 2005. Low-Temperature Oxidation of Oils in Terms of SARA Fractions: Why Simple Reaction Models Don't Work. Journal of Canadian Petroleum Technology 44 (3):584-601

Galas, C.M.F. and Ejlogu, G.C. 1993. Enhancement of in-Situ Combustion by Steam Stimulation of Production Wells. SPE Reservoir Engineering 8 (4): 270-274.

Garon, A.M., Kumar, M., and Lau, K.K. 1986a. A Laboratory Investigation of Sweep During Oxygen and Air Fireflooding. SPE Reservoir Engineering 1(5).

Garon, A.M., Kumar, M., and Lau, K.K. 1986b. A Laboratory Investigation of Sweep During Oxygen and Air Fireflooding. SPE Reservoir Engineering 1 (6).

Gates, C.F. and Sklar, I. 1971. Combustion as a Primary Recovery Process—Midway Sunset Field. SPE Journal of Petroleum Technology 23 (08): 981-986

Gerritsen, M., Kovscek, A., and Castanier, L. 2004. Experimental Investigation and High Resolution Simulator of in-Situ Combustion Processes; 1. Simulator Design and Improved Combustion with Metallic Additives. Paper SPE-86962 presented at the SPE International Thermal Operations and Heavy Oil Symposium and Western Regional Meeting, Bakersfield, California.

Glatz, G., Hascakir, B., Clemens and T. 2011. Kinetic Cell and Combustion Tube Results for a Central European Crude. Paper SPE-146089 presented at the SPE Annual Technical Conference and Exhibition, Denver, Colorado.

Graue, D.J. 2001. Upgrading and Recovery of Heavy Crude Oils and Natural Bitumen by In-Situ Hydrovisbreaking. Patent No. 6,328,104.

Greaves, M. and Al-Honi, M. 2000. Three-Dimensional Studies of In-Situ Combustion—Horizontal Wells Process with Reservoir Heterogeneities. SPE Journal of Petroleum Technology 39 (10)

Greaves, M. and Al-Shamali, O. 1996. In Situ Combustion ISC Process Using Horizontal Wells. Journal of Canadian Petroleum Technology 36 (4).

Greaves, M., Tuwil, A.A., and Bagci, A.S. 1993. Horizontal Producer Wells in in Situ Combustion (ISC) Processes. Journal of Canadian Petroleum Technology 32 (04).

Greaves, M., Xia, T.X., and Ayasse, C. 2005. Underground Upgrading of Heavy Oil Using Thai—'Toe-to-Heel Air Injection'. Paper SPE-5443 presented at the International Thermal Operations and Heavy Oil Symposium, Calgary, Alberta, Canada.

Gussis, G.L. 1987. Heavy Oil Recovery. Patent No. 1,228,533.

Gutierrez, D., Miller, R.J., and Taylor, A.R. 2008. Buffalo Field High-Pressure Air Injection Projects: Technical Performance and Operational Challenges. Paper SPE-113254 presented at the SPE/DOE Symposium on Improved Oil Recovery, Tulsa, Oklahoma, USA.

Gutierrez, D., Skoreyko, F., and Moore, R.G. 2009. The Challenge of Predicting Field Performance of Air Injection Projects Based on Laboratory and Numerical Modelling. Journal of Canadian Petroleum Technology 48 (4): 23-33.

Gutierrez, D., Taylor, A.R., and Kumar, V. 2007. Recovery Factors in High-Pressure Air Injection Projects Revisited. Paper SPE-108429 presented at the SPE Annual Technical Conference and Exhibition, Anaheim, California.

Gutierrez, D., Taylor, A.R., and Kumar, V. 2008. Recovery Factors in High-Pressure Air Injection Projects Revisited. SPE Reservoir Evaluation & Engineering 11 (6): pp. 1097-1106.

Hajdo, L.E., Hallam, R.J., and Vorndran, L.D.L. 1985. Hydrogen Generation During In-Situ Combustion. Paper SPE-13661 presented at the SPE California Regional

Meeting, Bakersfield, California.

Hallam, R.J. 1991. Operational Techniques to Improve the Performance of In-Situ Combustion in Heavy-Oil and Oil-Sand Reservoirs. Paper SPE-21773 presented at the SPE Western Regional Meeting, Long Beach, California.

Hallam, R.J., Hajdo, L.E., and Donnelly, J.K. 1989. Thermal Recovery of Bitumen at Wolf Lake. SPE Reservoir Engineering 4 (2): 178-186.

Hardy, W.C., Fletcher, P.B., and Shepard, J.C. 1972. In-Situ Combustion in a Thin Reservoir Containing High-Gravity Oil. SPE Journal of Petroleum Technology 24 (2): 199-208.

Hascakir, B., Glatz, G., and Castanier, L.M. 2011. In-Situ Combustion Dynamics Visualized with X-Ray Computed Tomography. SPE Journal (09).

Hayashitani, M., Bennion, D.W., and Donnelly, J.K. 1978. Thermal Cracking Models for Athabasca Oil Sands Oil. Paper SPE-7549 presented at the SPE Annual Fall Technical Conference and Exhibition, Houston, Texas.

He, B., Chen, Q., and Castanier, L.M. 2005. Improved In-Situ Combustion Performance with Metallic Salt Additives. Paper SPE-93901 presented at the SPE Western Regional Meeting, Irvine, California.

Horton, R.L. and Brandt, J.A. 1995. Continuous Method of In-Situ Steam Generation. Patent No. 5,458,193.

Islam, M.R. and Farouq Ali, S.M. 1992. New Scaling Criteria for in-Situ Combustion Experiments. Journal of Petroleum Science and Engineering 6 (4): 367-379.

Jha, K.N. and Verkoczy, B. 1986. The Role of Thermal Analysis Techniques in the in-Situ Combustion Process. SPE Reservoir Engineering 1 (4): 329-340.

Jia, N., Moore, R.G., and Mehta, S.A. 2006. Kinetic Modelling of Thermal Cracking and Low Temperature Oxidation Reactions. Journal of Canadian Petroleum Technology 45 (9).

Jia, N., Moore, R.G., and Mehta, S.A. 2003. Kinetic Modelling of Thermal Cracking and Low Temperature Oxidation Reactions. Paper PETSOC-2003-214 presented at the Canadian International Petroleum Conference, Calgary, Alberta.

Joseph, C. and Pusch, W.H. 1980. A Field Comparison of Wet and Dry Combustion. SPE Journal of Petroleum Technology 32 (9): 1523-1528.

Karacan, O.K., and Mustafa, V. 1997. Pyrolysis Analysis of Crude Oils and Their Fractions. Energy & Fuels 11 (2): 385 - 391.

Kisman, K.E. and Lau, E.C. 1994a. A New Combustion Process Utilizing Horizontal Wells and Gravity Drainage. Journal of Petroleum Scinece and Technology (03).

Kisman, K.E. and Lau, E.C. 1994b. A New Combustion Process Utilizing Horizontal Wells and Gravity Drainage. Journal of Petroleum Scinece and Technology 33 (3):39-45

Kisman, K.E., Nzekwu, B.I., and Lau, E.C. 1995. Horizontal Well Gravity Drainage Combustion Process for Oil Recovery. Patent No. 5,456,315.

Kumar, V., Gutierrez, D., and Thies, B.P. 2010. 30 Years of Successful High-Pressure Air Injection: Performance Evaluation of Buffalo Field, South Dakota. Paper SPE-133494 presented at the SPE Annual Technical Conference and Exhibition, Florence, Italy.

Lapene, A., Castanier, L.M., and Debenest, G. 2009. Effects of Water on Kinetics of Wet in-Situ Combustion. Paper SPE-121180 presented at the SPE Western Regional Meeting, San Jose, California.

Leaute, R. 1994. Recovery and Upgrading of Hydrocarbon Utilizing in Situ Combustion and Horizontal Wells. Patent No. 5,339,897.

Leider, H. R., Krikorian , O. H., and Young , D. A. 1973. Thermodynamic Properties of Carbon up to the Critical Point. Carbon, Vol II: 555-563.

Lewis, B. 1967. Modern Concepts of Combustion Phenomena. Paper WPC-17 presented at the 7th World Petroleum Congress, Mexico City, Mexico

Lin, L.C., Deo, M.D., and Hanson, F.V. 1991. Nonisothermal Analysis of the Kinetics of the Combustion of Coked Sand. Industrial & Engineering Chemistry Research 30 (8):795-1801.

Mamora, D.D. 1995. New Findings in Low-Temperature Oxidation of Crude Oil. Paper SPE-29324 presented at the SPE Asia Pacific Oil and Gas Conference, Kuala Lumpur.

Mohammad, A.A. and Mamora, D.D. 2008. In-Situ Upgrading of Heavy Oil under Steam Injection with Tetralin and Catalyst. SPE-117604 presented at the International Thermal Operations and Heavy Oil Symposium, Calgary, Alberta, Canada.

Nares, H.R., Schachat, P., and Ramirez-Garnica, M.A. 2007. Heavy-Crude-Oil Upgrading with Transition Metals. Paper SPE-107837 presented at the Latin American & Caribbean Petroleum Engineering Conference, Buenos Aires, Argentina.

Nasr, T.N. and Ayodele, O.R. 2005. Thermal Techniques for the Recovery of Heavy Oil and Bitumen. Paper SPE-95487 International Improved Oil Recovery Conference in Asia Pacific, Kuala Lumpur, Malaysia.

Oskouei, S.J.P., Moore, R.G., and Maini, B.B. 2010. Feasibility of in-Situ Combustion in the Mature Sagd Chamber. Paper SPE-137832 presented at the Canadian Unconventional Resources and International Petroleum Conference, Calgary, Alberta, Canada.

Oskouei, S.J.P., Moore, R.G., Maini, B.B. 2011. Feasibility of In-Situ Combustion in the Sagd Chamber. Jotrnal of Canadian Petroleum Technology 50 (04):31-44

Ovalles, C., Vallejos, C., and Vasquez, T. 2001. Extra-Heavy Crude Oil Downhole Upgrading Process Using Hydrogen Donors under Steam Injection Conditions. Paper SPE-69692 presented at the SPE International Thermal Operations and Heavy Oil Symposium, Porlamar, Margarita Island, Venezuela.

Parrish, D.R., Pollock, C.B., and Craig Jr., F.F. 1974. Evaluation of as a Tertiary Recovery Method, Sloss Field, Nebraska. SPE Journal of Petroleum Technology 26 (6): 676-686.

Parrish, D.R., Pollock, C.B., Ness, N.L. 1974. A Tertiary Cofcaw Pilot Test in the Sloss Field, Nebraska. SPE Journal of Petroleum Technology 26 (6): 667-675.

Pebdani, F.N. 1990. Enhanced Oil Recovery for Oil Reservoir Underlain by Water. Patent No. 4,961,467.

Pebdani, F.N. and Shu, W.R. 1986. Heavy Oil Recovery Process Using Cyclic Carbon Dioxide Steam Stimulation. Patent No. 4,565,249.

Popa, C.G. 1976. Immiscible Multi-Phase Fluid Displacement in a COFCAW Process. Paper SPE-5860 presented at the SPE California Regional Meeting, Long Beach, California, 7-9 April 1976.

Ramirez-Garnica, M.A., Mamora, D.D., and Nares, R. 2007. Increase Heavy-Oil Production in Combustion Tube Experiments through the Use of Catalyst. Paper SPE-107954 presented at the Latin American & Caribbean Petroleum Engineering Conference, Buenos Aires, Argentina.

Ramirez-Garnica, M.A., Perez, J.R.H., Cabrera-Reyes, M.D.C. 2008. Increase Oil Recovery of Heavy Oil in Combustion Tube Using a New Catalyst Based Nickel Ionic Solution. Paper SPE-117713 presented at the International Thermal Operations and Heavy Oil Symposium, Calgary, Alberta, Canada.

Ranjbar, M. 1995. Improvement of Medium and Light Oil Recovery with Thermocatalytic In-Situ Combustion. Journal of Canadian Petroleum Technology 34 (8).

Redford, D.A. 1978a. Viscous Oil Recovery Method. Patent No. 4,099,566.

Redford, D.A. 1978b. Viscous Oil Recovery Method. Patent No. 4,099,566.

Ren, Y., Freitag, N.P., and Mahinpey, N. 2007. A Simple Kinetic Model for Coke Combustion During an in-Situ Combustion (ISC) Process. Journal of Canadian Petroleum Technology 46 (4).

Ryttan, C.C. 2009. The THAI^{TM} Process Annual Report, Petrobank Energy and Resources Ltd, Calgary, Canada.

Shokoya, O.S., Mehta, S.A., Moore, R.G. 2002. Evaluation of the Miscibility and Contribution of Flue Gas to Oil Recovery under High Pressure Air Injection. Journal of Canadian Petroleum Technology 41 (10).

Thiez, P.a.L. and Lemonnier, A. 1990. An In-Situ Combustion Reservoir Simulator with a New Representation of Chemical Reactions. SPE Reservoir Engineering 5 (3): 285-292.

Turta, A.T., Lu, J., and Bhattacharya, R.N. 2005. Current Status of the Commercial in Situ Combustion (Isc) Projects and New Approaches to Apply ISC. Paper Petroleum Society of Canada 2005-002 presented at the Canadian International Petroleum Conference, Calgary, Alberta.

Venkatesan, V.N. 1988. Oil Recovery Method. Patent No. 4,722,395.

Verkoczy, B. and Freitag, N.P. 1997. Oxidation of Heavy Oils and Their SARA Fractions-Its Role in Modelling In-Situ Combustion. Paper PETSOC-97-167 presented at the Technical Meeting/Petroleum Conference Of The South Saskatchewan Section, Regina.

Verkoczy, B. and Jha, K.N. 1986. TGA/DSC Investigations of Saskatchewan Heavy Oils and Cores. Journal of Canadian Petroleum Technology 25 (3).

Vossoughi, S., Bartlett, G.W., and Willhite, G.P. 1982. Development of a Kinetic Model

for In-Situ Combustion and Prediction of the Process Variables Using TGA/DSC Techniques. SPE Annual Technical Conference and Exhibition, New Orleans, Louisiana.

Xia, T.X., Greaves, M., and Turta, A. 2003. Main Mechanism for Stability of Thai-"Toe-to-Heel Air Injection". Paper Petroleum Society of Canada 2003-030, presented at the Technical Meeting / Petroleum Conference, Calgary, Alberta,

Yang, X. 2009. Hybrid Steam-Air Heavy Oil Recovery Process Design. M.Sc. MR51168. University of Calgary (Canada), Canada.

Yang, X. and Gates, I.D. 2008. The Design of Hybrid Steam/In-Situ Combustion Bitumen Recovery Processes. Paper 2008-114-EA presented at the Petroleum Society of Canada Technical Meeting/Petroleum Conference, Calgary, Alberta

APPENDIX A

Scaling

Assumptions in the scaling technique include different porous media (porosity and permeability), same fluid, different pressure drop, same temperature, and geometrical similarity.

Scaling calculation is as follows:

$$\left[\frac{H}{X_2}\right]_{model} = \left[\frac{H}{X_2}\right]_{prototype} = \beta \quad \text{(A-1)}$$

here X_2 in Cartesian coordinate is in the Z direction and H is the pay thickness of the model or prototype. "β" is the scaling ratio. By considering 27 m for a net pay of the Peace River reservoir and 0.15 meter height and porous media of the CAGD cell, the scaling ratio can be calculated using the following geometric ration;

$$\left[\frac{H_{prototype}}{H_{model}}\right] = \frac{27}{0.15} = 180 \quad \text{(A-2)}$$

With 0.4 width of the laboratory model, the well spacing and horizontal well length can be estimated as,

$$\left[\frac{W_{prototype}}{W_{model}}\right] = \frac{W_{prototype}}{0.4} = 180 \quad \text{(A-3)}$$

$$W_{prototype} = 72 \ m$$

Where "*W*" is the width of the model or prototype.

The permeability of the sand pack was chosen to obtain similar $K \times h$ for both laboratory model and prototype. Permeability of the sand pack was estimated using Berg (1970) correlation.

$$[K \times h]_{model} = [K \times h]_{prototype} = [5.23 \times 27]_{prototype} = 141.21 \ D.m \quad \text{(A- 4)}$$

$$[K \times h]_{model} = [5.23 \times 27]_{prototype} = 141.21 \ D.m$$

$$k_{model} = 942 \text{ D}$$

Also, time can be scaled using the following similarity relationship;

$$\left[\frac{\mu \times \varphi \times S_o \times X_1^2}{t \times k \times \Delta P}\right]_{model} = \left[\frac{\mu \times \varphi \times S_o \times X_1^2}{t \times k \times \Delta P}\right]_{prototype} \quad \text{(A-5)}$$

In this calculation, it was assumed that the pressure drop in the field is "β" times more than the pressure drop in the model. Since the formation has lower permeability and larger vertical spacing that is a reasonable assumption. The average porosity of the sand pack is 39%, and typical porosity of the Peace River reservoir is in the range of 18 to 23%. Based on these assumptions, time can be scaled in the following form:

$$[t]_{prototype} = \frac{b^2}{2}[t]_{model} \quad \text{(A-6)}$$

$$[t]_{prototype} = 15{,}954 \times [t]_{model} \quad \text{(A-7)}$$

This means that 1 hour in the laboratory is corresponds to 1.8 years at the field scale. For both the laboratory model and the field prototype, a similar fluid was considered. However, operating pressure for each one is different. This will change the partial pressure of oxygen the same as the oxidation characteristics. It was tried to maintain similar oxygen partial pressure by changing the molar composition of the oxygen in the injection stream (100% O_2). This partial pressure of oxygen in the laboratory model corresponds to the field pressure of about 1641 kpa (238 psi) and injection of air (20.95% O_2). Another variable for reaction scaling was the permeability of the porous media. In the laboratory sand pack, lower permeability provides a larger surface for oxidation reactions (Mamora 1995, Oskouei 2010). However, to scale the gravity to viscosity ratio, the laboratory model must have higher permeability. Thus, the oxidation reaction in the field prototype can be expected to be more vigorous than in the laboratory model.

Another scaling parameter was the heat losses. Inner and outer insulation was installed

in the CAGD cell. The aim of the inner insulation was to prevent heat conduction through the stainless steel body of the laboratory cell. The Inner insulation properties (thickness, heat conductivity, and heat capacity) were selected to have heat losses similar to field conditions, where a semi-infinite sand formation is present at the bottom and top of the reservoir. The following calculation provides a related procedure for heat-loss scaling between the model and the field prototype. To determine how much error will be introduced by using inner insulation for the boundary effect, the heat loss rate was calculated and then compared to the hypothetical semi-infinite sand formation. Ceramic insulation and sand properties are summarized in Table 12. The heat loss rate for a semi-infinite sand formation with elevated temperature of about ΔT (593 °C) at the inner boundary can be described by:

$$q_{\infty} = 2 \times \bar{K}_{\text{sand}} \times \Delta T \sqrt{\frac{1}{\pi \times t \times \alpha_{\text{sand}}}} \quad \text{(A-8)}$$

Where α_{sand} is the thermal diffusivity of sand and is defined as:

$$\alpha_{sand} = \frac{\bar{K}_{sand}}{\rho_{sand}} \quad \text{(A-9)}$$

In addition, the rate of heat loss for a slab of ceramic insulation with thickness of h_c which the temperature of one end raised to ΔT (593°C) is as follow:

$$q_{insulation} = \frac{\bar{K}_{\text{sand}} \times \Delta T}{h_{insulation}} \times \Delta T \quad \text{(A-10)}$$

The Initial temperature of the model is about 30°C and the highest recorded temperature of combustion front is about 623°C. Therefore, the maximum ΔT experienced by the surrounding formations is 593°C. Moreover, time duration of the experiment is about 24 hours. Based on this information, Fig. 79 compares the heat loss rate for the laboratory

model with the field prototype and shows the amount of error introduced by using the ceramic insulation. This graph implies that at the first 5 hours of the experiment, the amount of heat lost was significantly lower for the model. However, in this period, combustion front was not fully developed and did not even touch the overburden or the underburden formation. Therefore, the temperature difference (593°C) which was used in this calculation is not fully established at the boundaries. After the first 5 hours, heat loss rate for both cases are more and less similar, and the introduced error is less than 30%. The heat loss rates of the model is initially lower than the field condition, but field heat loss was exponential and fell below the steady-state laboratory heat loss rate at the end of the experiment. Fig. 80 shows the cumulative heat loss after the first 5 hours of the experiment. Error was defined as a percentage deviation of laboratory heat loss compared to field condition.

Table 12: Thermal properties of ceramic insulation and sand formation.

Property	Sand	Ceramic Insulation	Unit
C	1.55	1.13	(kJ/kg K)
$\overline{K}$	0.64	0.05	W/(m.K)
ρ	1762.20	99.96	Kg/m^3
α	0.000836	0.001652	m^2/hr
T_{In}	623	623	°C
T_{Out}	30	140	°C
ΔT	593	482	°C
$h_{insulation}$	∞	1.28	cm

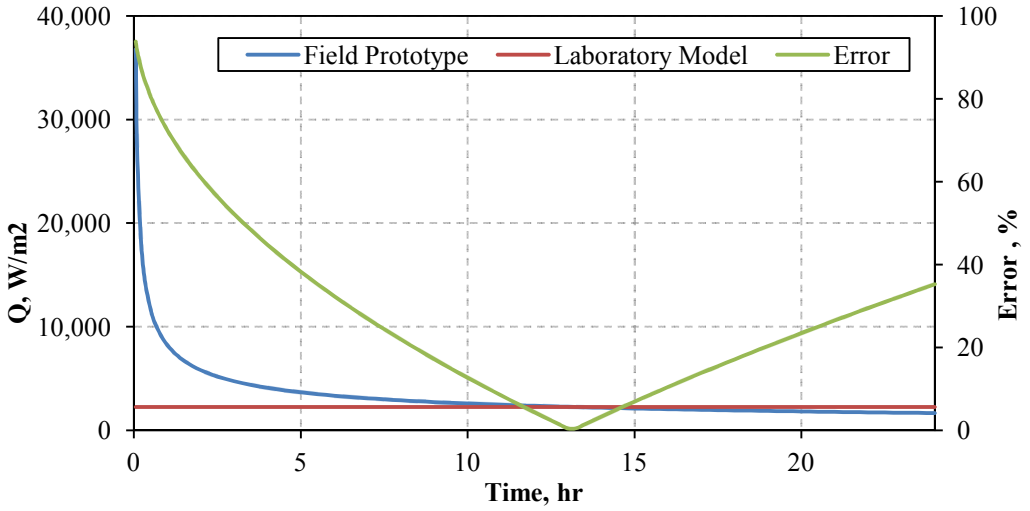

Fig. 79- Heat-loss rate comparison of laboratory model and field prototype. After the first 5 hours, heat loss rates for both cases are more and less similar or the introduced error is less than 30%.

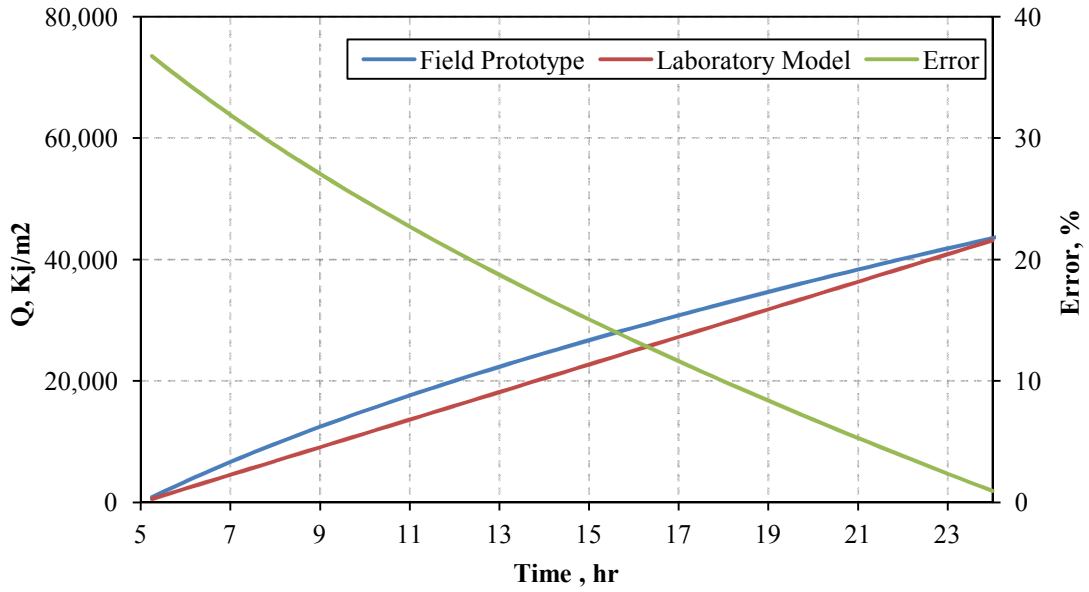

Fig. 80- Cumulative heat loss comparison of laboratory model and the field prototype. The cumulative heat loss of the field is higher than the experimental model. This graph implies that combustion reaction in the model is more vigorous than in the field condition.

APPENDIX B

Consumed energy calculation for steam and air injection

In this study consumed energy of SAGD process is calculated as the amount of energy that is required to convert water from ambient temperature of 25 °C to the steam with quality of 90% (Eq. B-1)

$$E = m\left(Sf_{@101\ \text{kpa}} - Sf_{@4000\ \text{kpa}}\right) + QS \times \left(hg_{@4000\ \text{kpa}} - Sf_{@4000\ \text{kpa}}\right) \quad \text{(B-1)}$$

Where Sf is the saturated water enthalpy, QS is the steam quality, m is the weight of water and hg is the saturated steam enthalpy. Table 13 summarized the water enthalpy at different condition.

Table 13: Summary of water enthalpy that was used in the energy consumption calculation

Condition	Enthalpy, Kj/Kg
water @101kpa	0.36722
Saturated water @ 4000 kpa	2.8102
Saturated steam @4000 kpa	2800.3
Steam quality	0.9

Air injection process (CAGD and THAI) require energy for preheating period and also compressing air. For preheating period the heating rate of 5.5×10^6 kJ/day was added to predetermine gird block (3.9 m3) of injection well for 6 month. Energy required to compress unit volume of air from atmospheric pressure to the injection pressure 4000 kpa (580 psi) was calculated by using Eq. B-2

$$E = 231.9 \times V \times \log\left(\frac{Pinj}{Psc}\right) \quad \text{(B-2)}$$

Where V is the air volume at standard condition, Psc (101.1kpa) is the atmospheric pressure and Pinj is the injection pressure (4000 kpa). Using these numbers Equation b-2 gives 341 (KJ) per cubic meter of air.

APPENDIX C

Reaction Kinetic Model

In addition to reaction schemes, Belgrave et al (1993) presented the properties of the pseudo-components. Table 14 listed the most important properties of these components. It should note that the proposed kinetic reactions are based on mass balance. For example in reaction number gives:

maltenes ➔ 0.372 asphaltens

This reaction implies that 1 mole of maltenes (406.7 g) converts to 0.372 moles of asphaltens (0.372×1092.8 = 406.7 g).

Table 14: Properties of the components used in fluid molding (Belgrave et al. 1993)

Component	Molecular Weight,g/mol	Tc, ºC	Pc, kPa
Maltenes	406.7	618.85	1478
Asphaltenes	1093.2	903.85	792
Coke	13.13	6536*	10436*
Water	18.02	373.85	22107
O_2	32	-119.15	5046
Gas	43.2	21.85	7176
CH_4	16.04	-82.55	4600
CO_2	44.01	31.05	7376
CO	28.01	-140.25	3496
N_2	28.01	-146.95	3394

* Reported by Leider et al. (1973)